UPTEC W05 016

Examensarbete 20 p
November 2005

Plant Extract Sensitised Nanoporous Titanium Dioxide Thin Film Photoelectrochemical Cells

Fotoelektrokemiska celler av nanoporös tunnfilmstitandioxid sensiterade med växtextrakt

Sigrid Hedbor
Linnéa Klar

Abstract

Plant Extract Sensitised Nanoporous TiO_2 Thin Film Photoelectrochemical Cells

Sigrid Hedbor and Linnéa Klar

Non-sealed photoelectrochemical dye sensitised solar cells (DSSC) with pressed nanoporous TiO_2 thin film photoelectrodes were manufactured for the purposes of finding out whether plant extract-based dye sensitised cells can perform as well as ruthenium complex-based dye sensitised cells and whether the pressing force affects the cell performance.

The cells were pressed with three different pressing forces and sensitised with plant extracts from red cabbage, beetroot, violet and henna, as well as with a ruthenium complex-based dye for comparison. The IPCE and iV values and the corresponding fill factors of the cells were evaluated and compared.

No significant difference between the cells pressed with different pressing forces could be established. Among the plant extract-based dye sensitised cells the ones sensitised with beetroot extract performed best. The cell that achieved the highest efficiency had a fill factor of 70%. Compared to the ruthenium-sensitised cells the overall performance of the plant dye sensitised cells were very poor and the produced photocurrents very low. The IPCE values were generally low: one of the best-performing cells had an IPCE value of slightly over 0.06 in the 440-470 nm wavelength ranges. One reason for this is that it is difficult to obtain a plant extract dye as intense and deep in colour as ruthenium complex-based dyes, since pigment saturation is obstructed by the presence of other chemical compounds in the plant extracts. Another is that it is a delicate and difficult matter to match the energy levels in the electrolyte-semiconductor system with the energy levels of the pigments in the plant extract dye.

keyword: photoelectrochemical cell, solar cell, nanoporous, thin film, titanium dioxide, dye sensitised, ruthenium, plant extract, beetroot.

Referat

Fotoelektrokemiska celler av nanoporös tunnfilmstitandioxid sensiterade med växtextrakt

Sigrid Hedbor and Linnéa Klar

För att undersöka skillnad i prestationsförmåga mellan celler sensiterade med växtextraktsbaserad färg, och celler sensiterade med ruteniumkomplex-baserad färg, samt huruvida presskraften påverkar en cells prestationsförmåga, tillverkades icke-slutna fotoelektrokemiska färg-sensiterade solceller med tunnfilmsfotoelektroder av pressad, nanoporös titandioxid.

Cellerna pressades med tre olika presskrafter och sensiterades med växtextraktsfärg från rödkål, rödbeta, viol och henna, samt en ruteniumkomplex-baserad färg som fick utgöra kontrollbetingelse. För varje cell uppmättes IPCE- och iV-värde och motsvarande fyllnadsgrad (fill factor) och dessa jämfördes.

Ingen signifikant skillnad kunde fastställas mellan celler pressade med olika presstryck. Bland cellerna sensiterade med växtextraktbaserad färg presterade rödbeta bäst. Cellen med högst effektivitet hade fyllnadsgraden 70%. Emellertid uppvisade de växtfärgade cellerna genomgående sämre effektivitet än de rutenium-sensiterade och fotoströmmarna var mycket låga. IPCE-värdena var allmännt låga: den bäst presterande cellen hade ett IPCE-värde på något över 0,06 i våglängdsintervallet 440-470 nm. En förklaring till detta är de övriga ämnen som förutom pigment återfinns i de växtbaserade färgerna. Dessa hindrar pigmentmättnad och förhindrar att växtfärgen når ruteniumfärgens intensitet. En annan anledning består i svårigheten att passa ihop energinivåerna i cellens elektrolyt-halvledarsystem med energinivåerna hos pigmentet i växtfärgen.

nyckelord: fotoelektrokemisk cell, solcell, nanoporös, tunnfilm, titandioxid, färgsensiterad, rutenium, växtextrakt, rödbeta.

Department of Engineering Sciences, Uppsala University, Ångströmlaboratoriet,
Lägerhyddsvägen 1, 751 21, Uppsala
ISSN 1401-5765

Preface

This thesis was performed at the Division of Solid State Physics, Depertment of Enginering Sciences and at the Department of Physical Chemistry. For Sigrid Hedbor it is part of a Master of Science degree in Environmental and Aquatic Engineering at Uppsala University and for Linnéa Klar it is part of a Master of Science degree in Physical Engineering at Uppsala University.

Claes-Göran Granqvist (Depertment of Engineering Sciences) and Sten-Eric Lindquist (Department of Physical Chemistry) were supervisors. Thank you for supervision and guidance! We would also like to thank Arne Roos, Nils-Olov Ersson, Kerstin Sunnerheim and Anders Herrmann for guidance, Torbjörn Lindgren, Justus Simiyu and Julius Mwabora for inspiration and families and friends for all kinds of support.

The responsibility distribution of the text is such that Linnéa Klar is responsible for sections 1.1 - 1.2, 1.4 - 1.5, 2.1.1, 2.3, 2.4, 3.1 and 3.2.1 through 3.2.4 and Sigrid Hedbor is responsible for sections 1.6, 2.1.2, 2.2 and 3.2.5. We both share responsibility for the Abstract, Referat, Preface and sections 1.3 4, 5, 6, 7, 8, 9 and 10.

Uppsala, November 2005
Sigrid Hedbor and Linnéa Klar

UPTEC W 05-016, ISSN 1401-5765
Printed at the Department of Earth Sciences, Geotryckeriet, Uppsala University, Uppsala, 2005.

Contents

1 Introduction

1.1 History

Photovoltaic cells utilise the photovoltaic effect, the discovery of which is most often attributed to Edmond Becquerel. (However, his father Antoine Cesar Becquerel might have been the true discoverer of this phenomenon; information is conflicting on this matter [1].) The experimental set-up, by help of which Becquerel let the photovoltaic effect appear before the eyes of the world, was a metal halide salt solution with two electrodes emerged in it. Upon illumination of the solution, a current between the electrodes were produced. This can be considered to be a remote ancestor to the modern-day photoelectrochemical (PEC) solar cell. Becquerel published an article on his (or his father's) discovery in 1839, but the phenomenon of the photovoltaic effect remained unexplained until the rise of quantum mechanics in the beginning of the 20th century, since wave theory cannot explain the mechanisms of the photovoltaic effect. Albert Einstein's 1905 paper on the photovoltaic effect elucidated the matter extensively [1], but even long before the mystery behind the photovoltaic effect was completely explained, scientists discovered a number of facts pertaining to photovoltaic cells. In 1837 Louis Daguerre created the daguerreotype, the very first type of photographic image, exploiting the light-sensitivity of silver iodide [2]. The photographic field was subject to comprehensive empirical research. William Henry Fox Talbot accidentally revolutionised photography when he employed silver halide crystals on a piece of film, which reduced the exposure time from one hour (the daguerreotypes) to one to three minutes; Talbot named his improved photographic process calotype [3]. This ignited discoveries in sensitisation: The semiconducting silver halides used by Talbot and others at that time had band gaps of 2.7 to 3.2 eV - therefore, they did not respond to wavelengths longer than 460 nanometres, since these wavelengths are not sufficiently rich in energy to admit energy transfer across the bandgap. In 1873, Hermann Vogel, (figure 1), a professor of photochemistry, spectroscopy and photography, discovered a way to extend the photo-response of the silver halide, using certain organic dyes, so that it became sensitive to wavelengths exceeding 460 nm. From having been sensitive only to white-blue light, photographs could now be sensitive to green light as well. The manufacturing of orthochromatic plates was born (the orthochromatic plates were sensitive to all the visible spectrum except red and deep orange). Some 25 years later, in the early 20th century, production of panchromatic films, sensitive to the entire visible spectrum, commenced [2], [4]. In 1887, James Moser became the scientist who carried dye-sensitisation over from photography to photo electrochemistry. The dye he used was erythrosine, a red substance formed by the oxidation of tyrosine. The first theoretical analysis of the photographic process was carried out in 1938 by Gurney and Mott [4]. Since the same photochemistry rules photography and photoelectrochemical cells, the same dyes for sensitisation can successfully be applied within the two fields. This was recognised by Hishiki and Namba at the International Conference on Photosensitisation of Solids in Chicago in 1964 [5]. It was also noticed that, to maximise the efficiency, the dye should be applied in a monolayer on the semiconductor electrodes. Later it was observed, by Gerischer, Tributsch and Hauffe, that electron transfer was the mechanism behind sensitisation. The post-war foundation of modern photo-electrochemistry is attributed to Gerischer [6], Brattain and Garret [4].

The first solid-state solar cell was constructed in 1876. The first silicon-based solar cells were created in the 1940s, but the breakthrough came in 1953, when Daryl Chapin, Calvin Fuller, and Gerald Pearson at Bell Laboratories produced a solar cell with a 4.5% efficiency. Their improvement was due to introducing impurities into the silicon, which render the silicon a considerably better conductor of electricity. Their innovation encouraged further research in the field, and before 1960 efficiency figures had reached 14%. Throughout the 1960s, with especially the US military demanding the technology, solar cells were mainly used to provide electrical power for earth-orbiting satellites. Boosted by the oil crisis, research in the field of photovoltaic cells waxed in the 1970s. The rise of amorphous silicon in the 1980s brought solar cells to common electronic consumer goods, pocket calculators, watches and more [7]. In 1989 a 37% efficiency was reported, when lenses to concentrate the sunlight had been employed [1].

Grätzel and O'Regan made a major contribution to the evolution of PEC cells in 1991, when they created the Grätzel cell, a nanoporous[1] TiO_2 PEC solar cell sensitised with a ruthenium complex dye and with acetonitrile or ethylene carbonate as organic solvents for the electrolytes [8]. The large surface area of the porous nanocrystalline TiO_2 layer and the ruthenium complex dye interact to harvest a large percentage of the incident photons; high conversion efficiencies are achieved in both simulated solar light and diffuse daylight.

Figure 1: Hermann W Vogel (1834 - 1898) performed the first sensitation. From [9].

1.2 Future

Photovoltaic cells are now (since the oil crisis-marked 1970s) generally appreciated as a promising alternative to non-renewable energy sources. Dye Sensitised Solar Cells (DSSC:s) are subjects for scrutinous study worldwide. In the constantly evolving field of research of PEC cells, many discoveries are yet to be made. Lately, the solar-cell industry has grown swiftly. In 2001, the global energy production generated from photovoltaic (PV) cells surpassed 300 Megawatt (MW) and in 2003 it reched 740 MW [10]. Silicon-based solar cells still dominate the PV energy market, holding roughly an 80% share of the present-day PV production. Predominant determinants in the fast growth in the PV energy production are a continuous decline of production costs and an increase of solar-cell efficiencies [11].

1.3 The Solar Cell Model Employed in This Study

The type of PEC solar cell under consideration in this study is a type of Grätzel cell. It is an open (non-sealed) two-electrode sandwich configuration, in which two glass substrates (the photoelectrode and the counter electrode) are pressed together with clips. (During measurements

---

[1] In the literature a number of terms are used synonymously: nanoporous, mesoscopic, nanostructured and (porous) nanocrystalline (for the case of crystalline substances). During the creation of this text the endeavour has been to use the word nanoporous consistently, except where the aim has been to emphasise e.g. the crystalline aspect.

the cell can be held erect by a holder and connected to measuring instruments by help of crocodile clips.) Figure 27 on page 38 depicts a schematic over this setup. The photoelectrode consists of a conducting glass substrate with a dye sensitised TiO_2 thin film deposited on it[2]. The counter electrode is made from a conducting glass substrate with a catalysing platinum chloride layer on it. The thin gap in between the glass substrates as well as the pores in the nanostructured film are filled with an electrolyte based on the I^-/I_3^- ion pair. Figure 2 shows a schematic over the physical cell, with the glass substrates, the dye coated nanoporous TiO_2 structure and the electrolyte, also including the electron path through the cell.

When an incident photon ($h\nu$) is absorbed by a DSSC the energy is transformed into the excitation of an electon in the pigment of the dye. The electron is then transfered to the semiconductor, induces as current, and is transfered through the conducting layer of the back contact and via the redox-couple to its original position in the pigment. Figure 3 shows a simplified schematic over the energy levels in a cell and the electron path through them. The mechanism of the cell is explained in more detail in chapter 2.1.2 where figure 5 on page 8 gives a more detailed picture of the energy levels.

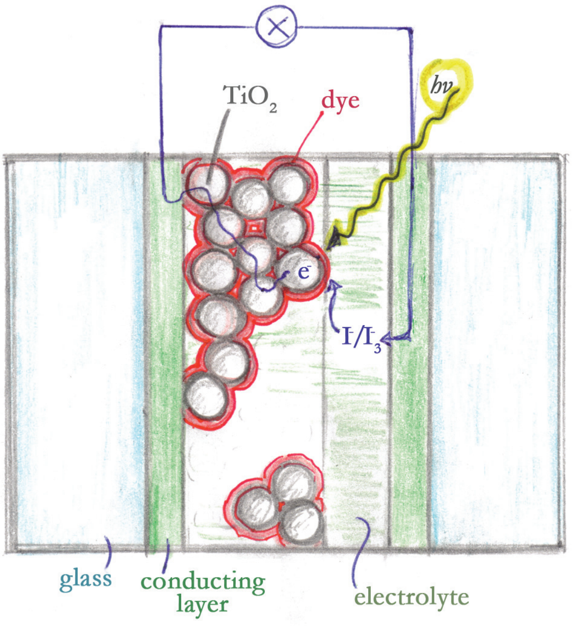

Figure 2: A schematic over a dye sensitised nanoporous TiO_2 cell with the electron path through it. An incoming photon ($h\nu$) causes excitation of an electron (e^-) and a current is induced.

---

[2] Generally, a thin film is not, as the name might suggest, a film having a specified thickness. Rather, a thin film is defined by its application. The thin films in this study have a thickness of approximately 0.005 mm, which is roughly a tenth of the thickness of scotch tape. Films pressed with a larger pressing force of course are thinner than those pressed with a lesser force.

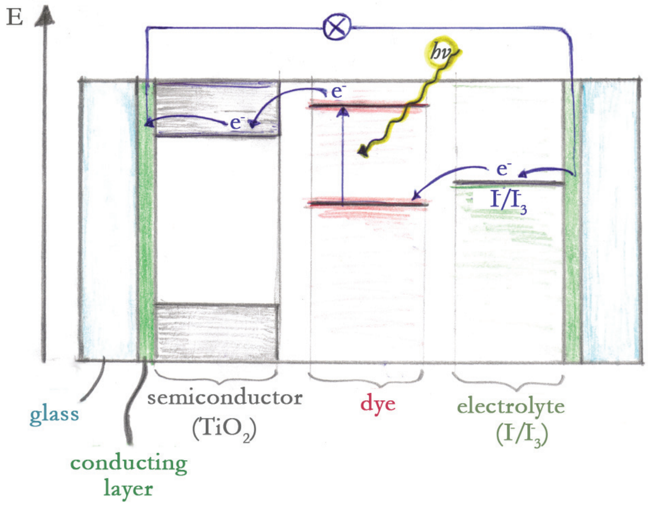

Figure 3: A simplified schematic over the energy levels in a cell and the electrons path through it. An incoming photon ($h\nu$) causes excitation of an electron (e^-) which then traveles to lower energy levels, induces a current and finally reaches its original position.

1.4 The Semiconductor and the Dye – Two Essential Components of the Nanoporous PEC Solar Cell

The semiconductor titanium dioxide, TiO_2, is long since a popular compound in various applications, such as toothpaste, paint, cosmetics, anti-reflexive coatings and so on, for its non-toxicity among other reasons. It is now much used in porous nanocrystalline thin film solar cells for its stability. The TiO_2 photoelectrode is under normal conditions not subject to any corrosion at the electrode-electrolyte interface [12]. Still, this type of solar cell faces problems with stability. Only because the TiO_2 is stable as showed by Honda and Fujishima [12], it does not necessarily mean that the compounded solar cell is stable. Dyes degrading from exposure to sunlight and problems with encapsulating the electrolyte shorten the lifetime of these solar cells.

A dye is essential to a PEC solar cell with a large bandgap semiconductor photoelectrode, in order to boost the efficiency of the cell. The photoelectrode semiconductor in itself may be practically transparent to visible and infrared light, which is the case with e.g. TiO_2. Therefore it is dyed for increased efficiency. The wider the part of the spectrum that can be absorbed, the more energy can be converted to electricity. Chlorophyll was a colouring agent alternative when research on dye sensitisation grew in the 1970s. Since then, far more effective dyes have been discovered, the most successful of which are the ruthenium complex dyes. Section 2.3.7 provides more information on effective ruthenium-based dyes.

Ruthenium dyes are frequently used since they so far are the most successful sensitisers in nanostructured thin film PEC solar cells. Ruthenium is an expensive element though. If an alternative dye, such as a plant dye, could be made to perform as well as ruthenium dyes, it would be interesting for environmental and economical reasons alike. Especially for investors in nanocrystalline thin film PEC solar cells, with developing countries regarded as potential investors, it would be of economic interest to replace the ruthenium with cheaper dyes. A goal for the research on plant-based dyes for PEC solar cell use is to come up with a dye as effective as the ruthenium-based dyes. Whether or not it is economically viable to substitute plant dyes for ruthenium depends on the rendered solar cell efficiency along with the long time stability of the dyes.

From an environmental point of view, substitutes for ruthenium would be preferable, as long as the substitutes are not even more toxic and detrimental to the environment. Even though a functional solar cell in use is not a threat to the ambient nature, undesired leakage or unsatisfactorily handling when the solar cell lifetime has expired, could cause environmental problems. For a PEC solar cell to function under working conditions, it must be well sealed, for the electrolyte must not evaporate. Therefore, leakage of toxic components will not be a problem unless the solar cell is damaged. These economic and environmental issues justify the search for alternative dyes.

1.5 Advantages of the Nanoporous PEC Solar Cell

Solar cells in general have obvious advantages. They are non-polluting in operation, and their source of energy, the sun, can be regarded as being close to inexhaustible, since its life time is estimated to be some 10 billion years [4].

The high conversion efficiency of the nanoporous PEC cell mentioned above adds to its attractiveness. Direct sunlight provides the best circumstances for photon harvesting, but diffuse light also gives an opportunity for this: compared to other types of photovoltaic solar cells, the nanoporous cell performs better in diffuse daylight. This distinctive characteristic makes nanoporous cells highly desirable in climates where a large fraction of the incident solar radiation is diffuse and for indoor consumer applications [13]. Another advantage of nanoporous PEC cells is that their manufacturing is simple and does not require expensive clean room techniques. The DSSC raises a hope for future large-scale use of photovoltaic cells for electricity generation.

1.6 The Purpose of This Study

The purpose of this study is to manufacture dye sensitised solar cells by means of a simple pressing tecnique and to examine whether it is possible to sensitise them with plant extract-based dyes instead of the commonly used ruthenium-based dyes which are expensive and known to be highly toxic [14].

The nanoporous TiO_2 thinfilm of the photoelectrodes are pressed with different pressing forces to investigate if the pressing force makes any difference in a cells performance.

The plant-extract dyes in this study are cheap, non-toxic and simple to manufacture and less harmful to the environment than ruthenium. We chose to concentrate on dyes obtainable from plants such as beetroot and red cabbage. The plants were chosen for their colour and their convenient accessibility.

The open sandwich configuration of the solar cells built for this study is designed for short-time use, since it is not sealed (so the electrolyte is allowed to evaporate). Therefore, issues of long-time use have not been considered in this study.

2 Theoretical Background

2.1 Fundaments of the Porous Nanocrystalline Solar Cell

2.1.1 The Semiconductor and its Nanoporous Structure

The basis of a solar cell is a semiconductor; its properties enabling electron separation and transport, allowing electricity to be yielded from sunlight. The semiconductor is a crystalline substance. All the atomic levels of the semiconductor crystal have merged to form two bands, the valence band (VB) and the conduction band (CB). The VB and the CB of the semiconductor crystal are analogues to the molecular concepts of HOMO (highest occupied molecular orbital) and LUMO (lowest unoccupied molecular orbital) [15]. The energy difference between the HOMO and the LUMO, or the valence and the conduction band, is the minimum amount of energy needed to excite an electron. For a semiconductor crystal with a large bandgap, only high-energy photons (i.e. short-wavelength photons) are energetic enough to excite electrons. A dye with a smaller difference between the HOMO and the LUMO can be used to sensitise the semiconductor crystal.

In this study the thin film semiconductor is titanium dioxide, TiO_2. It is a non-toxic, highly refractive, chemically resistant compound. It exists in three different crystal structures: rutile, anatase (see figure 4) and brookite. The two former are tetragonal phases and they are transparent in the visible range [4]. The TiO_2 powder used for the making of the thin film is composed of rutile and/or anatase. The TiO_2 particles are typically 5 to 50 nanometres. Rutile is the more thermodynamically stable of the two; rutile undergoes a transformation to anatase at atmospheric pressure at temperatures above 700 °C. Rutile has a density of 4.26 g/cm^3 and a bandgap of 3.0 eV. Anatase has a density of 3.89 g/cm^3 and a bandgap measuring 3.2 eV. These large bandgaps cause TiO_2 to have low conversion efficiencies, since only the ultra violet part of the solar spectrum (which is low in intensity) can be absorbed [5]. This is the reason a lot of energy is put into finding appropriate dyes for dyeing the titanium dioxide and thus “narrowing the bandgap”. [To “narrow the bandgap” is a somewhat hazy way of expressing it, since it is not the bandgap of the titanium dioxide itself that is narrowed, but the narrower bandgap of the dye which is used. A suitable dye, where the difference between HOMO and LUMO is small enough for low-energy photons (photons with longer wavelengths) to excite electrons, will “help” the titanium dioxide to absorb light in the visible spectrum.] The wide bandgap of TiO_2 is not only associated with insensitivity to the visible spectrum, but also with stability. Metal oxides are, due to the stability they exhibit, advantageous to work with, but for the sake of efficiency, they need be combined with a dye, absorbing visible light.

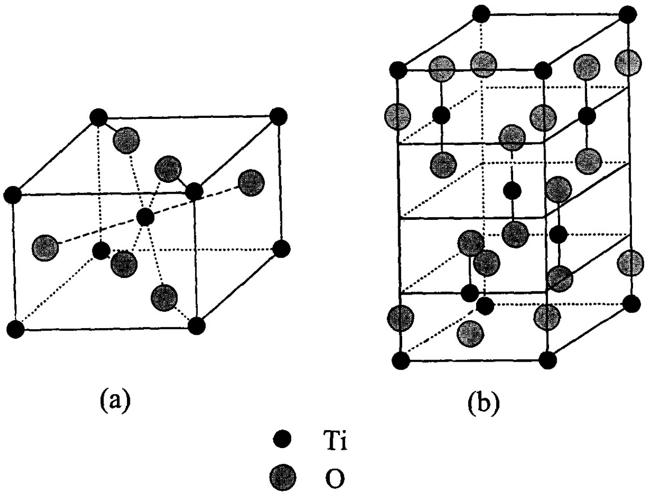

Figure 4: Crystal structures of TiO_2: (a) rutile, (b) anatase. From [4].

The thin film made from a mixture of anatase and rutile will be transparent to the eye if the particles are small enough, that is, less than 20 nanometres. If the particles are larger than that, the film will scatter light and appear white [16]. The reason to sinter the nanoporous thin film is that the particles (5-50 nanometres in diameter) get into electrical contact with one another and the conducting substrate [17]. Also, the sintering process makes the film devoid of any water molecules, which occupy the TiO_2 bonds, which could otherwise have hosted dye molecules. The presence of water in the film may have disastrous effects on the efficiency of the solar cell.

The porosity of a film measures how large a part of the volume of the sample is fluid- or gas filled. The porosity of the TiO_2 thin film is 50-60%, and it decreases with increasing pressure applied in the pressing step of the manufacturing process [17]. The porous structure of the film provides a very good contact area with the electrolyte and the dye solution during the dyeing process: The inner area of a part of the nanoporous thin film may be a thousand times as large as the two-dimensional area it covers [16]. In the dyeing process the whole film inner surface is impregnated with the dye. The cavities in between the particles are filled with the electrolyte in the solar cell, and the porous structure exhibits an advantage in the electron transfer, because of this immense contact area. The electrolyte, by nature a matrix in electrical contact with each part of itself, permeate the solid nanocrystalline TiO_2, which also is a continuous network, electrically in contact with all its parts (because of the sintering process, as mentioned above). In this favourable environment, electrons are easily transferred from the electrolyte to the titanium dioxide via the dye. In fact, the nanoporous structure and the monolayer dye admit a very efficient charge transfer from the electrolyte to the titanium dioxide. The key is that this electron transfer from the dye to the semiconductor is so much faster than the charge transfer constituting the recombination (which is otherwise, in solar cells not based on dye sensitised nanocrystalline structures, a main reason for loss of efficiency). The electron separation in the interpenetrating electrolyte-titanium dioxide-junction is readily measured in femtoseconds, whereas the time of the recombination process rarely gets faster than 10-100 ps [18], [19].

2.1.2 The Mechanism of the Solar Cell

When an incident photon is absorbed by a solar cell of this type it is a molecule of the dye that actually absorbs it, exciting an electron from a lower orbital or energy level to a higher. This higher level has to be slightly higher than the conduction band of the titanium dioxide so that the easiest path for the electron is to fall down to the conduction band and not back to the lower energy level of the dye in which case no energy can be gained. The latter is called recombination. The advantageous alternative process, when the electron is transferred from the dye to the semiconductor, is called injection. It is a part of the so-called separation: the electron and its corresponding vacancy are separated from each other [15] - a critical moment for avoiding recombination. The electron is transported from the dye through the nanoporous structure of the titanium dioxide to the back contact, inducing a current on its way to the counter electrode and there re-entering the cell via the red-ox-couple in the electrolyte. The red-ox-potential of the electrolyte has to be slightly higher than the lower energy level in the dye from which it was once excited and to which it will now return, waiting for a new photon to excite it to a higher energy level, see figure 5. The cycle can also be described in the opposite direction: when the electron is excited it leaves a vacancy that will be filled with an electron from the electrolyte. The positive charge wanders the same path as the electron but in the opposite direction.

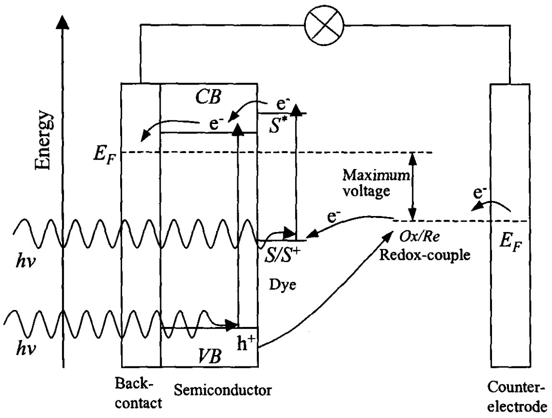

Figure 5: The mechanism of the solar cell. From [4].

It is crucial that the relationships between the energy levels in the cell are optimal. In general the excited electron always seeks to reach a lower energy level in small steps. Only if it can find a favourable path back to its lower original level a part of the voltage difference can be used to produce a current.

This description of the solar cell function also points at the importance of stability of the dye so that this cycle can occur again and again. The stability of dyes was however not considered in this investigation.

2.2 The Physics Behind the Colours

2.2.1 Atomic and Molecular Orbital Theory

The Schrödinger wave equation (1) describes the relationship between the energy and position of a particle, such as the electron, when it is regarded as a wave-motion rather than a solid particle. The Schrödinger wave equation in Cartesian coordinates [20]:

$$(\partial^2\Psi/\partial x^2) + (\partial^2\Psi/\partial y^2) + (\partial^2\Psi/\partial z^2) + ((8\pi^2 m_e)/h^2)[E - V(x, y, z)]\Psi(x, y, z) = 0 \tag{1}$$

where m_e is the electron mass, h is Planck's constant [21], E the total quantized energy of the atomic system and V the potential energy at point (x, y, z). Ψ is the wave function, a mathematical description of the electrons wave-motion [20].

Each solution to the equation (1) is associated with a wave function or atomic orbital. As for any wave function the only possible states are at the resonance frequencies. For each particle state there are so-called quantum numbers defined: n, l and m_l. Together they describe the specific particle state in question. The Schrödinger equation can only be solved when the quantum numbers n, l and m_l are integers. The total energy of the particle is the sum of those quantum numbers thus the energy is quantised. The allowed energy levels correspond to the orbits quantised according to Bohr's theory [22].

The wave function Ψ can be written as a product of three functions, one for each dimension [22]:

$$\Psi(x, y, z) = \Psi_x(x)\Psi_y(y)\Psi_z(z) \tag{2}$$

or in spherical coordinates [22]:

$$\Psi_{n,l,m}(r, \theta, \phi) = R_{n,l}(r)\Theta_{l,m}(\theta)\Phi_{m_l}(\phi) \tag{3}$$

where the quantum numbers n, l and m_l charachterise the orbital. The quantum number n is a positive integer (1, 2, 3...) representing the orbital's distance from the nucleus. l, ranging from 0 to n-1, is related to the shape of the orbital and m_l, ranging from -l through 0 to +l, corresponds to the spatial orientation of the orbital. When $l = 0$ the orbital is a spherical s-orbital (denoted 1s, 2s...) and when $l = 1$ the orbital is a two-lobed p-orbital with one of three possible orientations (denoted 2px, 2py, 2pz, 3px, 3py...). The shapes of orbitals with higher l are more complicated. Each orbital can host two electrons of opposite magnetic spin [20].

The orbitals of molecules are more complex than those of atoms but based on the same theory. The chemical bond in molecules, the covalent bond, occurs when atoms share electrons. The molecular orbitals are mathematical combinations of the electron orbitals of the atoms that the molecule consists of [20]. Hybridization is also a mathematical combination of orbitals but within an atom. This theory explains how the shapes of molecules arise. In a single bond in an organic compound the 2s-orbital and the three 2p-orbitals of a carbon atom are combined to four tetraedically oriented sp3-hybridization orbitals overlapping the valence orbitals of other atoms giving an explanation of the tetraedical orientation of a carbon atom's bond sites [20].

In the carbon-carbon double bond the 2s-orbit and two of the three 2p-orbitals of a carbon atom are combined in sp2-hybridization to three planar oriented orbitals, in this example effectively overlapping the 1s-orbitals of hydrogen atoms or the sp2-hybridiztion of another carbon atom, forming σ-bonds. The remaining 2p-orbitals are combined to a bonding π-bond as described in figure 6 [20]. When two orbitals are added, the result is a bonding molecular orbital with total lower energy than the orbitals added. When the same two orbitals are subtracted the result is a non-bonding molecular orbital with total higher energy and with a node between the nuclei. Figure 7 shows two cases of this. When the orbitals are lying along the internuclear axis and overlapping end to end a σ-bond is formed and when they are perpendicular to the internuclear axis and overlap side-to-side a π-bond is formed [20].

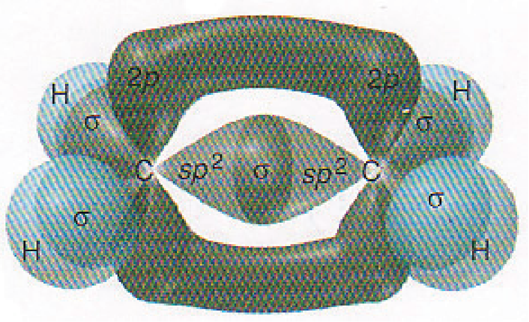

Figure 6: The bonding π-bond of the carbon-carbon double bond. From [20].

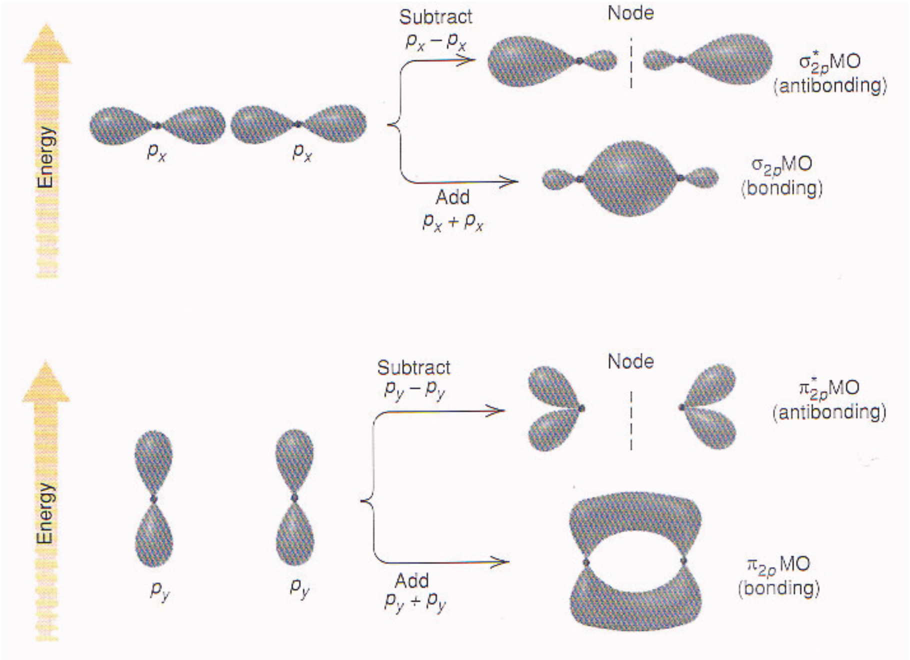

Figure 7: Non-bonding molecular orbitals of the carbon-carbon double bond. From [20].

In the case of conjugated double bonds, as in the aromatic compound benzene in figure 8, the bonding π-orbitals of the adjacent bonds are joined and the electrons in those orbitals are highly delocalised. This gives molecules with conjugated double bonds ability to absorb light of several different wavelengths. In the case of a larger molecule with a molecular group absorbing light at a specific frequency that group is denoted a chromophore.

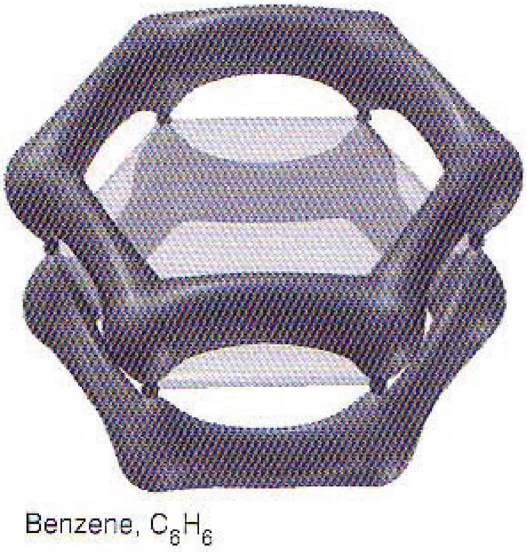

Figure 8: Benzene, an aromatic carbon compound and an example of a molecule with conjugated double bonds. From [20].

2.2.2 Molecule-Light Interaction

An electron can be excited from one energy level or orbital to another if it for example absorbs a photon. The energy difference between the energy level the electron is excited from and the one it is excited to must correspond exactly to the energy of the photon. The energy, ε, of a photon is correlated to its wavelength, λ, by the equation

$$\varepsilon = hc/\lambda, \tag{4}$$

where c is the speed of light in vacuum and h is Planck's constant. The absorption of light by a molecule can only occur at the specific wavelengths corresponding to the possible transitions in that molecule.

Most transitions in nature occur between the Highest Occupied Molecular Orbit (HOMO) and the Lowest Unoccupied Molecular Orbit (LUMO) in a molecule [23], which corresponds to the smallest energy quanta possible to absorb by that molecule. A complex molecule such as a dye has a distribution of electronic states in the HOMO and the LUMO. Thus a number of wavelengths defining the absorption spectra of that molecule can be absorbed.

2.2.3 Colours

What the human eye perceive as the colour of a dye is the combination of the wavelengths not absorbed but reflected. Figure 9 shows an example of two different absorption spectra, both perceived as the very same nuance by the human eye [24].

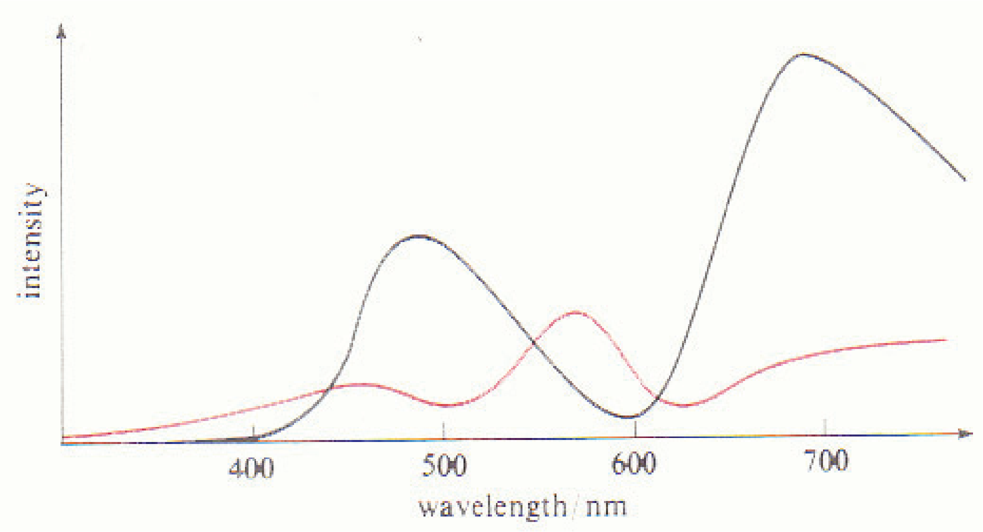

Figure 9: Two different absorption spectra, both perceived as the very same nuance by the human eye. From [24].

The light absorbed by the chromophore of a dye is of the complementary colour of the apparent colour of the dye. Chlorophyll, for example, absorbs mostly blue and red, reflecting green, and anthocyanins absorbs blue and green, giving us the perception of a red or violet colour. Table 1 gives the relationship between absorbed light and reflected (or transmitted) light for part of the visible spectrum.

The sunlight spectra contains much energy in the blue-green area which is the reason why the search for solar cell dyes is focused on green-absorbing red and purple dyes such as anthocyanins and betanins as well as the ruthenium dye.

Table 1: The relationship between absorbed and complementary colour (perceived) in the visible spectrum [25].

Absorbed wavelengths/nm	Absorbed colour	Complementary colour
380-420	Violet	Green-yellow
420-440	Violet-blue	Yellow
440-470	Blue	Orange
470-500	Blue-Green	Red
500-520	Green	Purple
520-550	Yellow-green	Violet
550-580	Yellow	Violet-blue
580-620	Orange	Blue
620-680	Red	Blue-green
680-780	Purple	Green

2.3 Pigments - Anthocyanins, Anthocyanidins, Betanins and Ruthenium

2.3.1 Structures and Chromophores of Anthocyanins and Anthocyanidins

Anthocyanidins is a subgroup of the flavonoids, polyphenolic compounds possessing 15 carbon atoms: two benzene rings joined by a linear three-carbon chain [26]. Anthocyanidins are aglycons of corresponding anthocyanins, which are weak acids and occur naturally in a great many plants. The colours of anthocyanins are typically red, blue, violet, orange and pink (in fact all colours except from green have been recorded) [27]. Chromophores of anthocyanins absorb different parts of the visible and ultraviolet spectrum, depending not only on the type of anthocyanin, but also on the type of sugar attached, where on the carbon skeleton this sugar is attached, pH, complexes formed with metal cations and the presence of colourless flavonoids. The sugar attached to the carbon frame characteristic for all anthocyanins, $C_6C_3C_6$, see figures 10 and 11, is most often a monosaccharide, such as glucose, rhamnose and xylose, but disaccharides and trisaccharides are not unusual. Figure 10 shows an example of an anthocyanin, the violet cyanidine-3,5-diglukoside [28]. Close to 300 different anthocyanins have been discovered [29], and they are further classified in subgroups, for example pelargonin, cyanin, delphinin, malvin and petunin, which are all glucosidic anthocyanins, and the corresponding aglycons are pelargonidine, cyanidine (which is the most common one), delphynidine, malvidine and petunidine. The six most common anthocyanidins share the 3,5,7,4'-tetrahydroxyflavylium structure [30], see figure 11.

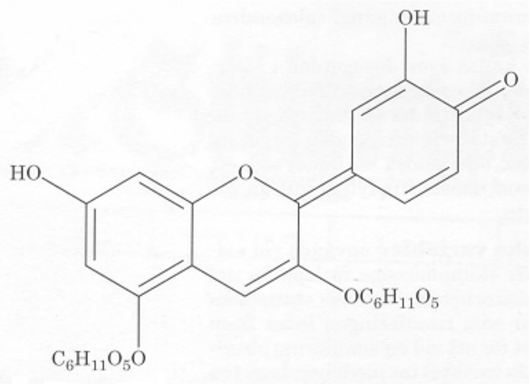

Figure 10: The violet cyanidine-3,5-diglukoside. From [28].

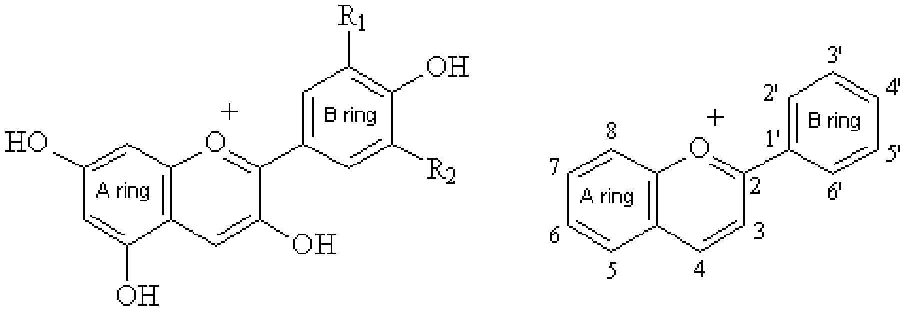

3,5,7,4'-tetrahydroxyflavylium

Structure common to many anthocyanidins

Figure 11: The 3,5,7,4'-tetrahydroxyflavylium structure, common to the six most frequently occurring anthocyanidins. From [30].

Anthocyanins are water-soluble and found in vacuoles in plant cells of angiosperm families (flowering plants). Red onion contains a large number of anthocyanins, among others cyanin, as do red cabbage. The anthocyanins can be used as pH-indicators, as many of them change colour depending on the pH of their surroundings. One example is an anthocyanin taking on a mauve-pink colour when the plant grows in acid soil, and blue colour in alkaline soil [31]. Also, it is the same anthocyanin, cyanin, which is the pigment of both roses and cornflower. In this case it is the alkali metal potassium, which in the cornflower forms a complex with the cyanin that gives rise to the blue colour. Generally, anthocyanins adapt to changes in acidity (or alkalinity) according to this outline: In acidic environments the chromophore[3] of anthocyanins is an aromatic flavylium (2-phenylchromenylium) cation, red in colour. In a more basic surrounding the double bond of the flavylium cation is disrupted by a water molecule, and the result is a colourless structure. This structure can regain colour under even more alkaline ambient conditions, since dehydroxylation restores a conjugated double bond in the anthocyanin structure. The key to this behaviour lies in the conjugated double bonds.

Conjugated double bonds make possible the absorption of photons of lower energy (and longer wavelengths) in the visible spectrum, i.e., with conjugated double bonds lower photon-energies are required to excite electrons. The more extensive the system of conjugated double bonds, the lower energies can be accepted for excitation. When a hydroxide is inserted into the structure, a double bond is broken and now the photon-energy required to excite an electron is higher than it was before the introduction of the hydroxide, so the absorption is pushed towards (and into) the ultraviolet. Conversely, removal of a hydroxide can restore double bonds and again lower the adequate excitation energy and bring the absorption back to visible regions [32]. An anthocyanin subject to traversing the pH scale from acid to alkaline environments, undergoes this very described procedure. The possible excitation energies allowed by the double bonds of the acid form of the anthocyanin do not coincide with the dittos of the basic form of the anthocyanin and that is the reason the colours of the different forms are not the same. Figure 12 shows the change in molecular structure and colour for cyanin for different pH-values.

---

[3] More on chromophores can be read in section 2.2.3.

Anthocyanins are not very stable in alkaline environments, or in environments with a high sugar concentration [29]. They are also heat-, oxygen- and light-sensitive.

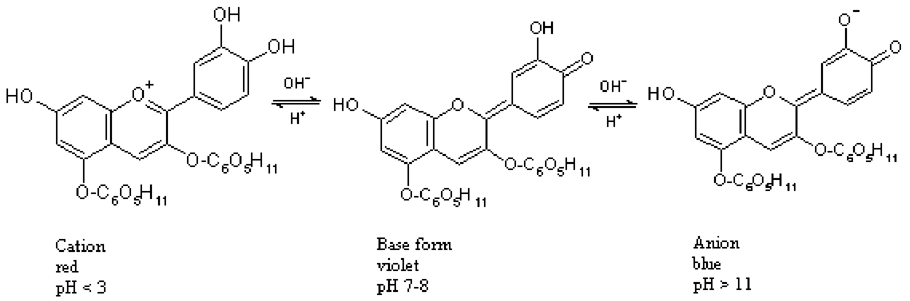

Figure 12: The molecular structure and thus colour of cyanin depends on pH. From [30].

2.3.2 Functions and Areas of Use of Anthocyanins

Anthocyanins have a number of purposes in the plants. They play a key role in the process of pollination. They attract insects with vivid colours, not only those visible to humans, and they can even be switched on and off: when they no longer are needed to attract pollinators to flowers they may get degraded by plant enzymes [27]. Anthocyanin-related pigments serve as UV screens and protects the plant's DNA from damage by sunlight. Also, anthocyanins serve as anti-feedents, their disagreeable taste serving to deter animals feeding on that plant.

In the food industry anthocyanins are used as colourants, and they share the E number E163. Anthocyanins used for food colouring are extracted mainly from the waste products from vinification of red wine [33]. Scientists working for the Agricultural Research Service (ARS), the chief scientific research agency of the U.S. Department of Agriculture, have documented the anti-oxidant and anti-inflammatory properties of anthocyanins [34]. Furthermore, the abilities of anthocyanins to inhibit LDL cholesterol and render dangerous carcinogens harmless, are also known [34], [29].

2.3.3 Betalains, Betacyanins and Betanins

The Eurasian biennial plant Beta vulgaris, the common beetroot, of the family Chenopodiaceae, is the most important source of betanin, a red-purple pigment, used as a colouring agent in food (the E number of betanin is E162). Betanin (figure 13(a)), makes up 75-95% of the total red colouring matter of the beetroot [35], [36]. It is a type of betacyanin, which is a larger group of red-violet pigments, and betacyanins are in turn part of a larger group of pigments, known as betalains. Betalains are water-soluble nitrogen-containing alkaloid pigments [37], which are found in vacuoles of cells of families of plants belonging to the order Caryophyllales. Only in this order, and in no other order of plants, betalains are found. Also in some fungi e.g. Fly Agaric, betalains exist. A finding, which so far remains unexplained, is why plants containing betalains appear to be void of anthocyanins [38] and vice versa. The two pigment groups seem to perfectly exclude each other in the paths of evolution [37]. Betalains are subdivided into red betacyanins and yellow betaxanthins - the yellow pigment can be found in golden beets, but also in beetroot, in the form of vulgaxanthins. Vulgaxanthine-I provides around 95% of the yellow colour of beetroot [36]. Betaxanthins are conjugation products of betalamic acid with different amino acids or amines [39]. Betacyanins are immonium conjugates of betalamic acid with cyclo-DOPA (dihydroxyphenylalanine) [37]. Betalamic acid (figure 13(c)) is the chromophore of all betalains, and depending on in which molecule it is found it gives rise to different colours. In betaxanthins it renders the molecule yellow, and in betacyanins it effects red and violet colours, (see figure 13(d)). Betanidin (figure 13(b)) is the aglycone of most betacyanins. In situ, betacyanins are most often glycosides of betanidin or its C-15 isomer.

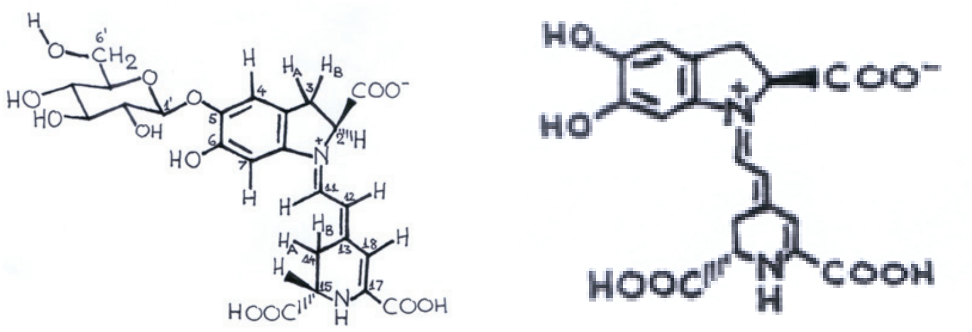

(a) Betanin, the 5-O-β-glucoside of betanidin.

(b) Betanidin.

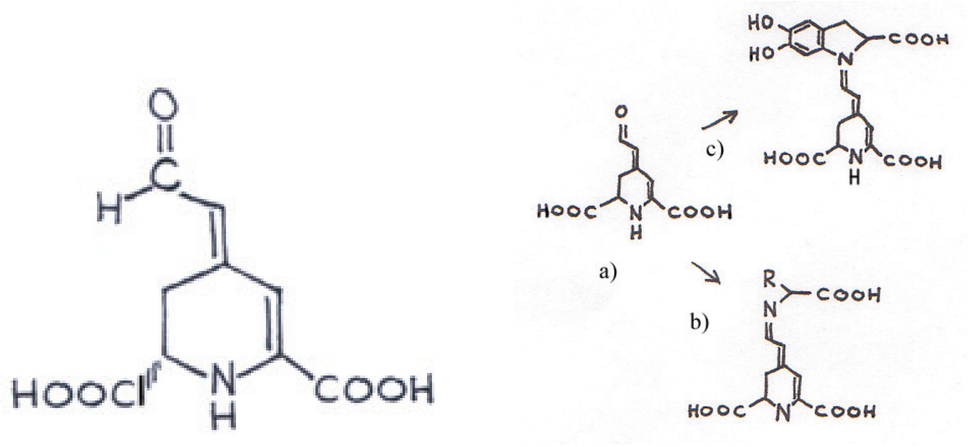

(c) Betalamic acid.

(d) The pigment chromophores a) betalamic acid, b) betaxathin, c) betacyanin.

Figure 13: Molecular structures of betanin and derivatives.

Betanin exists in different varieties. Some of these are: Phyllocactin, 2'-Apiosyl- phyllocactin, 2'-(5"-O-E-Feruloylapiosyl)-betanin and hylocerenin [37]. Betanin is generally unstable when exposed to heat, light and oxygen, all of which have a degrading (and cumulative) effect on betanin. Generally, betanins are stable in slightly acidic environments (between pH 4.0 and 7.0), a fact that is exploited by the food industry in the use of betanin as a colouring additive. At a neutral pH, heating in the presence of air causes breakdown to brown compounds. The temperature sensitivity of betacyanins is illustrated by the following observations: Half-life at 25 °C is 413.6 minutes versus 83.5 minutes at 60 °C [35]. Betacyanins are known to have antioxidant and radical scavenging activities, which could help counteract the onset of degenerative diseases in human [37].

2.3.4 The Absorption Spectra of Betanin

Betacyanins have visible spectra with maxima in the 535-550 nm ranges, and the exact absorption spectrum is dependent on pH and temperature. Figure 14 shows different absorption spectra of betanin at two different pH-values, one acid and one alkaline. The absorbance (see equation (32)) is plotted against wavelength for pH 3.5 and 8.5 respectively. Six of the samples have been treated at different temperatures for 4 hours, and the seventh curve is from a newly extracted sample that was not treated at all. As can be seen, the absorbance maximum of betanin is slightly shifted towards greater wavelengths in a more basic environment [35], [40]. In strongly acid and alkaline environments, degradation of betanin occurs to a larger extent than in slightly acid surroundings [35], but at high temperatures degradation is strong whatever the pH is [40].

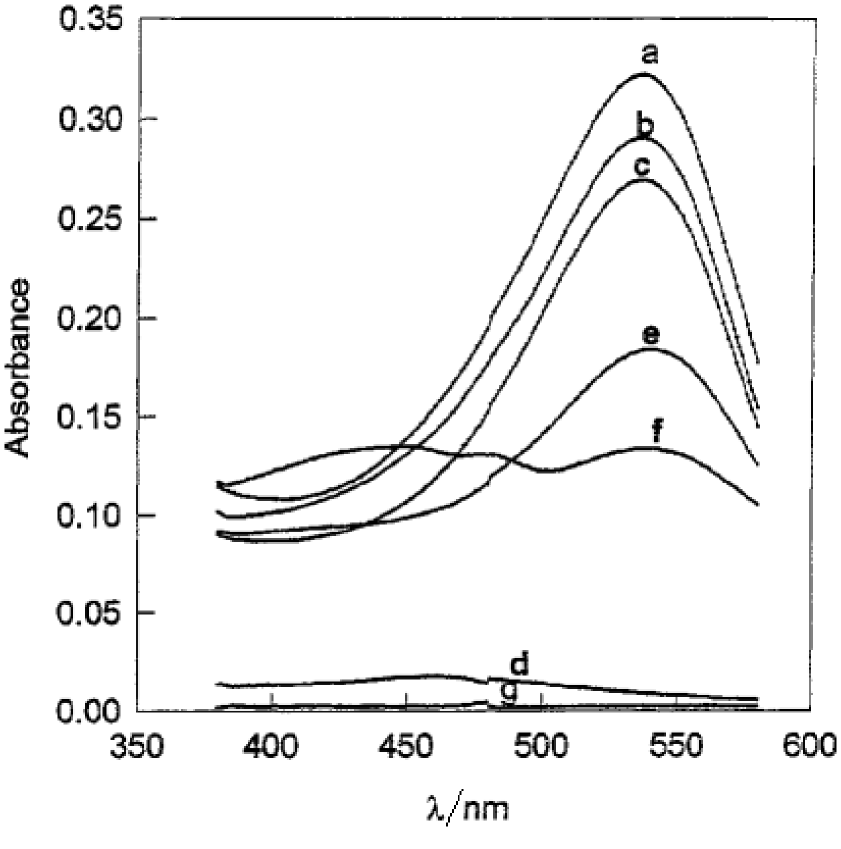

Figure 14: The absorbance of betanin is pH- and temperature-dependent. Visible spectra of betanin: (a) not treated at all, compared to specimens treated for 240 minutes: (b) treated at pH 3.5, 25 °C, (c) pH 3.5, 50 °C and (d) pH 3.5, 75 °C, (e) treated at pH 8.5, 25 °C, (f) pH 8.5, 50 °C and (g) pH 8.5, 75 °C. From [40].

2.3.5 Physical and Chemical Properties of Ruthenium and Areas of Use

The name ruthenium comes from the Latin word Ruthenia meaning "Russia". Pure ruthenium is a hard, silvery-white metal of the platinum group (which consists of platinum, palladium, iridium, rhodium, osmium and ruthenium) [41]. Ruthenium, atomic number 44, belongs to group 8, period 5 of the periodic table of elements. It is rarely used in pure form because of its being extremely difficult to work. It remains hard and brittle even at temperatures as high as 1500 °C. Under normal circumstances, ruthenium does not react with air, water, HNO_3 or HCl. On heating with oxygen, ruthenium yields ruthenium (IV) oxide, RuO_2. Ruthenium tetroxide, RuO_4, is highly toxic and in addition explosive, as is osmium tetroxide (osmium is immediately below ruthenium in the periodic table) [42], [14]. Generally, ruthenium compounds bear a remarkable resemblance to cadmium compounds (Cd, which is also in period 5). Ruthenium comes in four crystal modifications and twelve isotopes, of which five are radioisotopes. The radioactive isotopes have half-lives ranging from 1.64 hours (95-Ru) to one thousand and twenty years (106-Ru). This last-mentioned most stable radioisotope is since the 1960s used to cure eye tumours (retinoblastomas and melanomas) [43]. Ruthenium is one of the most effective hardeners of palladium and platinum; therefore it is used in the jewellery and electronics industries, to impart hardness in jewellery alloys and to improve resistance to abrasion in electrical contact surfaces [44]. Other important applications within electronics are for use in resistors and in computer hard discs to increase the density at which data is stored. The element's resistance to corrosion is conspicuous: By adding 0.1% of ruthenium to titanium, resistance to corrosion is improved by a factor of 100. Furthermore, ruthenium has good catalytic properties and is used as a catalyser in a large number of industrial applications, for example in the petroleum industry, for obtaining sulphur-free, high-quality fuels. At least eight oxidation states have been found, of which the most common are +2, +3 and +4. In the ruthenium complex-based dyes, used for dying semiconductor photoelectrodes of solar cells, the most common oxidation state of ruthenium is +2, see below. The ground state electron configuration of ruthenium is $[Kr]4d^7 5s^1$ and its term symbol is $^5F_5$. The atomic weight is 101.07 u and its density (at 293 K) is 12.2 g/cm^3.

2.3.6 Abundance of Ruthenium

Ruthenium is mined from ores together with other members of the platinum group in the Ural Mountains and in South and North America, in a nickel-mining region in Ontario, and in pyroxidine deposits in South Africa [42]. Table 2 expresses the abundance of ruthenium in the universe and on earth in terms of parts per billions (ppb), both with respect to weight and with respect to atoms.

Table 2: Abundance of ruthenium.

	ppb by weight	ppb by atoms
Abundance in the universe	4.0	0.05
Abundance in the earth's crust	1.0	0.2
Abundance in seawater	0.0007	0.000043

2.3.7 Ruthenium Complex Dyes for Solar Cell Applications

Of the ruthenium complex-based dyes, a few have become known to have an excellent impact on the efficiency of the solar cells. One of the more noteworthy is Ruthenium 353-bisTBA with the chemical name cis-bis(isothiocyanato)bis(2,2'-bipyridyl-4,4'-dicarboxylato)-ruthenium(II) bis-tetrabutylammonium and the chemical formula $C_{58}H_{86}O_8N_8S_2Ru$, formerly sold under the name N-719. Another is Ruthenium 353 with the chemical name cis-bis(isothiocyanato)bis(2,2'-bipyridyl-4,4'-dicarboxylato)-ruthenium(II) and the molecular formula $C_{26}H_{20}O_{10}N_6S_2Ru$, formerly sold under the name N3 [45]. A third of these renowned dyes is Ruthenium 620-1H3TBA with the chemical formula $C_{69}H_{117}O_6N_9S_3Ru$, formally named tris(isothiocyanato)-ruthenium(II)-2,2':6',2"-terpyridine-4,4',4"-tricarboxylic acid, tris-tetrabutylammonium salt (identical to the old products called Ruthenium 620 or N-749 or Black-Dye). These dyes (which can be seen in figures 15, 16 and 17) are all very expensive: 100 mg of the Ruthenium 620-1H3TBA dye cost $427, the same quantity of Ruthenium 353 dye cost $194, and the price for 100 mg of Ruthenium 353-bisTBA dye is $116. (These prices were provided by Solaronix, a Swiss shareholder company specialising in dye sensitised nanocrystalline titanium oxide solar cells [46].) As a comparison can be noted that the average price of platinum for the first half of June 2004 was $820 per troy oz (31.1 grams). Ruthenium 353 and Ruthenium 353-bisTBA are both dark purple powders, whereas Ruthenium 620-1H3TBA is a black to dark greenish powder. Ruthenium 353 sensitises very efficiently wide band-gap oxide semiconductors, like titanium oxide, up to a wavelength of 750 nm. Ruthenium 353-bisTBA excels over Ruthenium 353 and presents higher photo voltages by ca 50 to 100 mV in regenerative photo-electrochemical cells when compared Ruthenium 353. Ruthenium 620-1H3TBA sensitises efficiently wide band-gap oxide semiconductors, up to a wavelength of 920 nm.

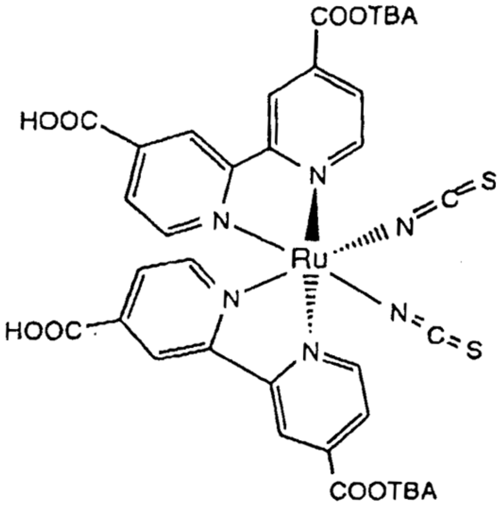

Figure 15: The molecular structure of Ruthenium 353-bisTBA, aka N-719. Provided by [47].

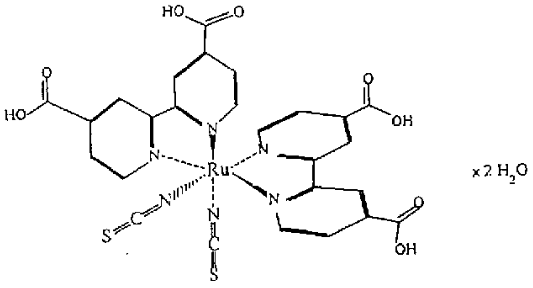

Figure 16: The molecular structure of Ruthenium 353, aka N3. Provided by [47].

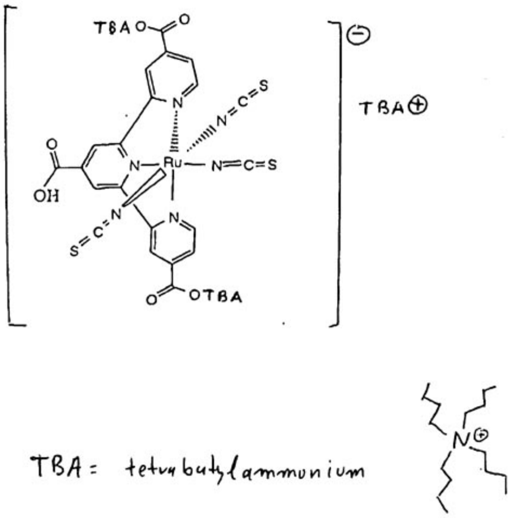

Figure 17: The molecular structure of Ruthenium 620-1H3TBA, aka N-749. Provided by [47].

2.4 The Rate of Chemical Reaction

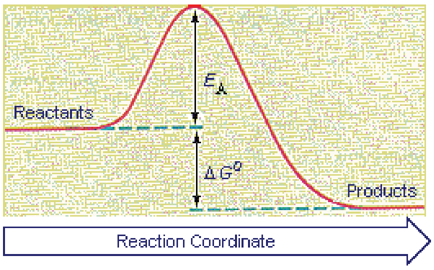

Figure 18: The energy relationship between reactants and products. From [48].

For any chemical process not occurring spontaneously, a certain amount of energy is required to be added to the system for the chemical reaction to be triggered. This energy quota is self-explainingly called the activation energy, E_A. Figure 18 illustrates the relationship: The horizontal axis represents the so-called reaction coordinates, which stand for the progress of the reaction (i.e., the reaction coordinates represent infinitesimally small changes converting the reactants into products). The vertical axis represents the relative energies of the states. The natural tendency is to always strive for as low an energy level as possible. The energy difference between the energy levels of the reactants and the products is the Gibbs Free Energy, and it does not influence the reaction rate. The activation energy is in the figure represented as a barrier, which has to be overcome in order for the chemical reaction to take place. If the energy barrier had not been there, the reaction would have occurred spontaneously, but being there, it acts as a threshold, ensuring that not all colliding reactant molecules actually undergo the reaction. Only those colliding molecules with energy equal to or exceeding the activation energy E_A will, if the molecular orientations are right, be able to perform the reaction [49]. As both the frequency of collisions and the kinetic energy of the particles increase with increasing temperature, the temperature and the activation energy are both crucial to the reaction speed of any chemical process. The fraction of collisions rendering actual reactions increases exponentially with temperature [49]. This is included in the

Arrhenius equation:

$$k = Ae^{-\frac{E_A}{RT}}. \tag{5}$$

k is the rate constant, T is the temperature, R is the universal gas constant and A, called the frequency factor, includes the determining factor of molecular orientation. Taking the natural logarithm of equation (5), a linear equation is obtained:

$$\ln(k) = -\frac{E_A}{R}\left(\frac{1}{T}\right) + \ln(A). \tag{6}$$

Most rate constants obey the Arrhenius equation [49]. Interlaced with the Arrhenius equation (5) is the rate of change of concentration of a reactant:

$$\frac{dc}{dt} = -k\,[c], \tag{7}$$

where c is the reactant concentration and t is the temporal variable. In the case of cyclic voltammetry, where the voltage is time-dependent, the concentration rate can also be considered with respect to voltage, see section 3.2.1.

The effect of the addition of platinum to the counter electrodes (see section 4.1.6) is that the activation energy barrier for the I^-/I_3^- ion pair of the electrolyte is essentially decreased to a level allowing for a much larger fraction of colliding reactant molecules to actually react. This is equivalent to a boost of the chemical reaction speed.

3 The Theory Behind the Methods used for the Characterization of the Dye Sensitised Solar Cells

3.1 Current-Voltage and IPCE Characterisation

Measurements of Current-voltage characterisation (iV) and Incident Photon-to-Current Conversion Efficiency (IPCE) were the main methods to characterise the dye sensitised solar cells.

3.1.1 Current-Voltage Characterization and Efficiency

The efficiency of the solar cell is of greatest importance, but it is not the only characteristic to be considered when the solar cell is evaluated.

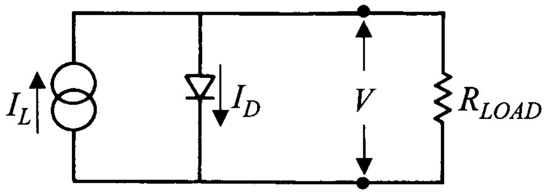

(a) The simplified equivalent circuit of a solar cell

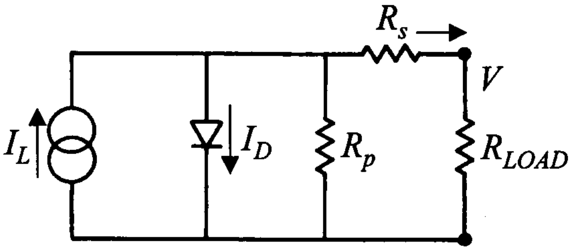

(b) Equivalent circuit for a solar cell

Figure 19: The simplified equivalent circuit of a solar cell (a) consists of a diode and a current source which are switched in parallel. The current source generates the photo current I_{Ph} or I_L, which is directly proportional to the solar irradiance. The p-n transition area of the solar cell is equivalent to a diode where I_D is the Diode current. V is the terminal voltage at the solar cell and R_{LOAD} is the external resistance. At real solar cells (b) a voltage loss on the way to the external contacts could be observed. These losses are represented by a parallel and a series resistance, R_P and R_S [50]. Pictures from [4]

To record the characteristics of photo-electrochemical (PEC) solar cells, the current density, alternatively the current, the voltage and the efficiency are measured. V denotes the voltage [V], I denotes the current [A] and i denotes the current density [A/cm^2]. The current density is the electrical current produced per unit area, and throughout this investigation the area is measured in cm^2. (In graphs, the y-axis represents either I or i). The current density and the voltage (the iV characteristics) are measured when the solar cell is connected to a simple circuit (see the equivalent circuit of the solar cell, figure 19(a)) and a spotlight, providing a known radiation, illuminates the solar cell. (The illumination should match up with one of the various internationally accepted standards. Our measurements were carried out with respect to the AM 1.5 standard, see section 3.1.3 for details.) The circuit of figure 19(a) is a simplified equivalent circuit for the solar cell, and in connection to it two conditions are considered: The short circuit condition, when there is no electrical potential difference ($V_{sc} = 0$), and the open circuit condition, when there is no current flowing ($I_{oc} = 0$).

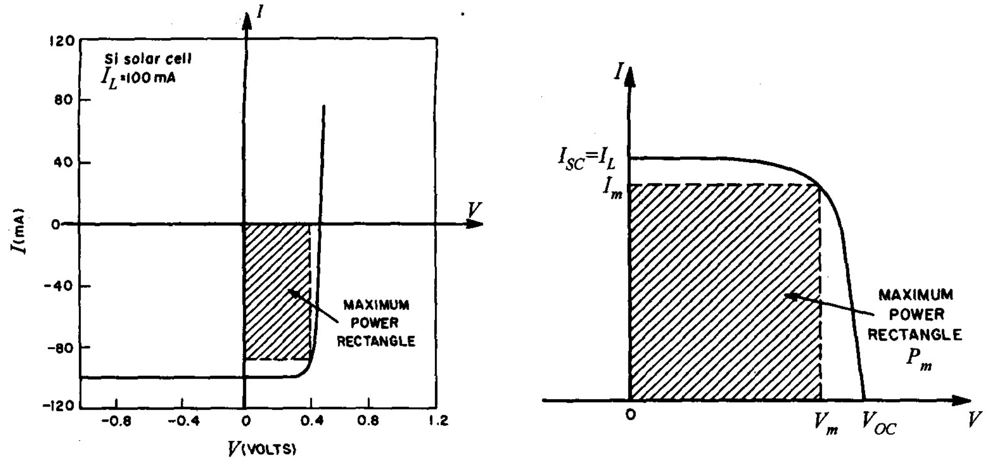

(a) (b)

Figure 20: The IV characterization gives the efficiency of the solar cell. (a) The IV graph as a whole. (b) The efficiency quadrant flipped over. Useful information is provided by the so-called maximum power rectangle. From [4].

The efficiency can be calculated from the iV characteristics by the relation

$$\eta = i_m V_m / P_{in} = \mathrm{FF} \cdot (i_{sc} V_{oc})/P_{in} \tag{8}$$

where, V_{oc} is the open circuit voltage, i_{sc} is the short circuit current density, P_{in} is the power of the incident radiation, i_m is the current density obtained for the maximum power, V_m is the voltage obtained for the maximum power and FF is the fill factor

$$\mathrm{FF} = i_m V_m / (i_{sc} V_{oc}). \tag{9}$$

The product $i_m V_m$ is called the maximum power rectangle (per unit area), see figure 20. If both the current density [A/cm^2] and the corresponding power density [W/cm^2] of a solar cell are plotted in the same graph, the justification of the maximum power rectangle concept can be observed: the maximum power is obtained for the voltage value where the maximum power rectangle has its vertex. One example of this can be seen in figure 21: the data is from one of the solar cells manufactured in this study.

The above formulas are all based on calculations for an ideal solar cell. Realistic solar cells suffer from losses such as relaxation processes of excited electrons and radiative recombination [4]. The equivalent circuit corresponding to a realistic solar cell is similar to figure 19(a), but made complete by added resistances (a parallel so-called shunt and a series resistance), see figure 19(b).

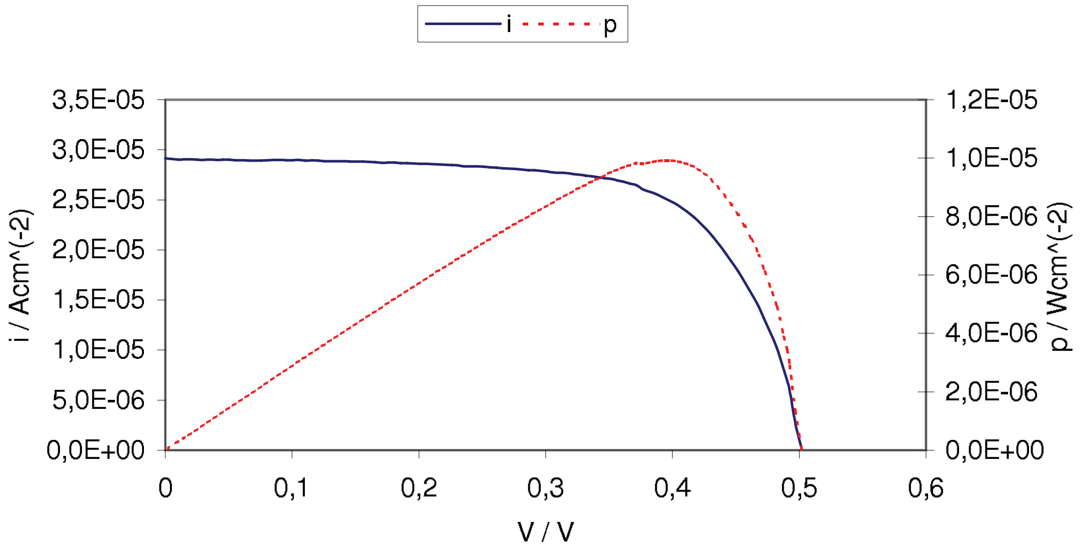

Figure 21: The maximum power rectangle has its vertex at the voltage where the maximum power density occurs. The data originates from a solar cell sensitised with a beetroot-in-methanol dye and pressed at 1500 kg/cm^2.

3.1.2 IPCE, the Incident Photon-to-Current Conversion Efficiency

Incident photon-to-current conversion efficiency, IPCE, is a quotient of the number of outgoing electrons (generated by the photovoltaic effect, justifying the use of the word photocurrent) to the number of photons incident in the system [4]. The photocurrent density is measured in short circuit mode (no bias applied). The flux of incident photons, $\Gamma(\lambda)$, which is a function of wavelength [4] and is measured in photons per square centimetre and second, is also measured, and the ratio of the flux of electrons to the flux of photons is formed. This ratio is the IPCE:

$$\mathrm{IPCE} = \eta(\lambda) = (i_{ph}/q)/(\Gamma(\lambda)) \tag{10}$$

where i_{ph} is the photocurrent density for a given wavelength, q is the elementary charge and $\Gamma(\lambda)$ is the photon flux. The IPCE is wavelength-dependent, and each wavelength is assigned its own IPCE value. This is a monochromatic aspect of the IPCE measurement: each wavelength is investigated separately and the interval of investigation is narrow, almost monochromatic. A crucial thing in the device set-up is that the short circuit current is directly proportional to the light intensity [51].

The photon flux $\Gamma(\lambda)$ can be expressed in terms of optical power P, using h for Planck's constant and ν for the frequency corresponding to wavelength λ:

$$\Gamma(\lambda) = P/(h\nu). \tag{11}$$

Utilizing the familiar frequency-wavelength relation

$$\nu = c/\lambda, \tag{12}$$

where c is the speed of light in vacuum, the IPCE quotient can be re-written as

$$\eta(\lambda) = (i_{ph}/q)/(P\lambda/hc). \tag{13}$$

Inserting numerical values for c, h and q and using SI-units only, the following expression is obtained:

$$\eta(\lambda) = 1240 \cdot 10^{-9} i_{ph}/(P\lambda). \tag{14}$$

A more common expression for the IPCE is obtained when allowing for λ to be expressed in units of nanometres:

$$\eta(\lambda) = 1240 i_{ph}/(P\lambda). \tag{15}$$

3.1.3 Atmospheric Influences and the Solar Radiation

Of great importance is to get good estimates of the incident photon-to-current conversion efficiency and efficiency of the solar cell when it is in operation. This efficiency is dependent on absorption effects and the distance the photons have to travel through the atmosphere. The amount of air the photons have to travel through varies with the angle; the photons travel through different so-called air masses. The air mass definition (AM) is the ratio of the optical thickness of the path the photons travel through the atmosphere to the optical thickness of the path the photons would have travelled through the atmosphere, had the sun been in zenith. Following [4] and letting θ denote the angle between the actual path taken through the atmosphere and the zenith direction, and letting $0< \theta <70$, then

$$\text{AM} = \sec\theta = 1/\cos\theta. \tag{16}$$

The sun is approximated by a black body radiator, supplying the earth with an almost constant amount of electromagnetic radiation per time unit. That is, in space the solar radiation is practically constant (but varies with a couple of thousandths over a few years [4]); on earth it varies with the latitude as well as with the time of day and year and weather. However, neglecting these variations and also absorption effects in the atmosphere caused by water vapour, carbon dioxide and ozone, the radiation power from the sun is 1367 W/m^2 [21]. (The numerical value of this so-called solar constant, denoted AM0, may however vary, depending on source of information.) The standard air mass condition for calculating efficiencies for solar cell applications on earth is AM1.5, corresponding to θ (the angle between the actual path and the zenith direction) = 48.28. This air mass condition dictates that when testing for efficiency, the light intensity should be 1000W/m^2 = 100 mW/cm^2, and this is considered in the design of the iV apparatus set-up.

3.2 Other Methods of Characterisation

To characterize both the cells and the dyes a few additional methods were used as complements to the iV and IPCE measurements of the photoelectrochemical cells. The cyclic voltammetry, the thin-layer chromatography and the spectrophotometry were used to obtain information about a dye in liquid form; its electrochemichal properties, if the dye is separable into several compounds and the dyes absorbtionspectra respectively. The X-ray-diffraction was used to investigate the crystal structure of unsensitised, solid, TiO_2 substrate and the integrating sphere to obtain absorbtionspectra for unsensitised as well as sensitised (dyed) subrates, the latter to compare with the obtained absorbtionspectra for same dye in liquid form.

3.2.1 Cyclic Voltammetry

Certain electrochemical characteristics of a system are obtainable through a method called linear potential sweep chronoamperometry or linear sweep voltammetry, LSV. (The name cyclic voltammetry is justified below.) It produces an electrochemical spectrum, indicating potentials at which processes occur. For example, one can investigate whether a redox reaction is reversible or not [52] and what the standard potential of a species is.

During voltage-scanning experiments it is a disadvantage if the electrodes are polarisable, that is, if the potential over the electrodes change when a current passed through them. The calomel electrode (the saturated calomel electrode, the SCE) is a reference electrode assembled from mercury and calomel:

$$\mathrm{Hg/Hg_2Cl_2/KCl}\ \text{(saturated in water)}$$

Calomel is an alternative name of mercurous chloride, or mercury (I) chloride (Hg_2Cl_2), which is a high-density, white and soft halide mineral [53]. The SCE is often employed in equilibrium electrochemical measurements on account of its being notably non-polarisable. The calomel electrode is equipped with a porous glass tip, designed for maintaining an electric potential without letting ions from the electrolyte diffuse into the electrode and vice versa.

The reference electrode serves as a benchmark – the potential of the working electrode is monitored with respect to the reference electrode. At sufficiently negative working electrode potentials, when the energies of the electrons are high enough to make the electrons occupy vacancies in the electrolyte, a reduction current is formed from the electrode into the electrolyte. Conversely, at positive enough potentials, a current from the electrolyte to the electrode is formed, called an oxidation current. The crucial potentials at which these currents arise are linked to the standard (electrode) potential, E^0, of a chemical species, and it is the standard reaction Gibbs energy expressed as a potential [54]. The potential of the saturated calomel electrode versus the standard hydrogen electrode (abbreviated SHE) is 0.242 V [55]. The standard hydrogen electrode, or the normal hydrogen electrode (NHE), with constituents at unit activity [55]:

$$\mathrm{Pt/H_2}(a = 1,\ \mathrm{g})/\mathrm{H}^+(a = 1,\ \mathrm{aq}),$$

is internationally accepted as a primary reference, and it has $E^0 = 0$ V. Another commonly used reference electrode is the silver/silver chloride electrode, $Ag/AgCl/Cl^-$. This electrode was used as the reference electrode in the cyclic voltammetry experiment presented in 4.3.1, and its standard potential versus the SHE is 0.2223 V [55].

The idea behind cyclic voltammetry is to study the interdependent relationship between current and time-dependent voltage for a specific redox couple present in an electrochemical cell. The results are recorded and depicted in a current-voltage or current-time graph, called a voltammogram (and the curve itself is called the response curve). Depending on the kinetics of the redox couple, the voltammogram will take on certain characteristics. The electrode potential is varied linearly with time, and as a response the current will vary, as will the concentration of the species close to the electrodes, where the reduction (at the cathode) and the oxidation (at the anode) take place. According to the electrical double layer model the solvated ions closest to the electrode, the specifically adsorbed ions, make up the innermost electrical layer, called the inner Helmholtz plane (IHP), and the solvated, non-specifically adsorbed ions just outside that layer constitute the outer Helmholtz plane (OHP). The OHP will experience a potential change as the concentrations of the anions and the cations respectively change, (see equation (20) below). The OHP marks the beginning of a three-dimensional layer named the diffuse layer. The thickness of the diffuse layer is, for concentrations exceeding 10^{-2} M, often less than 300 Å [55]. The electrical double layer remains unaffected by stirring and convection.

If the potential at the outset is positive of the potential "threshold for reduction", E^0, the initial current will be zero, and when the potential is closing in on E^0, reduction commences and a measurable current emerges. (E^0 is, as mentioned above, also called the standard electrode potential, and it is the potential of an electrode as compared to the standard hydrogen electrode [54].) As the potential drops further, reduction processes occur to a larger extent, and as a consequence the surface concentration of the cation decreases. The lowering of the concentration gives rise to an increase of the flux of the cation to the electrode surface, and thereby the current increases as well. The cation concentration reaches a minimum as the cation flow and the current reach their maxima. Depletion causes the current to decrease as the potential grows even more negative, and if now the potential scan is reversed, the system will follow a development which produces a current-voltage (or current-time) curve similar to the original current-voltage (or current-time) curve but inversed and with its starting point being the finishing point of the original curve and vice versa, see figure 44 on page 53, [55]. The coincidence of the starting and finishing points renders a closed curve and justifies the name cyclic voltammetry. The reversibility of the redox reaction decides the shape of the resulting voltammogram: Reversible processes give rise to symmetrical voltammograms and irreversible processes yield unsymmetrical voltammograms. The formulae describing the above-explained current-potential relations for a case where the redox couple is of the type M^{z+}, M, are briefly summoned as follows [54]:

Under zero-current conditions, the electrode potential is expressed by the Nernst equation:

$$E = E^0 + \left(\frac{RT}{zF}\right) \ln a, \tag{17}$$

with R being the molar gas constant, a the ion activity of the ions in the solution, F the Faraday constant and T the temperature. This can be expressed in a way more directly related to the ion concentration, using the coefficient of activity, $\gamma = (a/c)$, for a concentration c of the solution:

$$E^{\theta} = E^0 + (RT/zF) \ln \gamma, \tag{18}$$

where E^{θ} is the so-called formal potential of the electrode [54], and the electrode potential is

$$E = E^{\theta} + \left(\frac{RT}{zF}\right) \ln c. \tag{19}$$

Under current-producing conditions the potential at the outer Helmholtz plane is changed to

$$E' = E^{\theta} + \left(\frac{RT}{zF}\right) \ln c'. \tag{20}$$

The difference between the zero-current potential and the working value E' is the overpotential (here it may be called the concentration overpotential, since change of concentration is the reason for its arising):

$$\eta = E' - E = \left(\frac{RT}{zF}\right) \ln\left(\frac{c'}{c}\right). \tag{21}$$

Now, the bulk concentration in the solution is still c, so the concentration differs at the electrode surface as compared to the bulk solution. The distance from the electrode, which experiences a concentration difference, is called the Nernst diffusion layer and it is typically 0.1 mm thick and its thickness is here called δ. (This makes it dependent on hydrodynamics, so it will vary if the solution is stirred or subject to convection.) The Nernst layer experiences a concentration gradient, which is

$$\frac{dc}{dx} = \frac{(c' - c)}{\delta}. \tag{22}$$

The gradient motors the molar flux, J. Due to Fick's first law of diffusion, which says that if concentration varies steeply with position, then diffusion will be fast,

$$J = -D\frac{\partial c}{\partial x}, \tag{23}$$

here

$$J = -D\frac{(c' - c)}{\delta}, \tag{24}$$

where D is the diffusion coefficient, the SI unit of which is $\mathrm{m^2s^{-1}}$. This particle flux is directly related to the current density towards the electrode in that the current density j (measured in current per areal unit) is the product of the particle flux and the charge per mole of ions, Fz:

$$j = FzJ = FzD\frac{(c - c')}{\delta}. \tag{25}$$

As can easily be seen, the gradient maximum of equation (24) occurs when c' equals zero. This corresponds to an electron being transmitted from an ion in the solution to the electrode [54]. The theoretical upper limit for the current density is the limes value

$$j_{\mathrm{lim}} = FzJ_{\mathrm{lim}} = FzD\left(\frac{c}{\delta}\right). \tag{26}$$

Cyclic voltammetry provides a simple method for investigating the reversibility of an electrode reaction. The reversibility of a reaction closely depends upon the rate of electron transfer being sufficiently high to maintain the surface concentrations close to those demanded by the electrode potential through the Nernst equation. Therefore, when the scan rate is increased, a reversible reaction may be transformed to an irreversible one if the rate of electron transfer is slow [52]. Rate-determining factors are the diffusion and the kinetics of the redox processes. The faster the kinetics of the ions, the closer to the E^0-value will the current maxima of the voltammogram be (and the steeper will a line joining the maxima be). The maxima being situated on a vertical line at the very E^0-value is a sign that the kinetics are as fast as they can possibly get.

3.2.2 TLC, Thin-layer Chromatography

Thin-layer chromatography, or thin film liquid chromatography, is a method of separation that exploits the solubility of chemicals. Near an edge of a plate covered with an absorbent (it may be e. g. cellulose, aluminium oxide or silicon oxide) the solutions to be separated are applied dropwise. The plate is then placed in an eluent, so that the edge, near which the solvent drops are, is well in contact with the eluant, but the rest of the plate is not. This is most easily arranged so that the plate, resting against some kind of support, is positioned at an angle (approximately $\pi/4$) to the container holding the eluent. The eluent may be any solvent of choice. It is drawn up through the absorbent by the capillary effects, taking the drops of the chemicals to be separated with it. After some short time the TLC is interrupted (it has to be interrupted before the eluent has reached the farther edge of the plate), and then the distances the different chemicals have moved can be measured and compared. The plate then displays a so-called chromatogram.

A number of factors decide the rate at which a chemical travels through the absorbent, i. e. how far a distance it can travel in a limited time. The affinity between the substances is an important factor. The absorbent and the eluent both attract the chemicals to be separated, and from the travelled distance of a chemical it is possible to say which of the two that had the greatest affinity to it. Ions and charged particles affect the travelling speed, as well as phenomena as hydrofobic reaction, i. e. when in a polar environment hydrofobic particles group together. Sizes of particles are also significant: generally small particles travel slower than large ones, since they diffuse faster into the absorbent and get caught in small pores where the flow rate is slower.

3.2.3 X-ray Diffraction

Diffraction is the deflection of beams of radiation due to interference of waves that interact with objects whose size is of the same order of magnitude as the wavelengths. Molecules and solids typically have interatomic distances of a few Ångströms, comparable to the wavelengths of x-rays with energies of the order of 10 keV. X-ray diffraction has extensive applications in physics, chemistry, materials science, mineralogy and molecular biology. The most common application is determination of the structures of crystalline solids. Other important applications are electron microscopy and structural studies of amorphous solids, liquids and gases.

An X-ray diffractometer is an apparatus that exploits the x-ray diffraction of a known wavelength to gain information about a solid structure. Different data can be extracted from the diffraction patterns, for example the spacing of crystal planes and the sizes of particles of crystalline solids. The principle of the diffractometer is this: In an anode made from cupper, electrons are dislocated from the K-shell, and are replaced by electrons from the L-shell. The energy differences between the K- and the L-shells give rise to photon radiation. The photons emitted are almost (nominally, but not strictly) monochromatic. The angle at which the photons bombard the specimen is varied over an interval, and a means of detecting the scattered radiation counts the diffracted photons for each angle. Different solids and crystal structures diffract the rays at their own characteristic angles, so the linear count of diffracted photons can give information about what kind of solids are present in the specimen. X-ray diffraction cannot be described without the mentioning of Bragg's law, in which d is the spacing of the crystal planes, λ is the known wavelength, θ is the incident x-ray beam angle and n is the order of the interference:

$$n\lambda = 2d \sin\theta_B, \qquad n \in \mathbb{Z}+ \,. \tag{27}$$

The integer n is conventionally incorporated in the definition of d. Bragg's law explains the theory behind constructive and destructive interference, which are both consequences of the periodicity of atom arrangement. X-ray beams are reflected by different planes of the crystal and thus they are displaced in phase with respect to one another. Principal maxima (constructive interference) occur when reflected beams that differ an integer number of wavelengths coincide and reinforce each other. Minima (destructive interference) occur when crests differ exactly half a wavelength (or an integer number plus half a wavelength) in phase and thus annul each other.

When it comes to the linear count of diffracted photons, sharp peaks originate from crystals only, since only crystals can produce strong constructive (and destructive) interference. The reason the peaks have a broadness and are not needle-shaped, is that it is not only the Bragg angles that effect diffraction. The incident angle of the x-ray beams is only ideally strictly one; in reality the beams enters the specimen at angles that differ within a short interval (figure 22). The angles slightly larger and slightly smaller than the Bragg angle also yield diffraction, but of less intensity than the Bragg angle principal intensity maximum. This diffraction is not cancelled since the phenomenon of destructive interference is based upon the discrete matching of exactly half a wavelength [56].

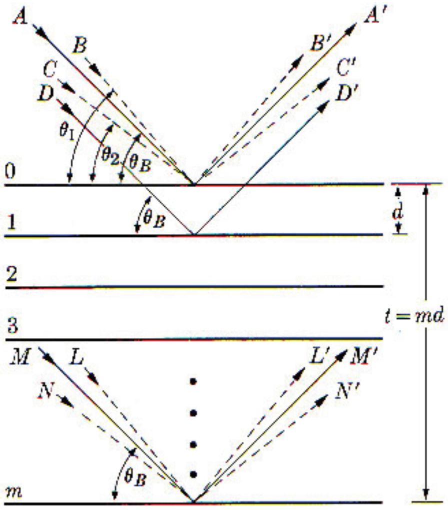

Figure 22: The crystal particle size influences the diffraction. θ_B is the angle which exactly meets the Bragg requirement (equation (27)), whereas θ_1 and θ_2 do not, but contribute with a blurring effect on the diffraction pattern, since the small size of the crystal inhibit their cancellation. From [56].

The size of the crystal influences the diffraction pattern (figure 22). If the size of the crystal is small there will be incomplete destructive interference [56]. That is, if adjacent layers give rise to a phase difference which is less than half a wavelength, then this phase difference could be cancelled by layers deeper within the crystal, but if the crystal is so small that these deeper layers do not exist, then there will be no cancellation and the diffraction pattern is rendered blurry. This is why the sharp peaks of crystals get broader as the crystal size decrease.

The broadness B, measured in radians, of an intensity peak is of a special interest, since it is related to the particle size, in particular the thickness (denoted by t). By convention, the broadness is measured where the intensity is half the maximum value (see figure 23(a)). An approximation of B, which is very illustrative and gives a good idea of the concept of B, is half the difference between the two outermost angles of a peak, at which the intensity is zero: $B = \frac{1}{2}(2\theta_2 - 2\theta_1) = \theta_2 - \theta_1$. (Note that θ is the incident angle, so 2θ is the diffraction angle.) For a specified solid and a specified crystal structure, the B-value of all the characteristic peaks will be approximately the same, and the particle size can be calculated from (or rather estimated by) B by help of Scherrer's formula:

$$t = \frac{0.9\lambda}{B\cos\theta} \tag{28}$$

For a simple deduction, see [56]. The Scherrer formula is designed for estimating diameters of approximately spherical crystals, but can be applied on non-spherical crystals as well. Most often the crystals are not spherical but ellipsoidal, lens-shaped, in which case it is not the diameter but the thickness, which is estimated. The thickness t is measured in a direction perpendicular to (a subset of) the reflecting planes of the crystal, see figure 22.

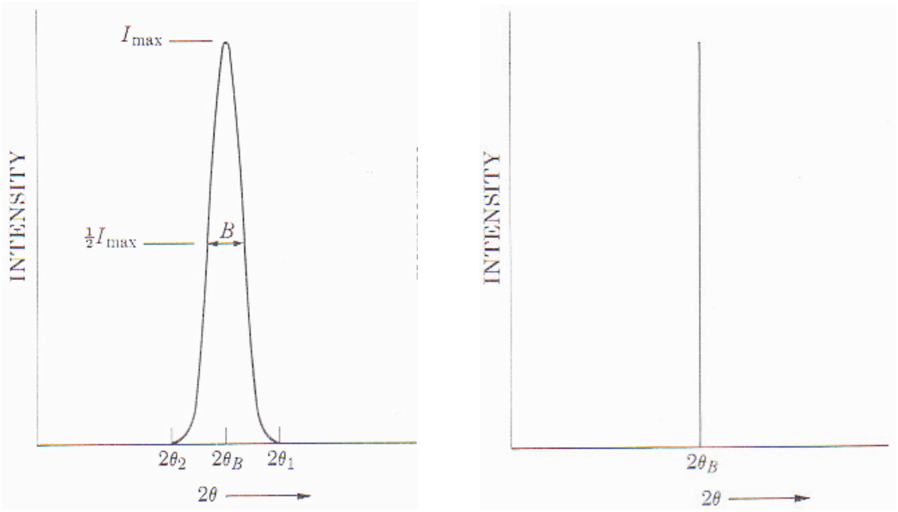

(a) The peak width B is measured where the intensity is half the maximum value.

(b) Ideal diffraction: Only the Bragg angle contributes to the diffraction (theoretically the case for infinite crystals).

Figure 23: The crystal particle size influences the broadness of the diffraction peaks. From [56].

The diffractometer consists of a cabinet in which the x-ray beams bombard the sample, held fixed in a sample holder. A mechanism supporting the sample holder and the detector, the goniometer, allows for precise movement of the detector. The door of the cabinet is made from x-ray radiation-proof glass, and a security device makes sure the x-ray beam is not engaged until the cabinet door is shut closed.

3.2.4 The Integrating Sphere

An integrating sphere is used for exploring what ratios of incoming light are transmitted, reflected and absorbed by a medium. The instrument is called “integrating” since an integration is performed for all the spherical inside of the sphere, in which the light is trapped and measured. The inside of the sphere is covered with a Teflon-like resin called spectralon. It is the best known material regarding diffuse reflectance [57]: Its reflectance exceeds 99% in the wavelength range 400 – 1500 nm. The equipment employed at the Ånström Laboratory can measure the transmittance and the reflectance. The absorption is then calculated using the intuitive relation

$$A = 1 - T - R, \tag{29}$$

where A is the absorption, T is the transmittance and R is the reflectance. Both diffuse and total transmittance and reflectance can be measured. The diffuse part of the reflectance or the transmittance is the part involving scattered light. The non-scattered part is called specular. From knowledge of the total and the diffuse parts, the specular part can be calculated by help of

$$T_{tot} = T_{spec} + T_{diff}, \tag{30}$$

and

$$R_{tot} = R_{spec} + R_{diff}, \tag{31}$$

where T is the transmittance, R is the reflectance, *diff* denotes the diffuse part, *spec* denotes the specular part and *tot* denotes the total part of the whole. Figures 24(a), 24(b), 25(a) and 25(b) are simple illustrations of the different cases for measuring diffuse and total transmittance and reflectance respectively. In the case of measurement of diffuse transmittance (24(a)), light is let into the sphere after having first been beamed through the sample. The location on the inner sphere wall where the undeviated beams would have hit the wall (i. e. on the spot diametrically opposite from where the light enters the sphere) a totally black cone is situated in an aperture. The undeviated beams hit the inside of the cone. The inside is really “very black”; it reflects only about 0.3% of the incoming light – so it is not a great exaggeration to say that what light goes into the cone will not come out. The remaining light left in the sphere is then the diffusely transmitted part and it can be measured without interference from the undeviated beams. In the case of the total transmittance (24(b)), light is again beamed through the sample into the sphere. The aperture is this time covered with a white Teflon slab, so as to make the inside of the sphere intact and enable measurement of the total transmittance, captured inside the sphere. When measuring reflectance, light is let into the sphere and the sample is placed in the aperture. In the case of total reflectance, all the light is captured inside the sphere (25(b)) and measured, and for the diffuse case (25(a)), the beams which are specularly reflected are let out of the sphere through another aperture so only the diffuse part of the reflected light remains for measurement inside the sphere. (The sample is not placed at an exact right angle to the sphere, since the specular beams leave the sphere at a spot different from the entrance opening.)

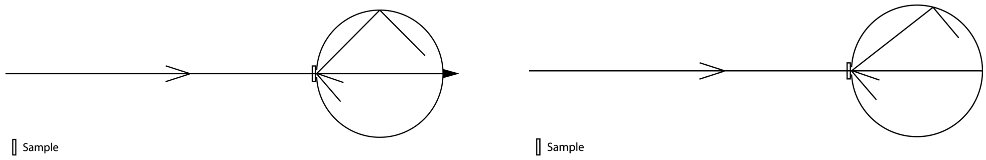

(a) (b)

Figure 24: Different modes of measuring transmittance with the integrating sphere: (a) Diffuse transmittance (b) Total transmittance

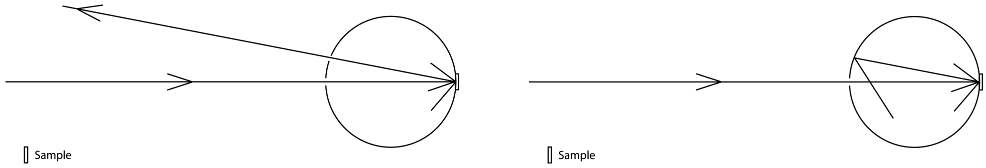

(a) (b)

Figure 25: Different modes of measuring reflectance with the integrating sphere: (a) Diffuse reflectance (b) Total reflectance

3.2.5 Spectrophotometry

The principle of a spectrophotometer is that light or other electromagnetic radiation of different wavelengths passes through a system often consisting of a sample of liquid, gas or solid in a compartment (a cuvette) of known length. The intensity of each wavelength is detected after having passed through the system and as a reference the intensity of each wavelength is also detected when the system or sample is not present (so that the light remains unrefracted). To get the absorbance of a specific substance the absorbance is detected for the same cuvette with the same solvent with and without the substance.

A typical spectrophotometer consists of a source producing radiation of different wavelengths, a monochromator that divides the light in different wavelengths, a sample holder and a detector [20]. Each wavelength is directed through the sample and detected for a certain time; a longer time gives higher accuracy and a shorter gives quicker measurement. A spectrophotometer could also be arranged the other way around; polychromatic light is send through the sample and then scattered into monochromatic light for measurement.

How much light is absorbed by a system when light is passing through it is described by Bouguer-Lambert-Beers law [58]:

$$A = \log(I_0/I) = elc, \tag{32}$$

where I_0 is the intensity before passing through the system and I the intensity after. l is the length of the system, c the concentration of the light-absorbing substance and e is the characteristic absorption coefficient for the substance at that wavelength [58]. A is the absorbance and is defined for every wavelength. In a spectrophotometer the absorbance A is measured at different wavelengths and A is then plotted against wavelength, giving an absorption spectrum.

As a quantitative method spectrophotometry can be used to measure the concentration of a substance in a sample if the absorbance is known at some wavelength and some concentration. It is in that case enough to have one sample of known concentration and relate its absorbance to the absorbance for each sample. Spectrophotometry can also be used in qualitative analysis where the absorption spectra can give information of which substance, or substances, is present in a sample.

4 Methodology

4.1 The Manufacturing of the solar cells

The solar cells were manufactured at the Department of Physical Chemistry at Uppsala University.

4.1.1 The Compounds of the TiO_2 Suspension

The only compounds of the TiO_2 suspension used were pure ethanol (Ethanol Absolute, 99.5%) and Degussa P25 TiO_2 powder [Japan]; the proportions (with regard to weight) were 4:1. The suspension was stirred with a magnetic stirrer [Bibby Sterilin Ltd, UK] overnight when first compounded, and for at least 30 minutes before use when used at later occasions. The suspension was stored in refrigerator.

A reason for using ethanol as suspending agent in the making of the TiO_2 suspension is that its surface tension is low and this will result in a smooth film [17].

4.1.2 The Film Substrates

The conducting glass substrates [F:SnO_2; Pilkington Kappa Energy, 18 Ω/cm^2] on which the films were deposited were prior to the deposition cleansed with 95% ethanol solution. The substrates were then left to dry. Any handling of the substrates was performed with a number of measures for securing the purity of the film: latex gloves or another kind of gloves were worn and tweezers were used. The substrates never left the laboratory environment unless they were carefully packed in aluminium foil. Bare hands never touched the substrates.

The films were applied onto the substrates using the doctor blading technique: the substrates were taped with scotch tape to the worktable, a few drops of the suspension were dropped onto the substrate by means of a pipette and a glass rod was used to evenly spread out the suspension. The solvent of the suspension exhibited a certain volatility and this presented one minor difficulty: It evaporates not extremely but rather quickly, so in order to get a nice, evenly deposited film, the spreading out by the glass rod had to be done as quickly as possible. The scotch tape frames not only served as fasteners, but also decided the initial film thickness (the glass rod raking tight over the taped edges will render the film thickness approximately that of the tape; this film thickness is later modified during the pressing process) and furthermore when the tape is removed, the edges are left uncoated, and there is space for mounting electric cables for subsequent iV characterization.

4.1.3 The Pressing Process

A few minutes after the substrates were coated, the films were pressed. The main purpose of pressing the substrates is to ensure mechanical stability. After pressing, the films are neither as likely to peel nor as predisposed to suffer scratching damage. Other effects of the pressing are that the transparency increases and the porosity decreases with increasing pressure forces [17]. The increase of the transparency is interconnected with the simultaneous decrease of light scattering effects of the TiO_2 powder, effects which are diminished since light dispersing aggregates are mashed into smaller pieces, which are less inclined to disperse light [17]. The pressing machine employed applied a uniform pressure force on a small area. The area involved in each case was the area of the deposited film. Since no mask, but only scotch tape was utilized, the areas of the different substrates could not be accurately but almost the same. On average the substrate film area was 1.8 cm^2. In order to prevent the films from sticking onto the surface facing it in the pressing device, the substrates were covered with aluminium foil (known for non-sticking properties) [17]. Each substrate was pressed for approximately three seconds. The pressing load was varied, the lowest being 5.89 kN/cm^2 (corresponding to the pressure force generated by the weight of 600 kg in the gravity field as perceived on the surface of the earth, applied on an area of 1 cm^2), the medium pressure force being 10.30 kN/cm^2 (corresponding to 1050 kg/cm^2), and the largest being 14.72 kN/cm^2 (corresponding to 1500 kg/cm^2). The pressure then depends on the film area, so with the average area these pressure forces correspond to pressures amounting to $27.0{\cdot}10^5$ Pa, $572{\cdot}10^5$ Pa, and $818{\cdot}10^5$ Pa. The pressing apparatus employed was the one at the Department of Physical Chemistry at Uppsala University, (figure 26).

Figure 26: The hydraulic pressing apparatus employed.

4.1.4 Preparation of the Dyes

Dyes were made from beetroot, red onion, red cabbage, henna and delphidinium. Cells were manufactured from substrates sensitised with the dyes made from beetroot, red cabbage and henna as well as with violet and ruthenium dyes, used as recieved.

The dyes made from beetroot, red onion, red cabbage and the delphinium dye were manufactured at the Department of Medichal Chemistry, Division of Pharmacognosy with assistance and guidance from Anders Herrmann.

Dyes Made From Beetroot, Red Onion and Red Cabbage

The dyes based on beetroot, red onion and red cabbage were made from fresh vegetables. 256.05 g red cabbage, 269.40 g red onion and 141.65 g beetroot was rinsed in distilled water and finely chopped. The vegetable pieces were separately immersed in 500 ml of ethanol (95%). The glass containers were covered with plastic laboratory film to prevent evaporation, covered with aluminium foils to prevent damage from light exposure and were left to shake for three days. Thereafter the vegetable-ethanol-mixes were filtrated. A Büchi Rotavapor-R was employed to rid the extracts of the ethanol. The rotavaporaton was executed at a low temperature (30 °) so as not to spoil the pigments too much due to heat. The viscous liquids were then left overnight, covered with evaporation-preventing plastic and aluminium foils in a cold-storage room. To void the extracts completely of water, they were transmitted to test tubes and freeze-dried. The freeze-drying process failed several times and had to be repeated. The remaining, dry substances were dissolved in ethanol (95%) or methanol (98.99%). Also ethanol (99.5%) was tried as a solvent, but unfortunately it turned out to be impossible to solvate the extracts in this solvent, so in this case a few drops of distilled water had to be added. (Water was otherwise avoided to as large an extent as possible.) Unfortunately the red onion extract was spoilt in an attempt to make the freeze-dried extract dissolve in a solvent.

After having obtained the best results with the beetroot extract, a new beetroot extraction was made: 486.7 g beetroot was rinsed in distilled water, chopped and mixed with 650 ml ethanol (95%) and was left to shake overnight according to procedures mentioned above. The following day it was filtered, made more concentrated by means of the rotavaporation and then an attempt to freeze-dry it in an e-flask was made, an attempt that failed (due to the shape of the e-flask). The next day the freeze-drying was repeated, this time in a round flask, an attempt that succeeded. The freeze-dried substance was dissolved in methanol, but the whole amount was not solvable at the first try, so dissolved liquid was decanted and more methanol was added in order to solve more of the dye. During the dissolving process the substance was left to shake with the solvent. The dissolved liquid was filtered and made more concentrated by yet another rotavaporation, where 1950 ml of liquid was reduced to 1150 ml.

The Ruthenium and Violet Dyes

The dyes based on ruthenium and violet were used as they were delivered, prepared in laboratory environment at the Department of Physical Chemistry (the ruthenium-based dye) and at the Department of Pharmacognosy at Uppsala University (the violet dye) respectively. The ruthenium-based dye was 0.5 mM Ruthenium 353-bisTBA (aka N719) in ethanol. The dyes made from violet (Viola Odorata of the family Violaceae) came in a number of shades, ranging from relatively dark pink to very light pink. The firsthand choice was to use the darker ones to the largest extent. The violet dyes contained water – a feature that much effort was put into avoiding in the other dyes. It also contained acetonitrile, a solvent which is also a part of the electrolyte used in all measurements.

The Henna Dyes

The dyes based on henna were made from dried henna leaves. Finely pulverised Henna; Lawsonia Inermis (of the brand Insan AB, the henna itself originating from Pakistan) and ethanol (99.5%) were the ingredients of the henna dye. These two compounds were thoroughly mixed together and blended with a magnet stirrer overnight (covered from light and protected against evaporation). There were two versions prepared: One in which the henna powder was used as received from the package, and one in which the henna was first made devoid of water by heating in a heat oven for well over one hour. The original henna powder weight was thereby reduced with 6.2%. The ethanol-henna mixtures were filtered, using Whatman Glass Microfibre filters GF/B, and then used for dyeing.

The Delphinium Dye

Blue delphinium flowers (of the family of Ranunculaceae) were also tested for dye extract making. 8.6 grams of the flowers were finely chopped and left to shake overnight in 45 ml ethanol (95%), but the blue pigment would not dissolve: the liquid was greenish and the flower parts were still blue. Methanol was then tried, with a slightly better result, but unfortunately the only testing tube with delphinium extract was spoilt in an attempt to make the extract dissolve in methanol. It is reasonable that the delphinium extract would not be solved in either ethanol or methanol, since the pigment molecule is charged. The making of a delphinium-based dye was cancelled when no appropriate solvent was found.

4.1.5 The Sensitising Process

Prior to sensitising, the photoelectrode substrates were sintered. The sintering makes the nanoparticles get into electrical contact with one another and the conducting substrate, but it also has another purpose, more important to the sensitising step which is to follow: the sintering rids the films of any water molecules. The water molecules must be eliminated; their presence can be detrimental to the efficiency of the solar cell. Any water molecules in the nanostructured titanium dioxide film prevent the dye molecules from adhering to the film itself. The substrates were sintered for 30 minutes in 350-4008 C, and after cooling they were ready for the sensitising step. The sensitising was performed in baths of dye solutions for approximately twelve hours, always immediately prior to the mounting and testing of the complete cells. The dying baths were glass containers filled with dye solutions, where the substrates were emerged and left overnight. The baths were always covered with plastic laboratory film (Parafilm "M" Laboratory Film, American National Can™, Chicago, Il. 60631) to prevent evaporation, and furthermore covered with aluminium foil to block out light. Upon removal from the dying baths the substrates were rinsed with 95% ethanol solution, in order to remove excess dye. (Dye particles, which do not adsorb properly on the thin film surface block out light from the solar cell and they should therefore be removed.) Thereafter they were left to dry, which usually took at most a couple of minutes. When dry, they were immediately used in mounted cells.

4.1.6 The Counter Electrode

Conducting glass substrates [F:SnO_2; Pilkington Kappa Energy, 18 Ω/cm^2] were cut to appropriate sizes (so as to match the sizes of the photoelectrodes). The glass substrates were cleansed with 95% ethanol solution to remove any stains. (As for the photoelectrodes, any handling of the counter electrode substrates was performed with gloves and tweezers.) A platinum chloride solution [$H_2PtCl_6 \cdot 6\ H_2O$, chloroplatinic acid hexahydrate(IV), 5mM] was applied onto the substrates to act as a "catalyser layer", to facilitate the conduction of the electric current, see section 2.4. Thereupon the substrates were sintered for 5-10 minutes in 400 °C. After cooling they were ready to be used in mounted cells.

4.1.7 The Electrolyte

The electrolyte was prepared according to what at the Department of Physical Chemistry at Uppsala University is known as "Hugo's recipe" or the standard electrolyte. It contains the following chemicals, solved in 10 ml of acetonitrile: 2.216 g tetrabutylammonium iodide (TBA I) (0.6 M), 0.253 g I_2 (0.1 M), 0.134 g LiI (0.1 M) and 0.676 g 4-tert-butylpyridine (0.5 M).

4.1.8 The Mounting of the Complete Solar Cells

The photoelectrode and the counter electrode were overlappingly placed in a holder so that the titanium dioxide covered area of the photoelectrode was the only part of the photoelectrode that was in contact with the counter electrode. The non-titanium dioxide covered area of the photoelectrode and the non-overlapping edge of the counter electrode were attached to the measuring equipment by means of cords and crocodile clips. The electrolyte was dropwise applied between the electrodes by means of a pipette. This set-up is called sandwich configuration, see figure 27.

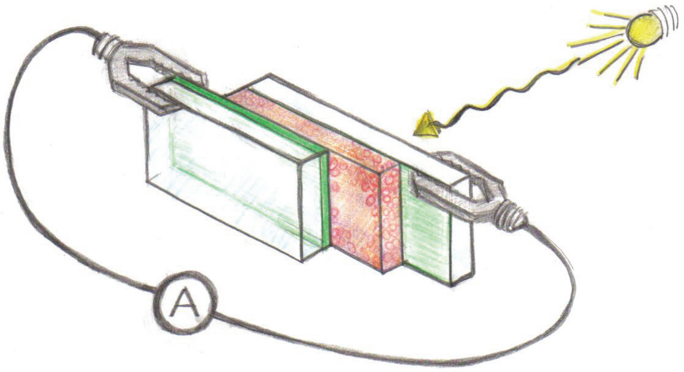

Figure 27: Schematic over the open sandwich configuration during an iV or IPCE measurement.

4.2 The Methodology of the Current-Voltage and IPCE Measurements

IPCE and iV measurements were conducted at room temperature, approximately 20 °C.

4.2.1 The Current-Voltage Measurements

The equipment used to record current and voltage was computerised Keithley Model 2400 source measure unit, and the lamp was a sulphur plasma lamp, Light Drive 1000. Its spectrum is very much alike the solar visible spectrum. The set-up had a dark compartment for the solar cells and a ruler for marking the exact distance corresponding to the specific light intensity 1000 W/m^2.

In analogy with the IPCE measurements, the cells were one by one connected to the current-voltage measuring equipment by means of cords and crocodile clips. Each measurement lasted for a couple of minutes. The cells were placed at a short distance from the sulphur lamp, a distance which corresponds to a solar illumination of 1000 W/m^2.

4.2.2 The IPCE Measurements

Here follows a shortened account of the IPCE set-up at the Department of Physical Chemistry.

Lamp: Collimated xenon arc lamp 300 W, Cermax Model LX300UV (ILC Technology); a water-filter with a quartz window and a quartz lens; Monochromator: Digikröm CM 110 (CVI Laser Corporation); Filterwheel; Suprasil lens; Beam splitter: quartz window; Reference detector: UV-enhanced Si-diode connected to a Keithley picoammeter Model 485; Calibrated detector: Optical Power Meter 1830-C (Newport) and a photo detector Model 818-UV; Current-meter: Model 2400 SourceMeter (Keithley).

The solar cells were compounded to form a two-electrode sandwich configuration: the two glass substrates are pressed together with clips, held erect by a holder and connected to measuring instruments by means of crocodile clips and cords, for more detailed information see section 4.1.8.

The cells were mounted immediately prior to the measuring of the IPCE and the current-voltage-characteristics. For the IPCE measurements the cells were connected one by one to the measuring equipment and the measurements were initiated. Each test had a duration of approximately 5 minutes.

4.3 The Methodology of the Other Methods of Characterisation

4.3.1 The Cyclic Voltammetry

For the cyclic voltammetry performance the apparatus at the Department of Physical Chemistry at Uppsala University was used. Its set-up is schematically drawn in figure 28. The laboratory experiment was performed with assistance and guidance by Sten-Eric Lindquist. A silver/silver chloride electrode was used as the reference electrode. The working electrode was made of gold.

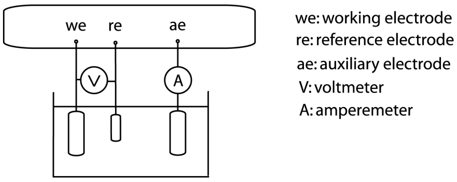

Figure 28: Schematic over the cyclic voltammetry set-up.

The working and auxiliary electrodes were cleaned in HNO_3 (oxidising) and H_2SO_4 (etching). The presettings were set to scan the voltage from -0.3 V to 1.0 V at a scan rate of 20 mV/s, 100 mV/s, 0.5V/s, 1 V/s. As a reference, a run with the compound dicyclopentadienyliron, commonly called ferrocene, $Fe(C_5H_5)_2$, was made. It is an aromatic, orange, crystalline metallo-organic substance consisting of two carbon rings symmetrically situated on either side of a central iron atom [59]. Its molecular weight is 186,04 g/mole, and since we needed a 10 mM concentration in a 125 ml volume, 0.2326 g ferrocene was solved in 98% methanol. Lithium perchlorate trihydrate, $LiClO_4 \cdot 3\ H_2O$, (with molecular weight 160.44 g/mole) provided the ion transfer, and 2.006 grams were added to make up a concentration amounting to 0.1 M. The preparations of the beetroot extract run were made accordingly. The lithium salt was directly solved in the beetroot extract solution, the solvent of which was also 98% methanol.

The determination of the E^0-values were done manually, by connecting the extreme points of the voltammogram curves with straight lines and noting where the lines incise the voltage axes. The potential of the silver/silver chloride electrode was then subtracted in order to place the tested substances in relation to the electrochemical series.

4.3.2 The TLC

TLC was performed with the beetroot extract, to verify that the extract contains several different pigments. Beetroot is known to contain betanin (a red pigment) and vulgaxanthins (yellow dittos). The TLC-plate used was an Macherey-Nagel Alugram SIL G/UV_{254}. The glass containers involved were prior to the experiment cleaned with ethanol (95%).

4.3.3 The X-ray Diffraction

To gain knowledge about the particle size in our TiO_2 specimens, an x-ray diffraction was performed at the Ånström Laboratory, Uppsala University, at the Department of Material Chemistry. Our specimens were carefully transported in clean glass containers and arrived unscathed. For the sake of comparison, 6 different specimens were brought: sintered and unsintered samples pressed with the three chosen pressing forces, i.e. sintered and unsintered samples pressed with correspondingly 600 kg/cm^2, 1050 kg/cm^2 and 1500 kg/cm^2. The diffractometer employed was a Siemens Diffractometer D5000 with an acceleration voltage of 45 kV and a current of 40 mA. The diffraction angles were scanned from 20° to 60° in increments of 0.05°. The wavelength bombarding the specimens was fixed: $\lambda = 1.5405981$ Å – this is the photon wavelength generated by the cupper anode (the CuK alpha line). The TiO_2 specimens were one by one fixed in the specimen holder and the diffraction measurements were automatically performed when the presettings were entered and the cabinet door was shut closed. The experiment was made under supervision of Nils-Olov Ersson.

4.3.4 The Integrating Sphere

To map out what percentage of the light is transmitted, reflected and absorbed by the photoelectrode the experiment of the integrating sphere was performed at the Ånström Laboratory at the Department of Solid State Physics, under guidance of Arne Roos. Four samples of TiO_2 thin film glass substrates were brought to the laboratory in a clean glass container and without becoming scratched or otherwise damaged under the transportation. Two of the samples were dyed with beetroot extract and the other two were not dyed at all. The instrument employed was a Perkin Elmer Lambda 900 UV/VIS/NIR spectrophotometer, a double beam type, in connection to a spectralon integrating sphere with a 15 cm diameter. The wavelength range traversed was 300 – 1000 nm, in 5 nm steps.

Measurements yielded information on transmitted and reflected radiation for each wavelength, and this information was corrected according to the correction instructions in [60]. The percentage of absorbed radiation was calculated using equation (29) on page 31 and compiled into table 8 and figure 52.

4.3.5 The Spectrophotometry

For each measurement a cuvette of length 1.00 cm with a sample of dye in methanol was placed in a Hewlett Packard 8453 UV-Visible Spectro-photometer shown in picture 29. To give a broad measurement spectrum two lamps were used, a tungsten lamp and deuterium lamp. The software used was UV-Visible Chem Station Rev. A. 09, 01 [76] Copyright Agilent Technologies 95-00.

Spectrophotometry measurements were made for the three dyes beetroot, red cabbage and red onion, all three with methanol as solvent. After choosing beetroot for further investigation another spectrophotometry measurement was done for five samples of the second fabrication of beetroot dye, also with methanol as solvent. In both cases a cuvette with methanol was used as a reference.

Spectrophotometry measurements was also done to compare unsensitised and violet dye sensitised TiO_2 photoelectrodes. In this case the photoelectrode itself was placed in the location for the cuvette. Since the solid TiO_2 scatter light in all directions and this kind of measurement is not reliable and therefore an integrated sphere measurement was done (see section 4.3.4) comparing unsensitised and beetroot dyed photoelectrodes.

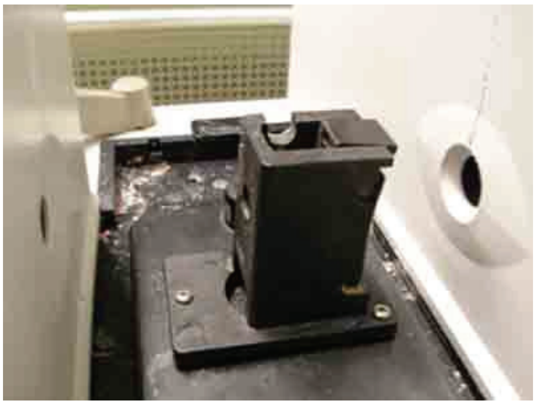

Figure 29: The spectrophotometer employed.

5 Results

5.1 The Results of the Current-Voltage and IPCE Measurements

5.1.1 The Current-Voltage Characterization

The current-voltage characteristics measurements produced both nice-looking and strange (failure-indicating) results. Two of the better results are the smooth iV-curves of figures 30(a) and 30(b), which both are products of solar cells with relatively high fill factors. Both cells are sensitised with the second-fabrication beetroot dye and they are pressed at 1050 kg/cm^2 (figure 30(a)) and 600 kg/cm^2 (figure 30(b)) respectively.

Three aspects of the current density-voltage curve are considered and compared. These are the fill factor, ff, which is a measure of the efficiency of a solar cell, the short circuit current density, i$_{sc}$, which is the highest current density and the open circuit voltage, V$_{oc}$, which is the highest voltage. Tables of fill factors and i$_{sc}$ and V$_{oc}$ values for a number of solar cells are shown in the appendix 10. The average values of ff, i$_{sc}$ and V$_{oc}$ and the corresponding distribution ranges are calculated for each dye and shown in tables 3, 4 and 5.

Under the assumption that samples are normal distributed the t-distribution is used to calculate he distribution range I$_m$ [61]:

$$I_m = (\bar{x} - t_{\alpha/2}(f) \cdot d, \bar{x} + t_{\alpha/2}(f) \cdot d), \tag{33}$$

where $\bar{x}$ is the average value and f is the degree of freedom, which equals (1-n), where n is the number of measurements (in this case the number of solar cells for each dye). d is the average error which equals $s/n^(0.5)$ where s is the standard deviation. The values for t$_{\alpha/2}$ are tabuled for each f [61]. The interval I_m covers the expectation value with the probability (1-α). Here α is chosen to be 0.05 so the probability will be 95%. This means that for each calculated average value the true expectation value for that parameter is with a probability of 95% found within the distribution range.

Figures 31 and 32 show diagrams comparing fill factors for cells sensitised with different dyes and pressed with different pressing forces respectively. The later figure also makes a comparison between the second fabrication of beetroot extract dyed cells and the rest of the cells. Generally the differences between dye averages are small and a difference is statistically significant only in the cases where two ranges do not overlap, as with ruthenium and second-fabrication beetroot.

The average V_{oc} values with ranges are shown in figure 33 and also here the differences are small and many ranges are overlapping. The average i_{sc} for each dye is shown in 34 and here the differences between the Ruthenium dye and the others are obvious. Most plant dye-sensitised cells have low current densities. The average i_{sc} for ruthenium sensitised cells is $4.6 \cdot 10^{-3}$ A/cm^2 and for the plant dye sensitised cells the best average is $6.5 \cdot 10^{-4}$ A/cm^2 for those sensitised with beetroot extract solved in ethanol, and between $1 \cdot 10^{-5}$ and $2 \cdot 10^{-4}$ A/cm^2 for the others. The average i_{sc} values for the plant dye sensitised solar cells is thus only between 0.2% and 14.2% of the average i_{sc} value for the ruthenium dye sensitised cells.

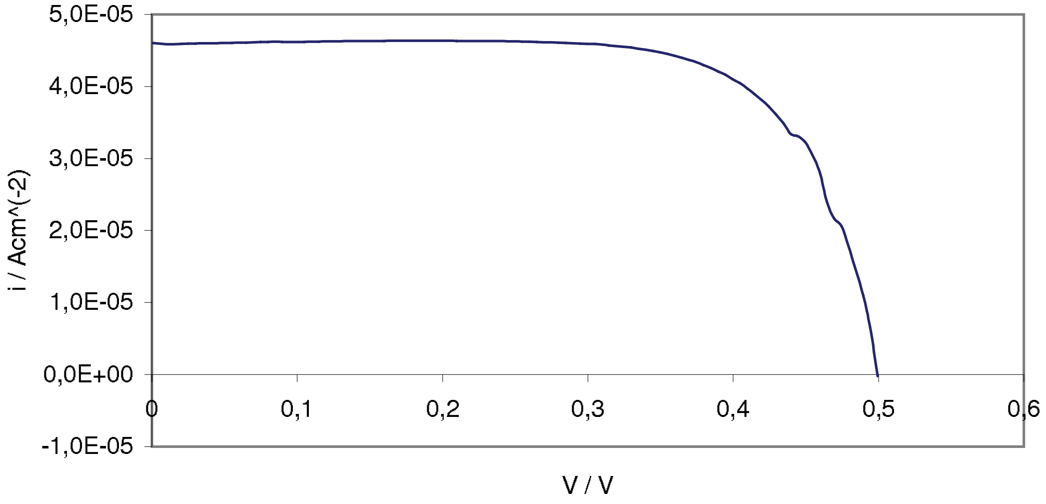

(a)

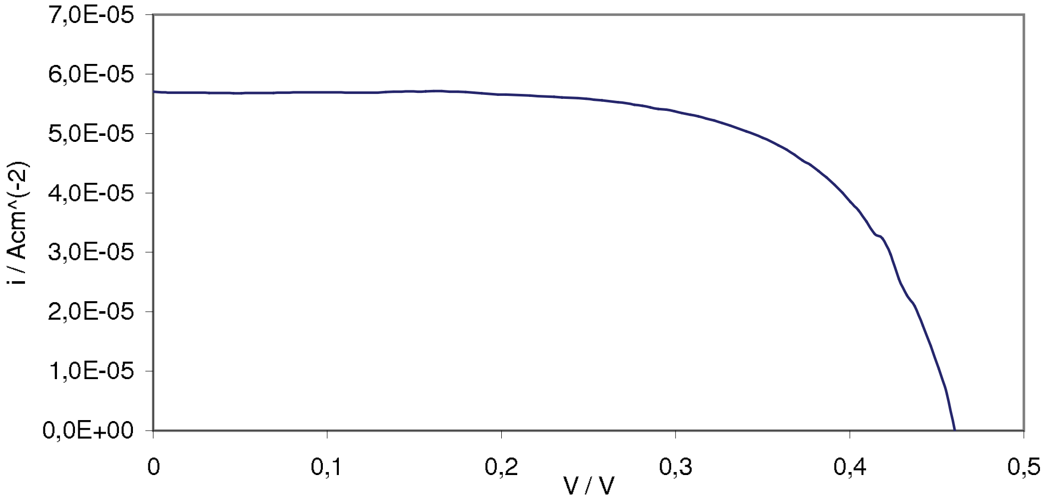

(b)

Figure 30: The iV-curves of two beetroot dye sensitised cells pressed with different pressure forces: (a) 1050 kg/cm^2 (b) 600 kg/cm^2.

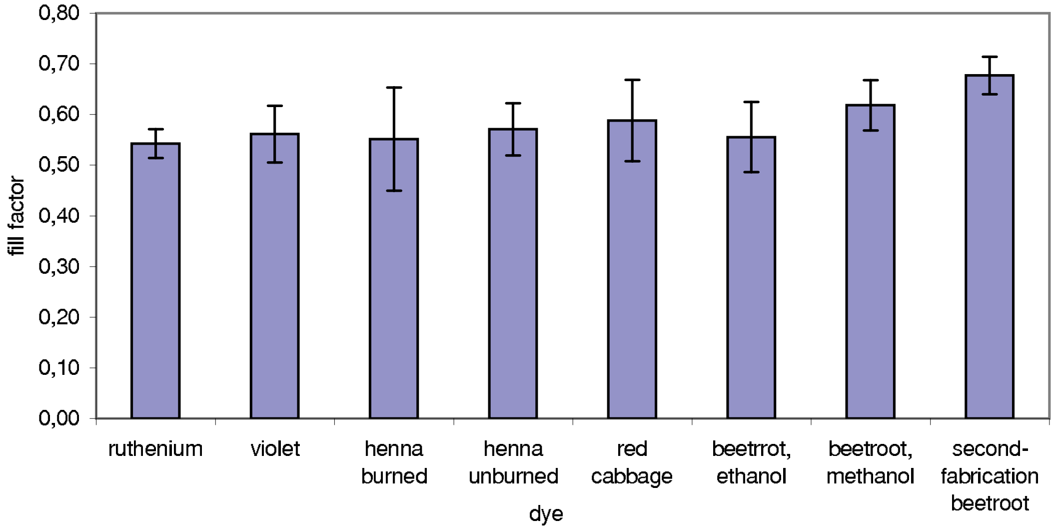

Figure 31: Average fill factor values and distribution ranges for different dyes.

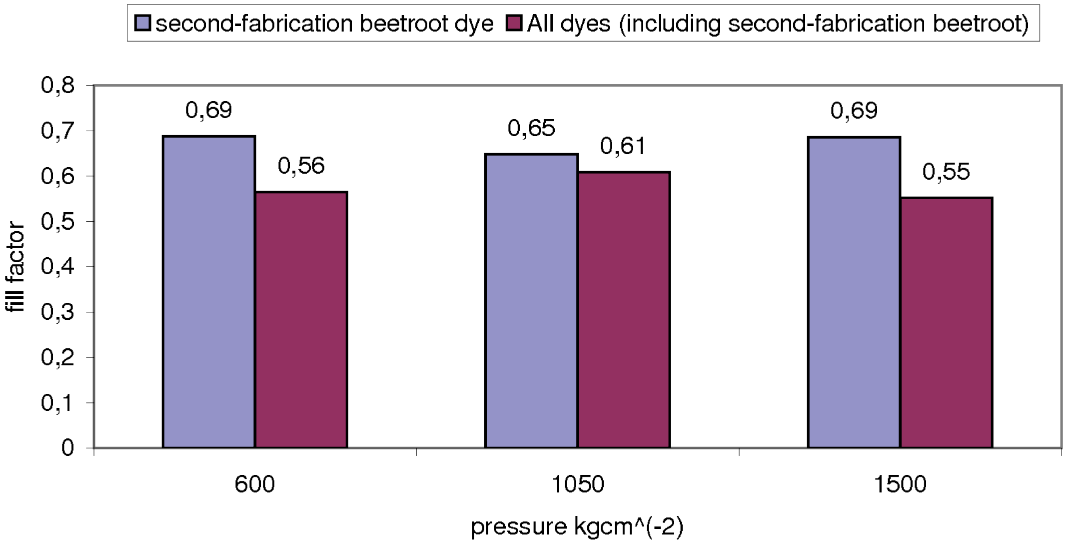

Figure 32: Average fill factors. A comparison between different pressing forces.

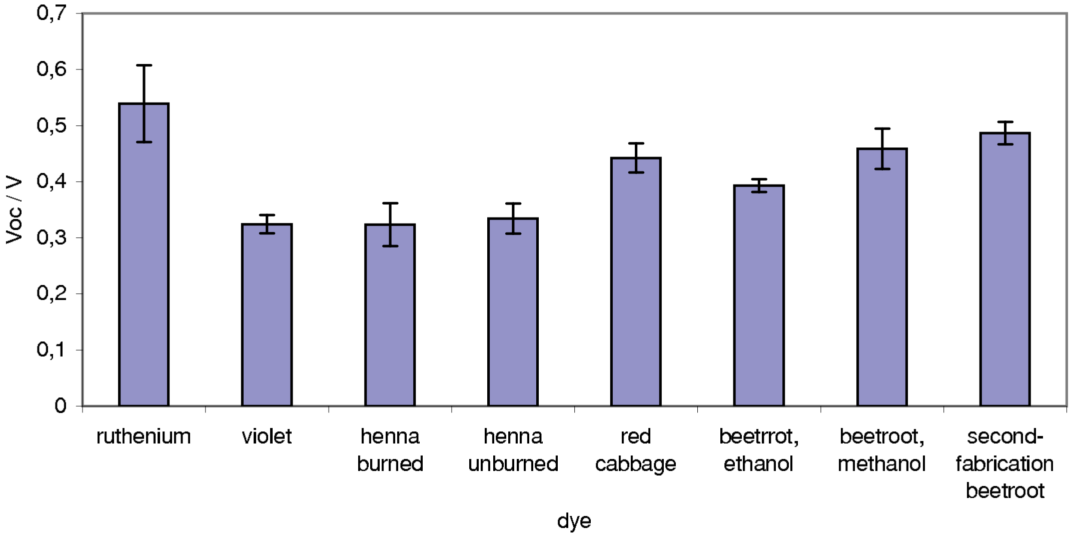

Figure 33: Average V_{oc} values and distribution ranges for different dyes.

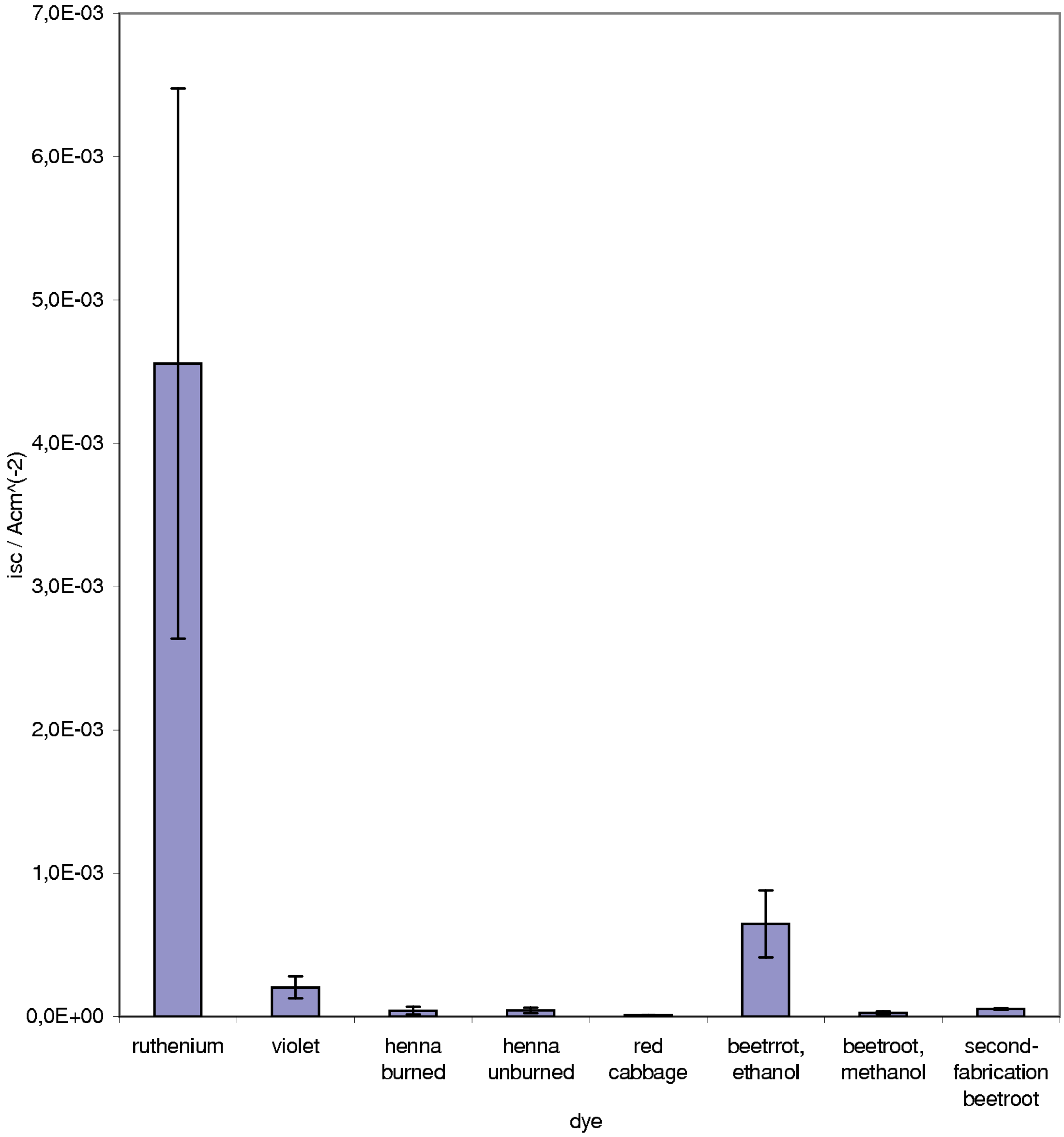

Figure 34: Average i_{sc} values and distribution ranges for different dyes.

Table 3: Average i_{sc} values.

Solar cell	Average $i_{sc}/\mu\text{Acm}^{-2}$	Distribution range/μAcm^{-2}
Ruthenium	4500	2000
Violet	200	80
Henna, burned	41	30
Henna, unburned	43	20
Red cabbage methanol	10	1
Beetroot ethanol	650	200
Beetroot methanol	27	10
Second-fabrication beetroot	54	6

Table 4: Average V_{oc} values.

Solar cell	Average V_{oc}/mAcm^{-2}	Distribution range/mAcm^{-2}
Ruthenium	540	70
Violet	320	20
Henna, burned	320	40
Henna, unburned	330	30
Red cabbage methanol	440	30
Beetroot ethanol	390	10
Beetroot methanol	460	40
Second-fabrication beetroot	490	20

Table 5: Average fill factors.

Solar cell	Average fill factors	Distribution range
Ruthenium	0.54	0.03
Violet	0.56	0.06
Henna, burned	0.55	0.1
Henna, unburned	0.57	0.05
Red cabbage methanol	0.59	0.08
Beetroot ethanol	0.56	0.07
Beetroot methanol	0.62	0.05
Second-fabrication beetroot	0.68	0.04

5.1.2 The IPCE

The graphs presented in figures 36, 37, 38, 39, 35, 40, 41 and 42 are the averaged IPCE results for different categories of solar cells. The categorization is made on the basis of which kind of sensitiser and what pressure force was applied to the photoelectrodes. For the sake of comparison, figure 41 contains the IPCE of an unsensitised solar cell alongside with the averaged results of the burned henna-sensitised cells. The IPCE graph in figure 43 shows the IPCE of the two individually best-performing plant extract sensitised solar cells, sensitised with red cabbage extract and beetroot extract respectively. As can be seen from the below figures, all plant extract sensitised solar cells performed poorly compared to the ruthenium-complex sensitised solar cells.

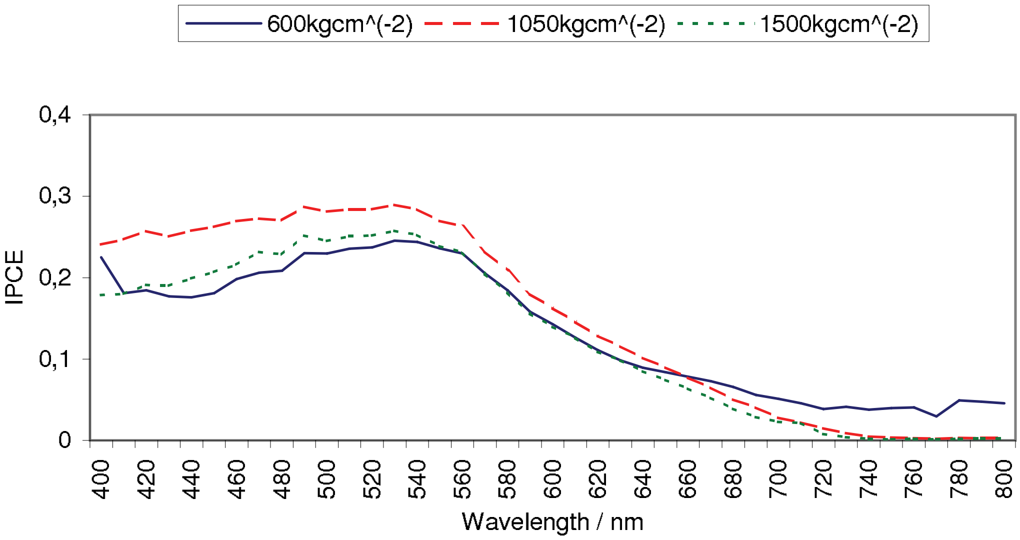

Figure 35: The average IPCE of cells sensitised with ruthenium-based dye dissolved in ethanol.

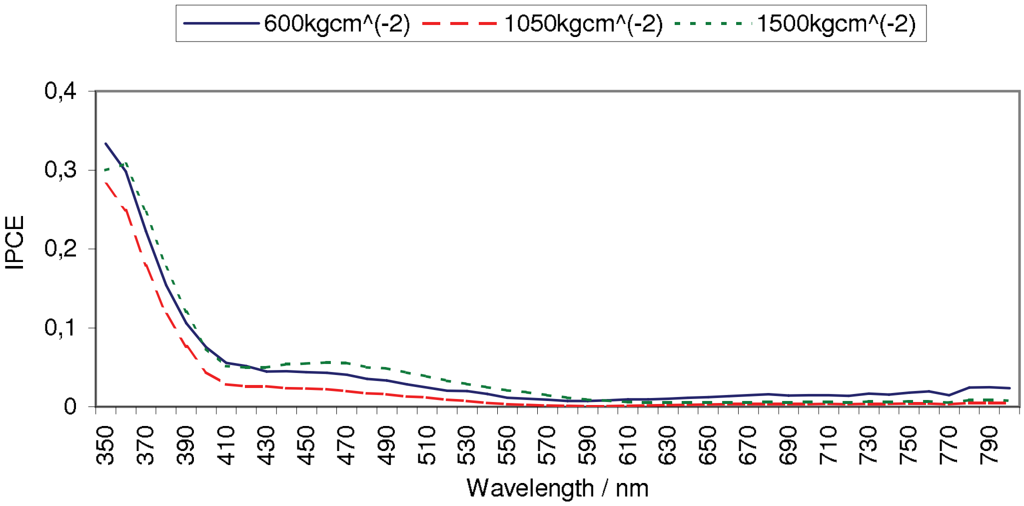

Figure 36: The average IPCE of cells sensitised with the first-fabrication beetroot extract dissolved in ethanol (99%) and a few drops of water.

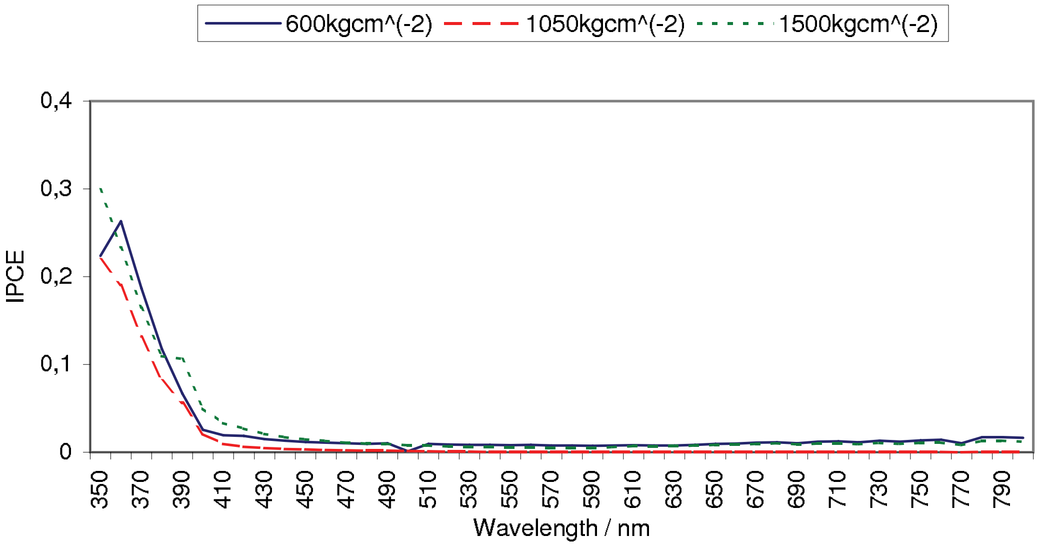

Figure 37: The average IPCE of cells sensitised with the first generation beetroot extract dissolved in methanol (98.99%).

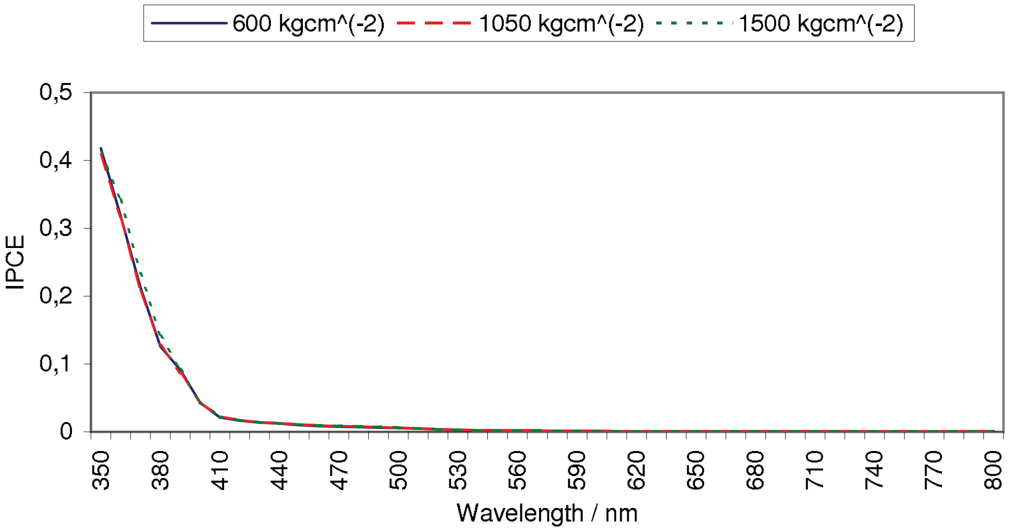

Figure 38: The average IPCE of cells sensitised with the second-fabrication beetroot extract dissolved in methanol (98.99%).

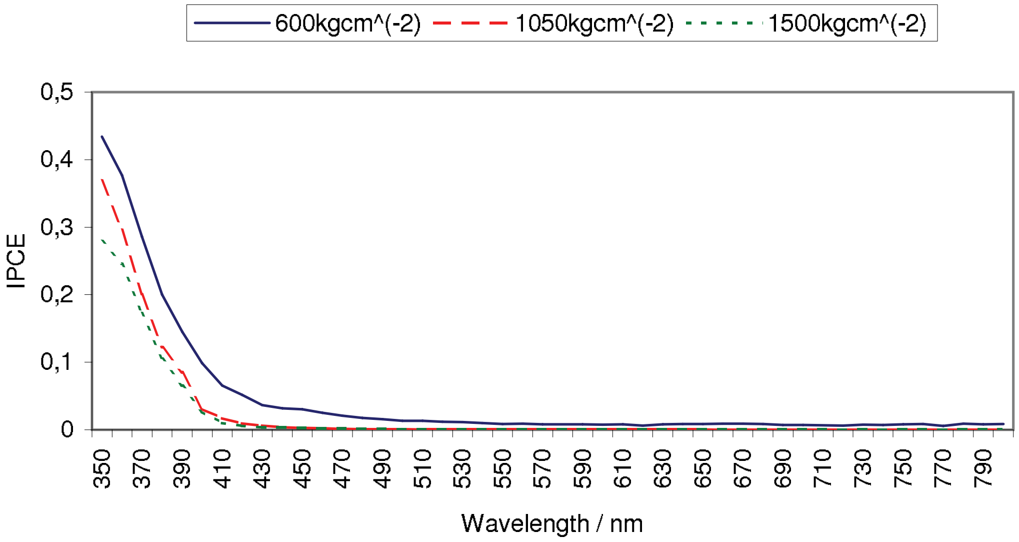

Figure 39: The average IPCE of cells sensitised with red cabbage extract dissolved in methanol (98.99%).

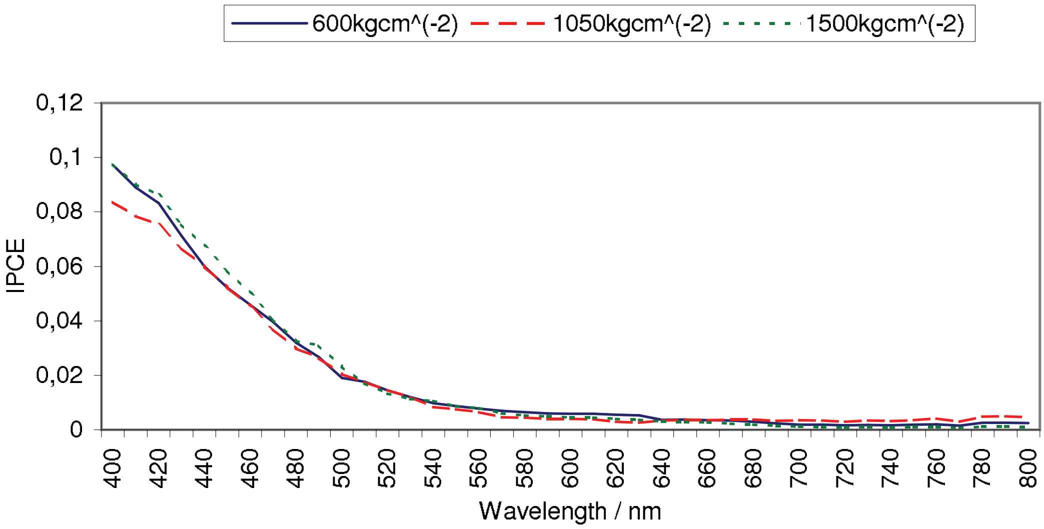

Figure 40: The average IPCE of cells sensitised with the violet extract dissolved in water and acetonitrile.

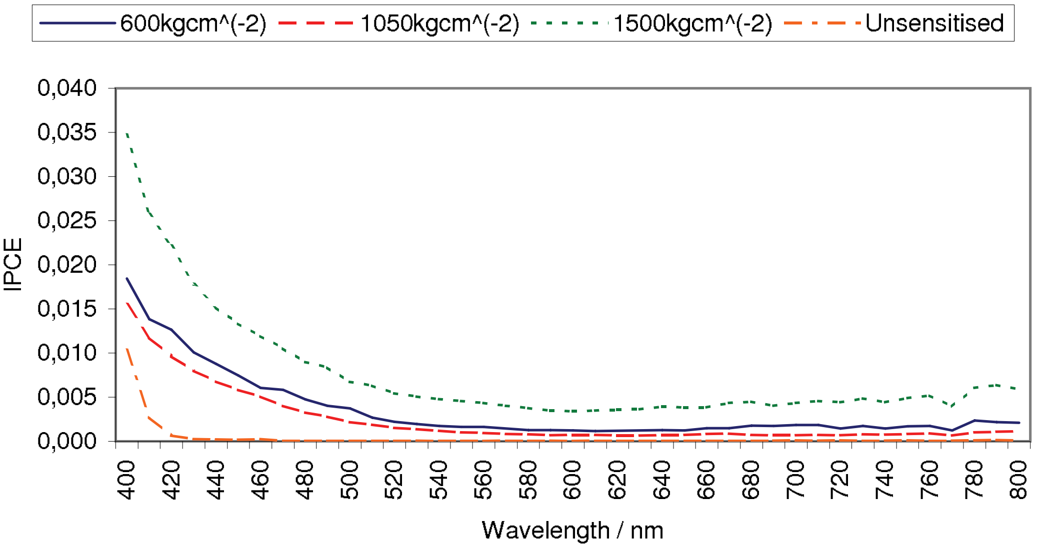

Figure 41: The average IPCE of cells sensitised with burned henna extract dissolved in ethanol (99.5%), and for comparison the IPCE of an unsensitised solar cell.

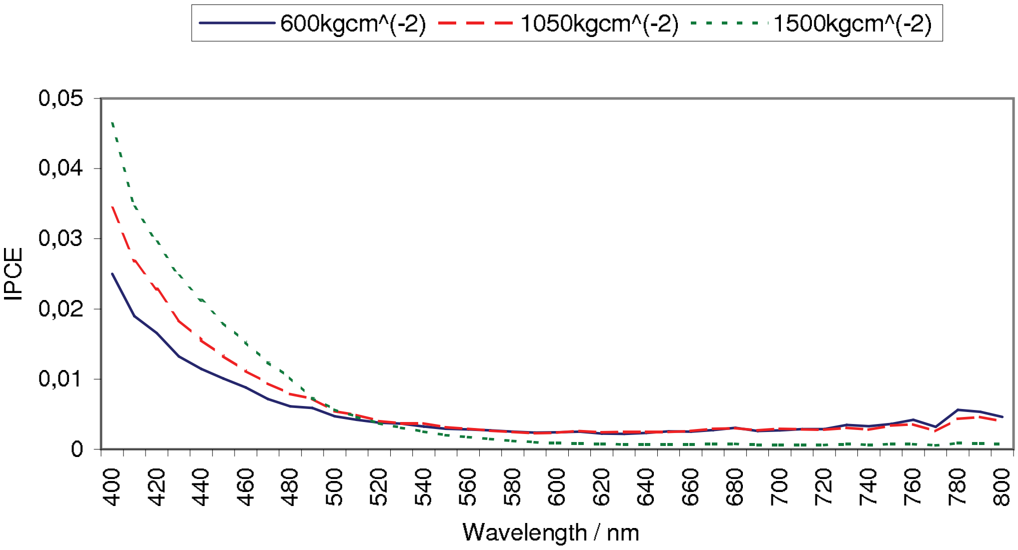

Figure 42: The average IPCE of cells sensitised with unburned henna extract dissolved in ethanol (99.5%).

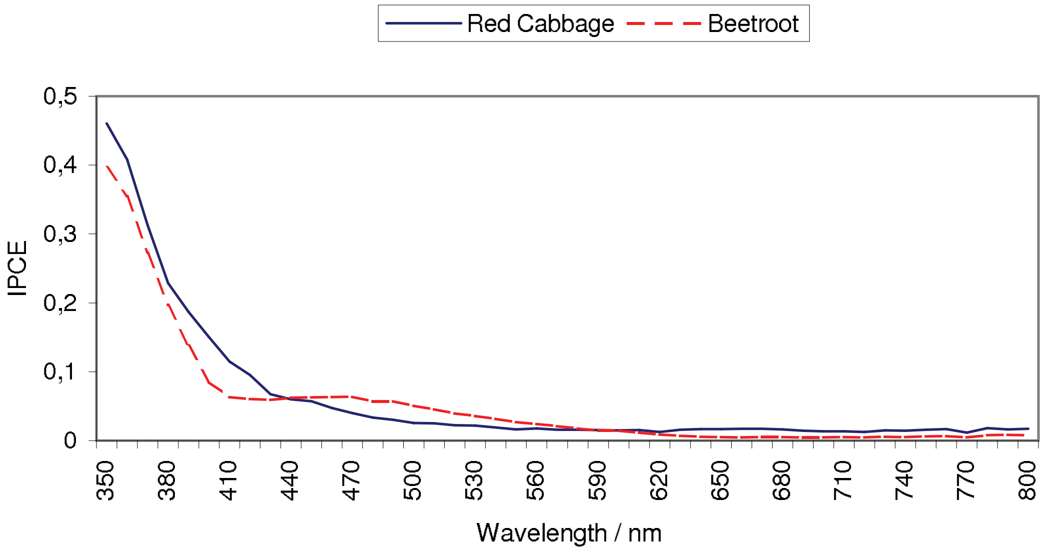

Figure 43: The IPCE of the best-performing cells, sensitised with red cabbage and beetroot extract dissolved in methanol and ethanol respectively.

5.2 The Results of the Other Methods of Characterisation

5.2.1 The Results from the Cyclic Voltammetry

Voltammograms resulting from the cyclic voltammetry can be seen in figures 44 and 45. The voltammogram for the beetroot extract differs from the reference voltammogram, but just as the reference the curve is symmetrical and closed, which means that the chemical processes occurring during the linear sweep voltammetry are all reversible. Had the kinetics of the electrolytes in question been very fast, these extreme points would have been situated on a vertical line parallel to the current axis. Now, since the kinetics only comparatively slowly reacts on the concentration changes, there is a displacement of the extreme points. Into the voltammograms lines connecting the extreme values of the curves have been drawn, to mark the E^0-values where the lines incise the voltage axes. The E^0-value for the reference ferrocene is 0.36 V with respect to the reference Ag/AgCl electrode and for the beetroot extract it is $E^0 = 0.30$ V. By subtracting the standard potential of the reference Ag/AgCl electrode, the E^0-values for the two substances can be placed in relation to the electrochemical series (see table 6), in which elements are ordered according to their ability to reduce. The more positive an element is, the easier it is to be reduced, i.e. the weaker is their reducing ability. Since the silver/silverchloride electrode has an E^0-value of 0.2223 V versus the SHE, the positions of the solutions in the electrochemical series are (0.30-0.2223) V = 0.0777 V $\approx$ 0.08 V for the beetroot extract, and (0.36-0.2223) V = 0.1377 V $\approx$ 0.14 V for the ferrocene. If the ferrocene position does not cohere with the general ferrocene standard potential, it is because in this experiment the standard concentration 1 M was not used.

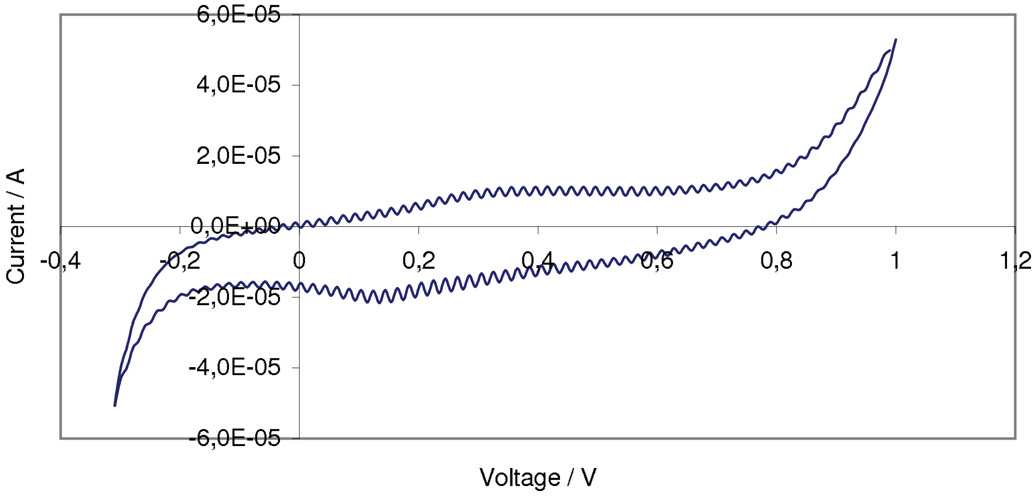

Figure 44: The beetroot run: $E^0 = 0.30$ V with respect to the Ag/AgCl electrode.

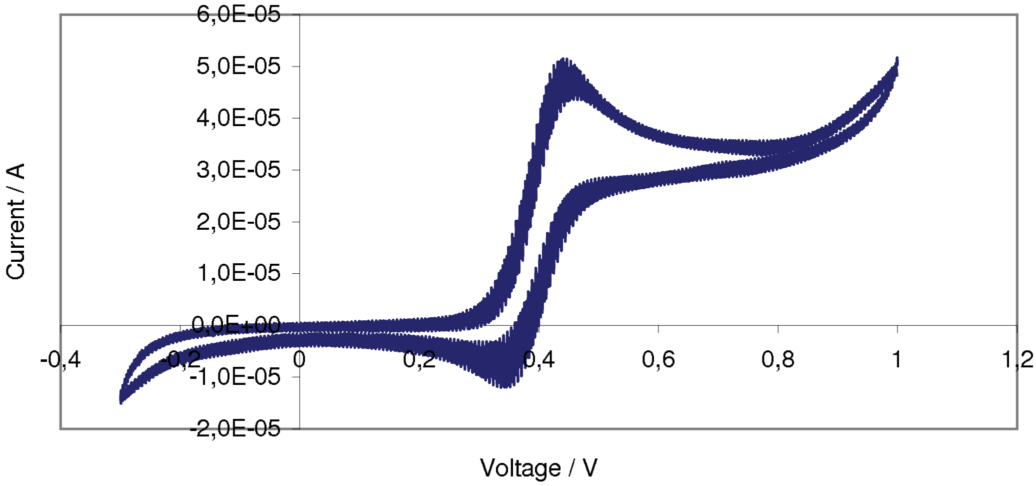

Figure 45: The ferrocene run: $E^0 = 0.36$ V with respect to the Ag/AgCl electrode.

Table 6: The electrochemical series with ferrocene and beetroot extract inserted.

Electrode	Standard potential E^0/V
Li^+ | Li	-3.05
K^+ | K	-2.92
Na^+ | Na	-2.71
Mg^{2+} | Mg	-2.37
Al^{3+} | Al	-1.66
Zn^{2+} | Zn	-0.76
Fe^{2+} | Fe	-0.44
Cd^{2+} | Cd	-0.40
Ni^{2+} | Ni	-0.23
I^- | AgI(s) | Ag	-0.15
Sn^{2+} | Sn	-0.14
Pb^{2+} | Pb	-0.13
H^+ | H_2 | Pt	0
Br^- | AgBr(s) | Ag	0.07
The Beetroot Extract	*0.08*
Ferrocene	*0.14*
Cl^- | AgCl(s) | Ag	0.22
Cl^- | Hg_2Cl_2(s) | Hg	0.27
Cu^{2+} | Cu	0.34
OH^- | O_2 | Pt	0.40
Cu^+ | Cu	0.52
I^- | I_2(s) | Pt	0.54
Fe^{3+}, Fe^2+ | Pt	0.77
Ag^+ | Ag	0.80
Br^- | Br_2(l) | Pt	1.07
Cl^- | Cl_2(g) | Pt	1.36
Au^{3+} | Au	1.50
F^- | F_2(g) | Pt	2.87
HF(aq) | F_2(g) | Pt	3.06

5.2.2 The Results from the TLC

The TLC experiment with the following eluents gave no useful results: pentane/ethyl acetate (1:1), ethyl acetate (pure) and ethanol (pure). When deionised water (solely) and deionised water/ethanol with the proportions (1:1), (1:10), (1:4) and (1:3) were used, the results were the chromatograms in figure 46. The red spot is mostly made up of betanin (betanin makes up 75-95% of the total red colouring matter of beetroot [36], [35]. The yellow part is presumably predominantly vulgaxanthine-I (which provides approximately 95% of the yellow colour in beetroot [36]), but it also contains flavonoids and carotenoids (e.g. beta-carotene). The experiment confirmed the hypothesis that the beetroot extract contains a lot of different pigments, since the traces on the chromatograms have oblongated shapes, indicating that different component substances travelled with different speeds, in turn indicating that there are a number of components.

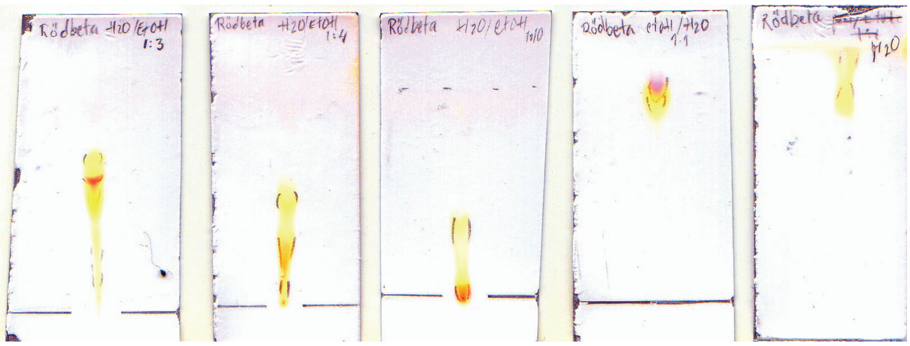

Figure 46: Chromatograms from the TLC.

5.2.3 The Results from the X-ray Diffraction

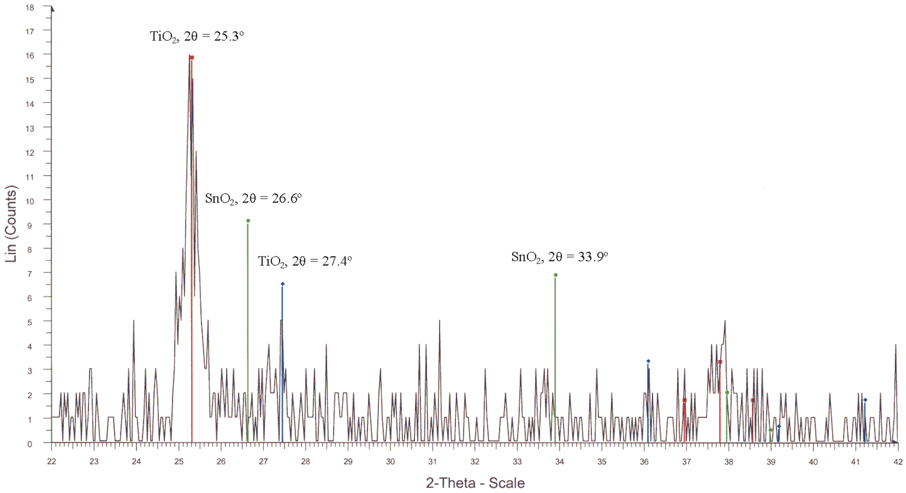

Figure 47: The x-ray diffraction pattern generated by a TiO_2 sample with characteristic peaks marked explicitly. On the y-axis is a linear count of diffracted photons and on the x-axis is the diffraction angle 2θ.

Figure 47 shows a typical diffraction pattern for a TiO_2 thin film covered substrate. The particular figure shows the diffraction pattern received by the sintered 1500 kg/cm^2-specimen. The vertical bars with dots on top mark where the characteristic peaks for the different crystals should be expected. The first bar from the left marks the main anatase peak (with diffraction angle $2\theta \approx 25.3°$) and the third marks the main rutile peak. The second and the fourth bars are inserted just for the sake of comparison: they mark two characteristic peaks for cassiterite, which is a crystal phase for SnO_2. No significant peaks being situated at those marked locations suggest that if a contamination substance is present, then it is probably not SnO_2. Estimates of the particle sizes (the crystal thicknesses) for the different TiO_2 samples is gathered in table 7. The rutile phase is generally better (to a higher extent) crystallised than the anatase phase, which makes the greater numbers for the rutile peak (with diffraction angle $2\theta \approx 27.4°$) quite plausible. There is a tangible congruence between the automatically computed crystal sizes and the manually computed dittos. A crystal size difference related to the different pressing forces applied to the substrates cannot be discerned anywhere, and a size difference related to the substrates having been sintered or not cannot be concluded from these tests. Thus we may well conclude that regardless of the preceding manipulations, the different photoelectrode substrates show the same crystal sizes. In figures 49, 50 and 51, depicting the two largest diffraction peaks for anatase and rutile for the substrates with the three different pressing forces applied, the sintered and the unsintered diffractions patterns are put together in the same graph. This also verifies there being no appreciable differences between the various specimens. The B-values in table 7 have been determined directly from graphs like the one in figure 48. The horizontal line at the height of the peak where the intensity is half the maximum value indicates the quantity B. White noise can be seen as small peaks along the bottom line of the graph.

Table 7: Particle size and related data for each combination of pressing force and sintered and unsintered TiO$_2$.

Anatase: Software-generated data	$2\theta/^\circ$	B/rad	Particle size/Å
Sintered 1500 kg/cm^2	25.22	0.0083	170
Unsintered 1500 kg/cm^2	25.23	0.0079	180
Sintered 1050 kg/cm^2	25.23	0.0081	180
Unsintered 1050 kg/cm^2	25.27	0.0083	170
Sintered 600 kg/cm^2	25.27	0.0076	190
Unsintered 600 kg/cm^2	25.30	0.0076	190
Anatase: Data computed manually	$2\theta/^\circ$	B/rad	Particle size/Å
Sintered 1500 kg/cm^2	25.21	0.0070	200
Unsintered 1500 kg/cm^2	25.26	0.0084	170
Sintered 1050 kg/cm^2	25.25	0.0070	200
Unsintered 1050 kg/cm^2	25.25	0.0082	170
Sintered 600 kg/cm^2	25.26	0.0076	190
Unsintered 600 kg/cm^2	25.30	0.0077	180
Rutile: Data computed manually	$2\theta/^\circ$	B/rad	Particle size/Å
Sintered 1500 kg/cm^2	27.45	0.0047	300
Unsintered 1500 kg/cm^2	27.45	0.0067	210
Sintered 1050 kg/cm^2	27.38	0.0050	280
Unsintered 1050 kg/cm^2	27.38	0.0054	270
Sintered 600 kg/cm^2	27.44	0.0070	200
Unsintered 600 kg/cm^2	27.35	0.0070	200

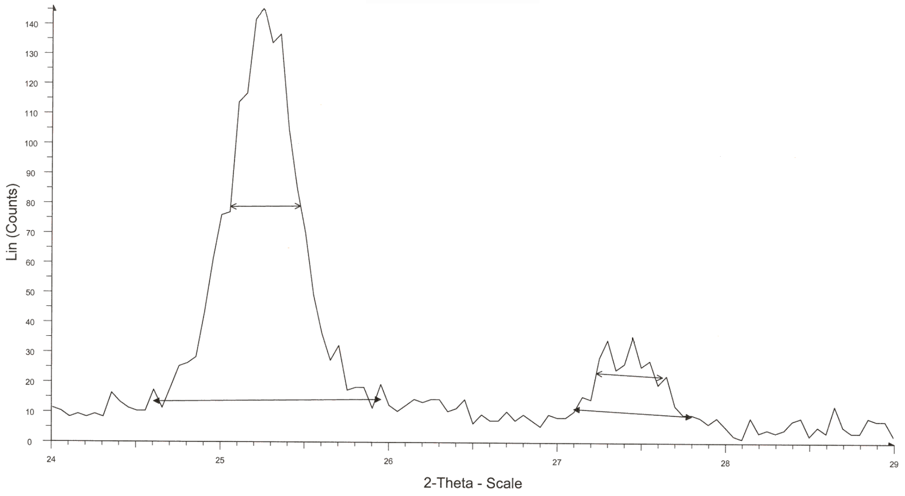

Figure 48: The broadness of a characteristic diffraction peak where the intensity is half the maximum value is the quantity B. This specific example depicts the sintered 600 kg/cm^2 sample, which has a B-value measuring 0.0070 radians.

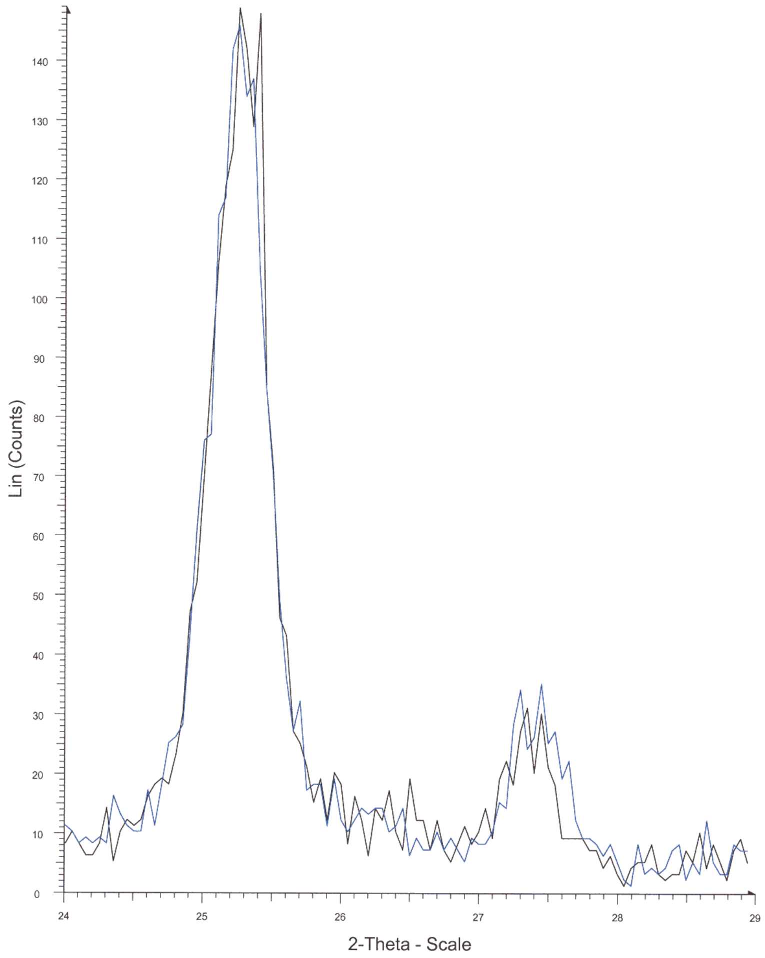

Figure 49: Diffraction patterns for the sintered and the unsintered specimens pressed at 600 kg/cm^2.

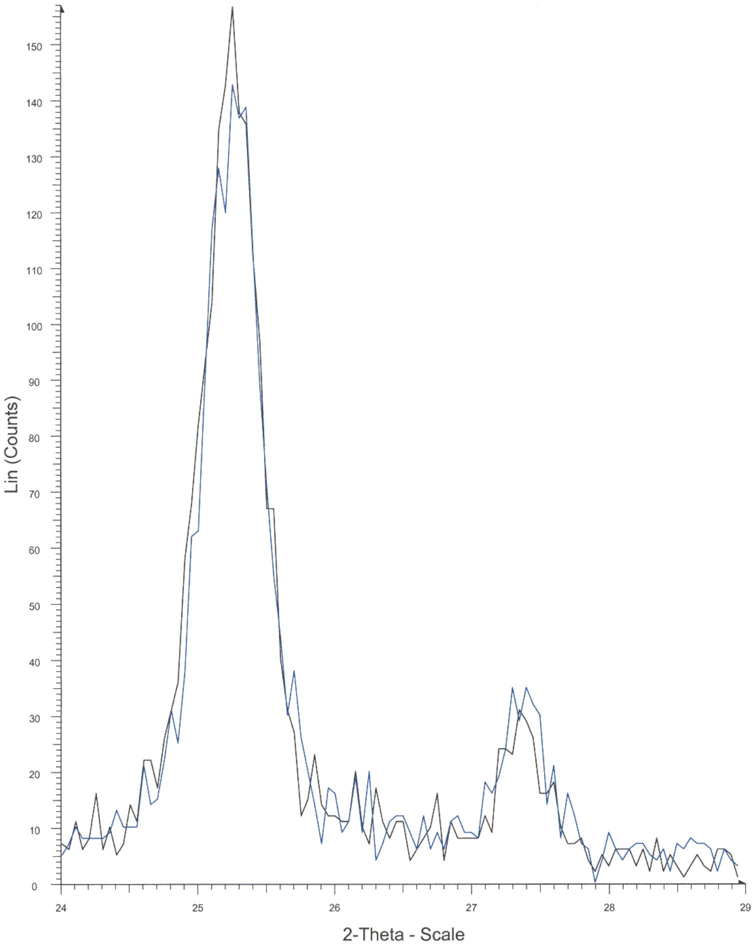

Figure 50: Diffraction patterns for the sintered and the unsintered specimens pressed at 1050 kg/cm^2.

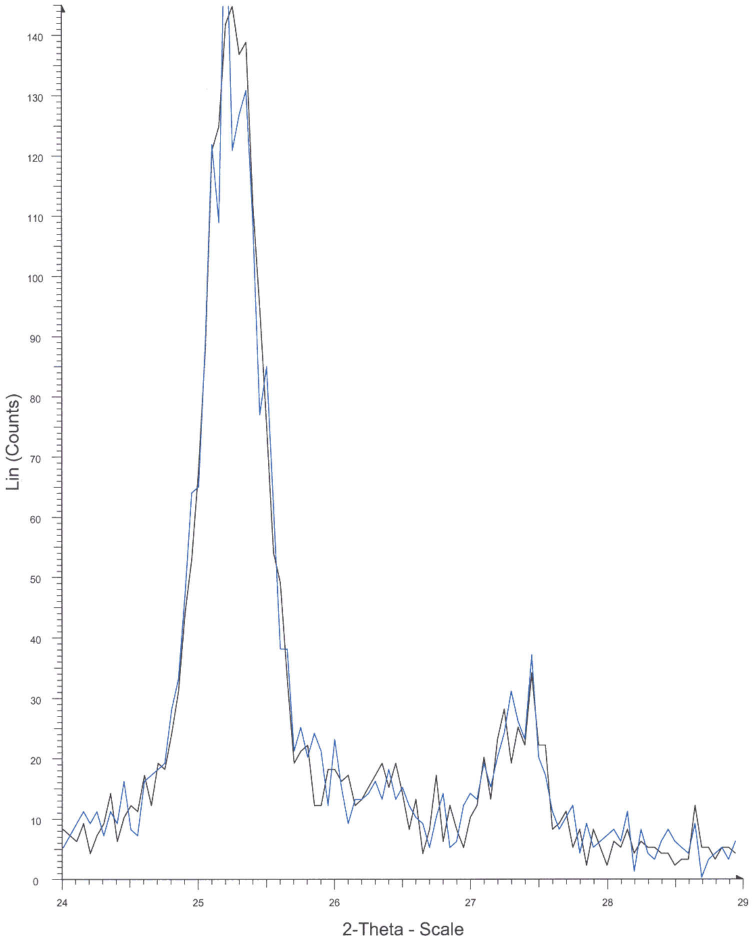

Figure 51: Diffraction patterns for the sintered and the unsintered specimens pressed at 1500 kg/cm^2.

The figures 49, 50 and 51 show the main diffraction peaks for anatase and rutile. The sintered and the unsintered diffraction patterns are merged into the same graphs to illustrate that there is no observable difference between sintered and unsintered TiO_2 regarding x-ray diffraction.

5.2.4 The Results from the Integrating Sphere

Four samples underwent the integrating sphere experiment, two sensitised with beetroot extract and two unsensitised. After having been corrected according to correction instructions, the information on transmittance and reflectance was used to infer the absorption of the photoelectrodes, and the results can be seen in figure 52 and table 8. In the table only a few wavelengths have been picked. The entire information material involves every fifth wavelength from 300 nm to 1000 nm, that is 141 data entries for each sample.

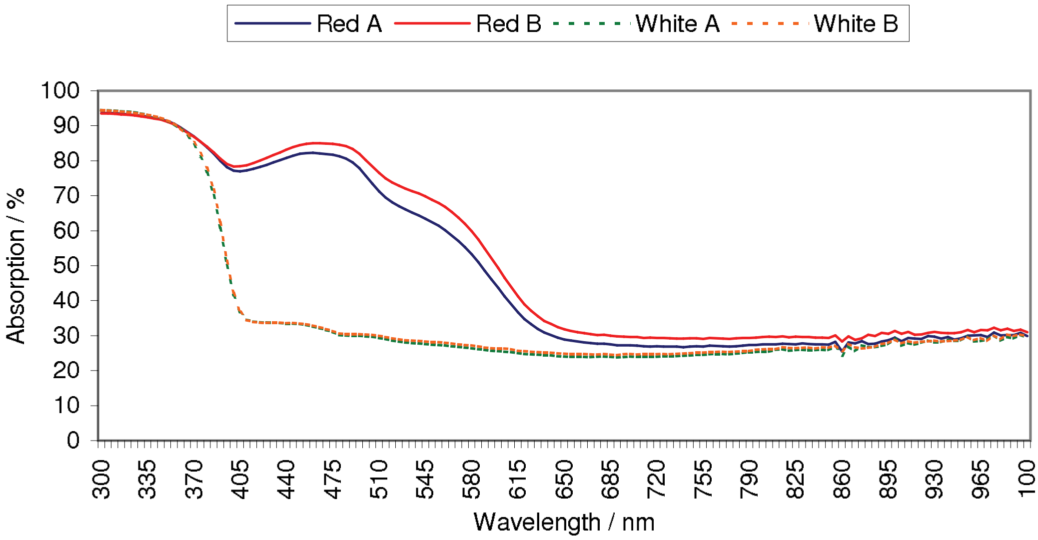

Figure 52: The photoelectrode absorption for two unsensitised samples (denoted White A and White B, lower curves) and two beetroot dye sensitised films (denoted Red A and Red B, upper curves).

Table 8: Absorption of TiO_2 thin film, sensitised with beetroot extract (Red A and B) and unsensitised (White A and B).

Wavelength/nm	Red A	Red B	White A	White B
300	93.6	93.5	94.5	94.3
400	77.2	78.4	41.5	42.2
500	75.7	80.2	29.8	30.3
600	43.7	49.3	25.6	26.3
700	27.3	29.6	24.0	24.7
800	27.5	29.6	25.4	26.0
900	29.4	31.3	28.9	28.9
1000	29.9	31.0	29.3	29.8

5.2.5 The Results from the Spectrophotometry

Absorption spectra have been obtained for the three dyes made from red onion, red cabbage and beetroot. As can be seen from the spectra in picture 53 all three absorbs most in the region 400-500 nm i.e. blue-green wavelengths, which reflections are perceived as orange-red-purple (see table 1).

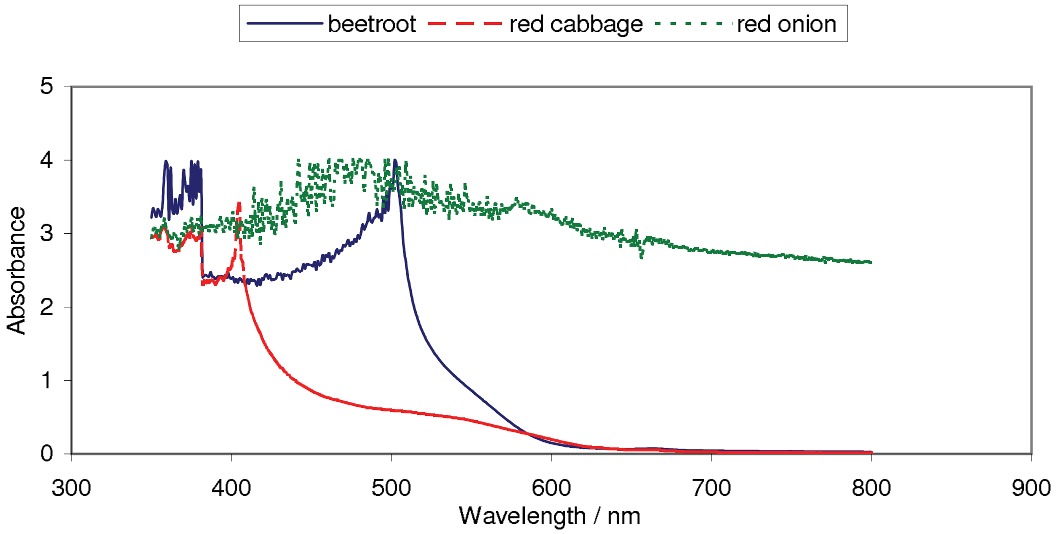

Figure 53: The absorbance of red onion, red cabbage and beetroot extracts.

Red onion has an absorption maximum at 480 nm in the blue-green area reflecting red, red cabbage has a maximum at 400nm in the violet area, reflecting green-yellow light and beetroot has two maxima at 400nm in the violet area and at 500 nm in the green area reflecting yellow and red-purple respectively.

The thorough investigation of beetroot shows its absorption spectrum in more detail, see figure 54. The figure shows three absorption maxima, at 320 nm (outside the visible spectra), at 400 nm (absorbing violet, reflection appearing green-yellow), and at 500 nm (absorbing green, reflection appearing red-purple) This corresponds well to the TLC test (see section 5.2.2) that separated the beetroot extract into one red-purple pigment and one or several green-yellow pigments.

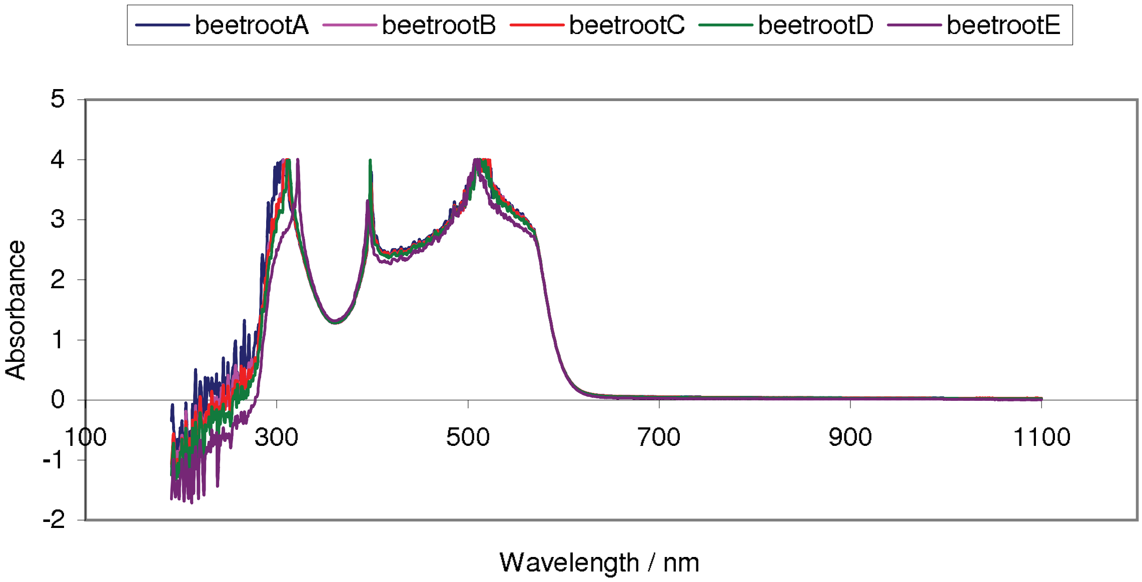

Figure 54: The absorbance of the second-fabrication beetroot extract.

6 Sources of Errors

6.1 The Manufacturing

The Semiconductor Suspension

The semiconductor TiO_2 suspension may have contained lumps despite many hours in the magnetic stirrer equipment. Furthermore, the earliest fabrications of cells were made with another batch of TiO_2 suspension than the later fabrications. There might have been small differences between the two batches of TiO_2 suspension.

The Photoelectrode Film Substrates and the Sintering Process

The evanescence of the ethanol in the semiconductor suspension invoked difficulties with the doctor blading process. Anomalies in the surface and the thickness of the semiconductor layer were consequences thereof. The thickness may also have been affected by the inexact doctor blading technique itself and the equipment used in the process: the glass rod and the scotch tape. The later could not be applied in precisely the same way each time, resulting in a small variance of the semiconductor surface area. Dust and minute grime particles might have adhered to the glass substrate or the semiconductor surface and the sintering process may have caused additional dirt particles to get attached to the electrode surfaces. The thermometer used in the sintering process was not always to be trusted, and therefore there was at times some uncertainty regarding in which temperature the sintering actually took place, but it was never interrupted if there was a suspicion that the sintering had been performed at too a cold temperature.

The Pressing Process

Measurements of the semiconductor surface areas were performed with a ruler, the exactness of which is limited by itself and the reading off it. Also the pressing apparatus itself, with a rather large-step reading scale, might have been the cause of inexact pressing forces. The aluminium foils attached to the substrates during the pressing in certain cases brought TiO_2 powder with them when peeled away; this was more common at higher pressing forces.

It is unlikely that the pressing apparatus applied an uneven pressing force during a given pressing. The steel blocks, between which the substrates were pressed, were so finely polished that it seems very remote to think that they could cause some kind of irregularity in this case.

The Preparation of the Dyes

In the manufacturing of a dye the time scope is of interest. Since it is a rather time-consuming business, the dye may be exposed to several causes of degradation before it is refined enough to be used. Even if not much time passed between the accomplishing of the dye extract fabrication and the dye's being used in a sensitising bath, the time lapse may be long enough for the dye to undergo degrading processes, which are hard to avoid. The rotavaporisation involved a low temperature, but still a temperature above normal room temperature. This warmth will certainly to some extent have contributed to dye degradation. Several unknown chemicals have been extracted along with the colour pigments in the dye solutions – this could hardly be avoided. These unknown molecules might have negative effects, like taking the place of the pigment molecules when the dye solution is applied on the semiconductor surface. Also they make it difficult to get a very concentrated dye extract because the extract gets saturated earlier than it would if it had contained only the colour pigments.

The Sensitising Process

Despite efforts to shut out light (with aluminium foils) and prevent vaporisation (by help of plastic film), light and vaporisation might still have affected the sensitisation baths through a degradation of the dye solutions. Alien species (from e.g. the plastic laboratory film) might have solved into the baths and this might also have affected the process.

The Counterelectrode

As in the case with the manufacturing of the photoelectrode, the counterelectrode was fabricated by means of a somewhat imprecise technique. The platinum chloride solution was applied dropwise and smeared out over the substrate surface by means of a glass rod. Dust particles and so on might have been involved (since the relatively clean laboratory is not a cleanroom after all). The counterelectrode was also sintered: the sources of errors connected to the sintering process are mentioned above.

The Electrolyte

The electrolyte was fabricated at the Department of Physical Chemistry, according to the standard recipe (see chapter 4.1.7). As only a small amount of electrolyte was fabricated at a time, a number of different fabrications were used. There might have been differences between the batches.

The Mounting of the Solar Cell

Several different clips were used to press the electrodes together, some stronger than others. Some electrodes might not have been optimally pressed together. In addition to this the relatively heavy cords and crocodile clips attached to the cell might have pulled the electrodes apart so that they were not tightly fastened to each other. These problems could in turn enhance or lead to the evaporating of the electrolyte. The electrolyte evaporating is a problem associated with the manufacturing of this type of small-sized open sandwich cells.

6.2 The Measurements

The iV Measurements

The lamp may at some runs not have been warm enough to give a good illumination spectrum. There might have been intermittent connections or short circuits in the solar cell set-ups for some runs, and the electrolyte might have partly evaporated. A software implementation fault may have caused strange "shark fins" on a number of the iV-curves. Air bubbles in the nanoporous surface of the semiconductor might have caused errors resulting in misshaped curves. The measures taken in cases when the iV-curves were clearly disturbed vary. If the error was a "shark fin" or a slightly deformed curve, it was dealt with manually and as far as possible compensated for in order to extract useful information from the curve anyway. In cases when the curve told of grave errors, the curve was not further considered.

The IPCE Measurements

The same type of errors occurring during the iV-measurements might have caused negative effects on the IPCE measurements: Not properly warmed-up lamp, intermittent connections, short circuits, air bubbles in the system and partial evaporation of the electrolyte.

The Cyclic Voltammetry

Apart from equipment-related errors, there might have been contaminations in the solutions and the cleaning of the electrodes prior to the test runs might have been insufficient.

The TLC

The eluents used were chosen arbitrarily. Perhaps there would have been a solvent at hand that would have been preferred.

The X-Ray diffraction and the Integrating Sphere

Since both experiments were entirely automated, the main errors can only have been that the substrates experienced damages (too small to be perceived by the naked eye) during the transport from the Department of Physical Chemistry at BMC to the Departments of Material Chemistry and Solid State Physics respectively, both at the Ånström Laboratory, (of course under the assumption that the computerised integrating sphere equipment and the x-ray diffractometer functioned faultlessly).

Photospectrometry

The run with a solid piece of substrate glass was evidently going to fail, since the solid scatter light in all directions and the photospectrometer equipment is designed for use of a cuvette with solution. The lamps were maybe at some runs not warm enough to give good illumination spectra. Apart from equipment-related errors, the tested extracts might have been turbid to some extent. Particles suspended in the extract scatter light and this might have interfered with the results.

Molecules other than the pigment molecules may also absorb light, and this too may be a cause of disturbed results.

7 Discussion

The manufacturing of this type of open sandwich cells of small size is difficult and sensitive as the electrolyte easily evaporates and heavy crocodile clips pull the tiny electrodes apart. Because of the sensitivity of the open sandwich configuration several different errors, such as short circuits, high series resistances and intermittent connections, occurred during iV-and IPCE-measurements leading to solar cells being discarded from the comparison.

Though IPCE-results were corrupt from no more than 2 cells of the total 95 solar cells produced and investigated, the iV-results from as many as 32 of 94, or 34.04% were discarded. The cells in this study where only made for a short lifetime, just enough for investigation, and this kind of loss is perhaps necessary or at least acceptable.

Problems with low pigment concentrations are to be expected when producing dye by extracting pigments from plants without any further refining. Each plant dye was made as a saturated solution but since there are probably hundreds or even thousands of chemical compounds in any plant extract, saturation of the solution is reached long before the solution is saturated with the pigment[4]. The presence of unknown chemicals in the plant extracts is the main reason for the efficiencies of the cells in this investigation being so low. The unknown chemicals bind to the TiO_2 surface and thereby they hinder the pigment molecules to do the same.

The TLC experiment confirmed the presence of several different compounds in the beetroot dye. The plant dyes having lower concentrations of pigment than the ruthenium dye was also indicated by the pale colours of the plant dyes compared to the very dark and intense colour of the ruthenium dye.

The comparison between the average IPCE-curves for different pressure forces as well as between iV-results for different pressure forces (see figure 32) and different solvents showed no significant differences either between different solvents or between different pressures forces. The conclusion can be drawn that the pressure force applied does not matter much. There are however some differences between cells sensitised with different dyes.

The low V_{oc} values of the cells result from poorly matched energy levels and are connected to the low E^0-value of the dye. Since the open circuit voltage is the theoretical upper bound for the voltage that can be produced by a unit, a high V_{oc} value is to be aimed for. When solar cells are combined into modules, the V_{oc} values of the individual solar cells are added into a total array open circuit voltage, so the higher the individual V_{oc} values are, the less units will be needed to attain a specific array voltage. The low V_{oc} values obtained in this investigation tell of how ineffective it would be to employ these cells in a compound module.

In the iV-measurements most of the plant dye sensitised solar cells gave quite high fill factors compared to the fill factors of the ruthenium dye sensitised cells. The cells sensitised with the second-fabrication beetroot extract dye gave especially good results, slightly better than the others, including ruthenium.

The fill factor of an iV-curve is one measure of how effective a solar cell is but there are also other

---

[4] It is basic chemical knowledge that much less salt can be dissolved in a sugarwater solution than in pure water.

aspects to consider. Several of the iV-curves have surprisingly smooth and "nice" shapes, thus high fill factors, despite the fact that they have extremely low current densities. In those cases the fill factor indicates that the cell is a really good one, but with an extremely low current density it is obviously not, since the whole idea of a solar cell is to produce an electrical current.

The highest current density of an iV-measurement is the short circuit current density, i_{sc}. The average i_{sc} values for the plant dye sensitised solar cells are only between 0.2% and 14,2% of the average i_{sc} value for the ruthenium dye sensitised cells (table 3).

The IPCE results are generally poor, except for the ruthenium dye sensitised cells (see chapter 5.1.2).

A comparison between a spectrophotometry absorbance spectrum for beetroot dye and an absorption spectrum from the integrating sphere experiment for a photoelectrode sensitised with the same beetroot dye (figure 55) shows that the beetroot dye sensitised solar cell does absorb light at roughly the same wavelengths as the beetroot dye dissolved in methanol.

A comparison between the same absorption spectrum and the IPCE-curve for the best performing solar cell sensitised with beetroot dye (figure 56) shows that despite the fact that there is absorption in parts of the visible spectrum, the IPCE response is close to zero at the same wavelengths. Light is absorbed by the solar cell, but the energy is clearly not transferred to the semiconductor thus not transformed in to electrical current to a matching degree.

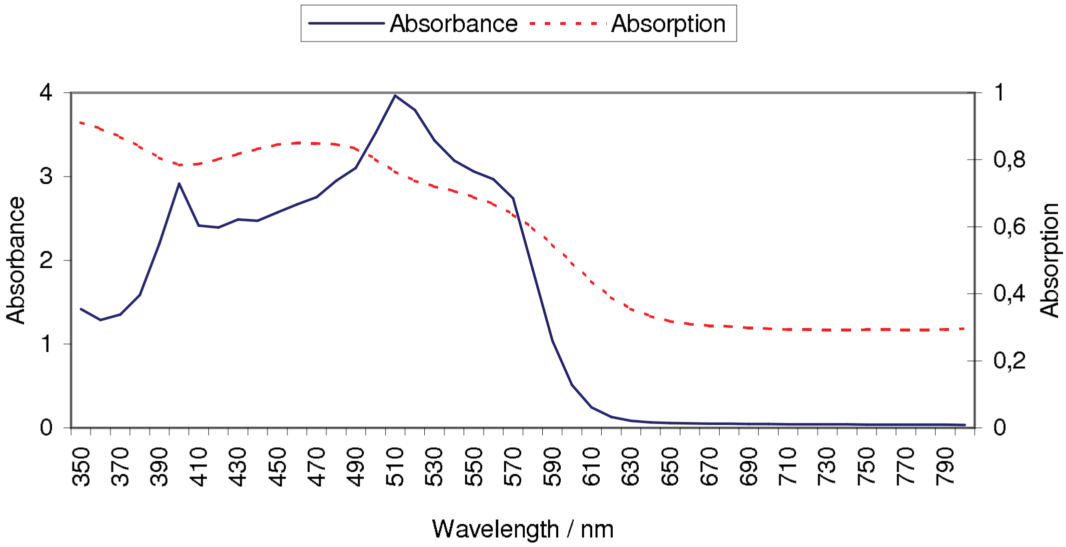

Figure 55: The Absorbance of beetroot dye and absorption of a beetroot dye sensitised electrode.

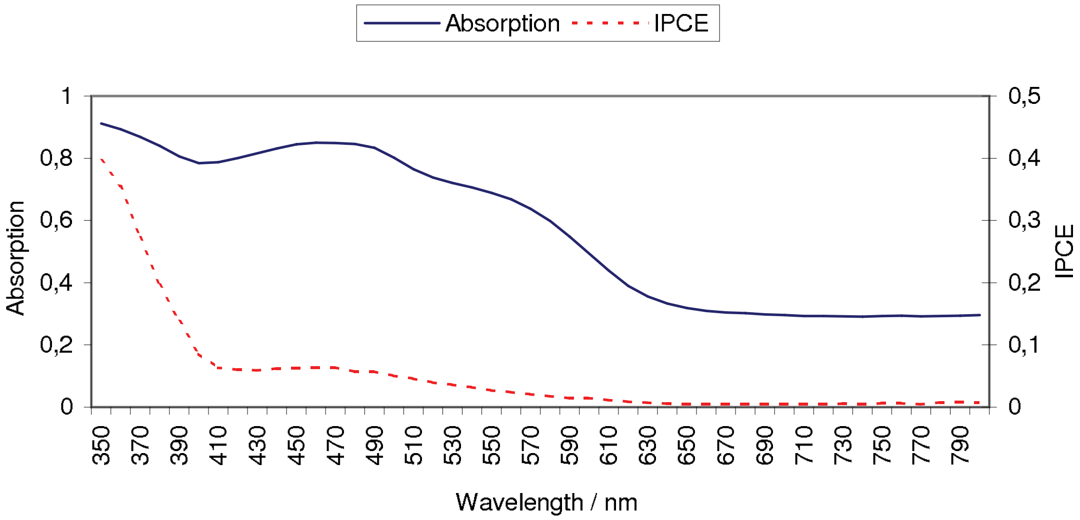

Figure 56: The absorption of a of beetroot dye sensitised electrode and the IPCE of a beetroot dye sensitised cell.

When choosing red colour for a dye it is roughly known how large the difference is between the energy levels that an absorbed photon is excited to and from, since, as explained in chapter 2.2.3, this corresponds to the absorbed wavelengths and thus to apparent colour, but it is not known where the absolute values for those energy levels are. As mentioned in chapter 2.1.2 the relationships between the energy levels of the semiconductor-electrolyte system and the energy levels in the pigment are critical. The energy level that the electron is excited to in the pigment must be slightly higher than the lower edge of the conduction band of TiO_2 and the energy level that the electron is excited from must be slightly lower than the E^0-value of the electrolyte and much higher than the valence band of TiO_2 (figure 5). The probability of this actually occurring is perhaps not so high when, since the absolute energy levels of an unknown pigment in a plant is rarely known, a plant for dye production is picked more or less by chance.

It is of course not impossible to find an optimal dye and further investigations might lead to the discovery of a plant, which will provide an excellent dye for thin film solar cells and safe energy for the future. In a further investigation of plant-based sensitising dyes a more successful strategy could be to first of all try to evaluate the standard potentials of the dyes (through literature studies for already known dyes and through cyclic voltammetry for not yet known dyes), i.e. their E^0-values. This is an important clue in the work of matching the energy levels of the dye to the Fermi level of the titanium oxide. It is also connected to the maximum V_{oc} value of the cell, and it is desirable to achieve larger V_{oc} values than was done in this investigation. High V_{oc} values are to strive for, to keep the number of units in solar cell modules (arrays) down. Another part of a further investigation should be to as far as possible purify the dye extract solutions, in order to eliminate present chemicals which do not contribute to the dye concentration, and in that way make possible an enhancing of this concentration. This would be the most crucial improvement, since in this investigation, the high concentration of unidentified chemicals was the chief obstructor of a high efficiency. Had it not been for these unidentified chemicals, the results would have been much better, as can also be concluded from the high fill factors. Even though the measured iV characteristics and the IPCE data are low, they are not too bad regarding the impurities of the extracts. By and large this investigation shows that there is certainly a hope for plant extract sensitised solar cells.

8 Figure Index

Figures depicting graphs resulting from our own measurements are not included in this index.

Introduction

Figure 1 on page 2 from [9]. Figures 2 on page 3 and 3 on page 4 drawn by Sigrid Hedbor.

Theoretical Background

Figures 4 on page 7 and 5 on page 8 from [4]. Figures 6 on page 10, 7 on page 10 and 8 on page 11 from [20]. Figure 9 on page 12 from [24]. Figure 10 on page 13 from [28], figures 11 on page 14 and 12 on page 15 from [30]. Figures 13(a) on page 16, 13(b) on page 16, 13(c) on page 16 and 13(d) on page 16 drawn by Linnéa Klar. Figure 14 on page 17 from [40]. Figures 15 on page 19, 16 on page 19 and 17 on page 20 provided by [47]. Figure 18 on page 20 from [48], with a slight modification to suit our needs.

The Theory Behind the Methods used for the Characterisation of the DSSC

Figures 19(a) on page 22, 19(b) on page 22 and 20 on page 23 from [4]. Figures 22 on page 30, 23(a) on page 31 and 23(b) on page 31 from [56]. Figures 24(a) on page 32, 24(b) on page 32, 25(a) on page 32 and 25(b) on page 32 drawn by Linnéa Klar.

Methodology

Figure 26 on page 35 photographed by Linnéa Klar. Figure 27 on page 38 drawn by Sigrid Hedbor. Figures 28 on page 39 and 29 on page 41 photographed by Linnéa Klar.

9 Acronyms and Abbreviations

aka	also known as
AM	air mass
ARS	Agricultural Research Service
BMC	(Uppsala) biomedicinska centrum
CB	Conduction band
DOPA	dihydroxyphenylalanine
DSSC	dye sensitised solar cell
e.g.	exempli gratia
etc	et cetera
HOMO	highest occupied molecular orbital
i.e.	id est
i_{sc}	Current density under the short circuit condition
IHP	inner Helmholtz plane
Il.	Illinois
IPCE	Incident Photon-to-Current Conversion Efficiency
IV	Current-Voltage
iV	Current density-Voltage
LDL (cholesterol)	low-density lipoprotein (cholesterol)
LSV	linear sweep voltammetry
LUMO	lowest unoccupied molecular orbital
NHE	normal hydrogen electrode
OHP	outer Helmholtz plane
PEC	photoelectrochemical
PV	photovoltaic
SHE	standard hydrogen electrode
Teflon	A proprietary name for polytetrafluoroethylene
TiO_2	Titanium dioxide
TLC	Thin-layer Chromatography
V_{oc}	Voltage under the open circuit condition
VB	Valence band

10 Appendix

Table 9: Fill factors for different solar cells. The numbers 600, 1050 and 1500 indicate the pressing force applied (in kg/cm^2) in the making of the TiO_2 film. The letters A-F are used to give unique names to different cells with the same dye and pressure force applied.

Solar cell	Fill factor
Ruthenium 600 C	0.56
Ruthenium 600 D	0.55
Ruthenium 1050 A	0.52
Ruthenium 1050 B	0.51
Ruthenium 1050 C	0.61
Ruthenium 1050 D	0.60
Ruthenium 1500 A	0.45
Ruthenium 1500 B	0.54
Ruthenium 1500 C	0.58
Ruthenium 1500 D	0.50
Violet 600 D	0.50
Violet 600 E	0.44
Violet 600 F	0.48
Violet 1050 D	0.63
Violet 1050 E	0.53
Violet 1050 F	0.53
Violet 1500 D	0.60
Violet 1500 E	0.54
Violet 1500 F	0.55
Henna burned 600 C	0.49
Henna burned 1050 C	0.55
Henna burned 1500 D	0.61
Henna unburned 600 A	0.48
Henna unburned 600 B	0.61
Henna unburned 600 C	0.53
Henna unburned 1050 B	0.65
Henna unburned 1500 B	0.60
Henna unburned 1500 C	0.55
Red cabbage methanol 600 A	0.62
Red cabbage methanol 600 B	0.67
Red cabbage methanol 1050 A	0.62
Red cabbage methanol 1050 B	0.63
Red cabbage methanol 1500 A	0.53
Red cabbage methanol 1500 B	0.42
Beetroot ethanol 600 A	0.40
Beetroot ethanol 600 B	0.55
Beetroot ethanol 1050 A	0.58
Beetroot ethanol 1050 B	0.65
Beetroot ethanol 1500 A	0.56
Beetroot ethanol 1500 B	0.58
Beetroot methanol 600 C	0.62
Beetroot methanol 600 D	0.67
Beetroot methanol 1050 A	0.66
Beetroot methanol 1050 D	0.63
Beetroot methanol 1500 A	0.68
Beetroot methanol 1500 C	0.49
Beetroot methanol 1500 D	0.58

Table 10: Fill factors for solar cells sensitised with the second-fabrication beetroot dye. The numbers 600, 1050 and 1500 indicate the pressure force applied (in kg/cm^2) when preparing the TiO$_2$ film. The numbers 1-6 are used to give each cell a unique name.

Solar cell	Fill factor
Beetroot final 600 3	0.71
Beetroot final 600 4	0.69
Beetroot final 600 5	0.66
Beetroot final 1050 1	0.53
Beetroot final 1050 2	0.74
Beetroot final 1050 3	0.75
Beetroot final 1050 4	0.60
Beetroot final 1050 5	0.71
Beetroot final 1050 6	0.54
Beetroot final 1500 2	0.75
Beetroot final 1500 3	0.66
Beetroot final 1500 4	0.70
Beetroot final 1500 5	0.68
Beetroot final 1500 6	0.64

Table 11: i_{sc} values for different cells.

Solar cell	$i_{sc}/\mu A cm^{-2}$
Ruthenium 600C	6900
Ruthenium 600D	7300
Ruthenium 1050A	620
Ruthenium 1050B	740
Ruthenium 1050C	8100
Ruthenium 1050D	7500
Ruthenium 1500A	960
Ruthenium 1500B	750
Ruthenium 1500C	5700
Ruthenium 1500D	7100
Violet 600D	62
Violet 600E	150
Violet 600F	220
Violet 1050D	62
Violet 1050E	360
Violet 1050F	290
Violet 1500D	73
Violet 1500E	250
Violet 1500F	370
Henna Burned 600B	29
Henna Burned 1050C	48
Henna Burned 1500D	53
Henna Unburned 600A	35
Henna Unburned 600B	39
Henna Unburned 600C	16
Henna Unburned 1050B	83
Henna Unburned 1500B	61
Henna Unburned 1500C	27
Red cabbage methanol 600A	10
Red cabbage methanol 600B	11
Red cabbage methanol 1050A	8.2
Red cabbage methanol 1050B	8.0
Red cabbage methanol 1500A	10
Red cabbage methanol 1500B	12
Beetroot ethanol 600A	500
Beetroot ethanol 600B	730
Beetroot ethanol 1050A	400
Beetroot ethanol 1050B	310
Beetroot ethanol 1500A	1000
Beetroot ethanol 1500B	910
Beetroot methanol 600C	20
Beetroot methanol 600D	28
Beetroot methanol 1050A	57
Beetroot methanol 1050D	18
Beetroot methanol 1500A	29
Beetroot methanol 1500C	17
Beetroot methanol 1500D	19

Table 12: i_{sc} values for cells sensitised with the second-fabrication beetroot extract dissolved in methanol (98.99%).

Solar cell	i_{sc}/μAcm^{-2}
Final Beetroot 600 3	41
Final Beetroot 600 4	51
Final Beetroot 600 5	57
Final Beetroot 1050 1	40
Final Beetroot 1050 2	55
Final Beetroot 1050 3	51
Final Beetroot 1050 4	52
Final Beetroot 1050 5	46
Final Beetroot 1050 6	44
Final Beetroot 1500 2	46
Final Beetroot 1500 3	81
Final Beetroot 1500 4	56
Final Beetroot 1500 5	58
Final Beetroot 1500 6	74

Table 13: V_{oc} values for different cells.

Solar cell	V_{oc}/mV
Ru 600C	630
Ru 600D	630
Ru 1050A	370
Ru 1050B	390
Ru 1050C	670
Ru 1050D	640
Ru 1500A	440
Ru 1500B	430
Ru 1500C	600
Ru 1500D	600
Violet 600D	300
Violet 600E	270
Violet 600F	320
Violet 1050D	330
Violet 1050E	330
Violet 1050F	320
Violet 1500D	320
Violet 1500E	350
Violet 1500F	360
Henna Burned 600B	290
Henna Burned 1050C	320
Henna Burned 1500D	350
Henna Unburned 600A	320
Henna Unburned 600B	360
Henna Unburned 600C	290
Henna Unburned 1050B	370
Henna Unburned 1500B	360
Henna Unburned 1500C	300
Red cabbage methanol 600A	470
Red cabbage methanol 600B	480
Red cabbage methanol 1050A	400
Red cabbage methanol 1050B	450
Red cabbage methanol 1500A	450
Red cabbage methanol 1500B	400
Beetroot ethanol 600A	400
Beetroot ethanol 600B	400
Beetroot ethanol 1050A	400
Beetroot ethanol 1050B	400
Beetroot ethanol 1500A	390
Beetroot ethanol 1500B	370
Beetroot methanol 600C	460
Beetroot methanol 600D	480
Beetroot methanol 1050A	520
Beetroot methanol 1050D	440
Beetroot methanol 1500A	500
Beetroot methanol 1500C	380
Beetroot methanol 1500D	430

Table 14: V_{oc} values for the cells sensitised with the second-fabrication beetroot extract dissolved in methanol (98.99%).

Solar cell	V_{oc}/mV
Final Beetroot 600 3	520
Final Beetroot 600 4	520
Final Beetroot 600 5	460
Final Beetroot 1050 1	400
Final Beetroot 1050 2	530
Final Beetroot 1050 3	520
Final Beetroot 1050 4	450
Final Beetroot 1050 5	500
Final Beetroot 1050 6	400
Final Beetroot 1500 2	520
Final Beetroot 1500 3	490
Final Beetroot 1500 4	510
Final Beetroot 1500 5	480
Final Beetroot 1500 6	500

References

[1] http://stage.itp.tsoa.nyu.edu/˜pr442/solar/pv_history.html.

[2] http://www.rleggat.com/photohistory/.

[3] http://micro.magnet.fsu.edu/optics/timeline/1834-1866.html.

[4] Mónica Marcela Gómez León. *Photoelectrochemical and Physical Properties of Sputter Deposited Titanium Oxide Electrodes – A New Option for Dye-sensitised Nanocrystalline Solar Cells*. PhD thesis, Faculty of Science, National University of Engineering, Lima, 2001.

[5] Michael Grätzel. Photoelectrochemical cells. *Nature*, 414:338–344, 2001.

[6] H. Gerischer. Electrochemical behavior of semiconductors under illumination. *The Journal of The Electrochemical Society*, 113:1174–1182, 1966.

[7] http://www.fsec.ucf.edu/pvt/pvbasics/index.htm.

[8] M. Grätzel and B. O'Regan. A low-cost, high-efficiency solar cell based on dye-sensitized colloidal tio$_2$ films. *Nature*, 353:737 – 739, 1991.

[9] http://msp.rmit.edu.au/Article_04/05.html.

[10] http://www.peopleandplanet.net/doc.php?id=2360.

[11] Bhushan Sopori. Silicon Solar-Cell Processing for Minimizing the Influence of Impurities and Defects. *Journal of Electronic Materials*, 31(10), 2002.

[12] A. Fujishima and K. Honda. Electrochemical Photolysis of Water at Semiconductor Electrode. *Nature*, 238(37), 1971.

[13] Greg Smestad and Leticia Cowan. Photography, photosynthesis, and photons yield power. OE Reports August 1994 Issue, http://www.spie.org/app/Publications/magazines/oerarchive/august/solar_tech.html.

[14] http://www.lenntech.com/Periodic-chart-elements/Ru-en.htm.

[15] Torbjörn Lindgren. Solceller - en första introduktion, 2002.

[16] Sten-Eric Lindquist, Anders Hagfeldt, Henrik Lindström, Sven Södergren, Håkan Rensmo, and Anita Solbrand. Det artificiella lövet - en solcell med möjligheter. *Fysikalisk-kemiska institutionen, Uppsala Universitet*, 1900.

[17] Henrik Lindström, Eva Magnusson, Anna Holmberg, Sven Södergren, Sten-Erik Lindquist, and Anders Hagfeldt. A new method for manufacturing nanostructured electrodes on glass substrates. *Solar Energy Materials & Solar Cells*, 73:91–101, 2002.

[18] http://www.chm.bris.ac.uk/motm/solarcells/understanding.htm.

[19] Yasuhiro Tachibana, Saif A. Haque, Ian P. Mercer, Jaques E. Moser, David R. Klug, and James R. Durrant. Modulation of the Rate of Electron Injection in Dye-Sensitized Nanocrystalline Tio_2 Films by Externally Applied Bias. *The Journal of Physical Chemistry B*, 105:7424–7431, 2001.

[20] M Silberberg. *Chemistry - The Molecular Nature of Matter and Change, international edition.* McGraw-Hill, 1996.

[21] Carl Nordling and Jonny Österman. *Physics Handbook for Science and Engineering.* Studentlitteratur, 1996.

[22] F. J. Blatt. *Modern Physics, international edition.* McGraw-Hill, 1992.

[23] P. W. Atkins and R. S. Friedman. *Molecular Quantum Mechanics.* Oxford University Press, 3 edition, 2000.

[24] J.D. Cole, R. R. Hill, and D. R. Roberts, editors. *Chemical change and life - a source book in photochemistry.* The Open University, 1982.

[25] D. C. Harris, editor. *Quantitative Chemical Analysis.* W. H. Freeman and Company, 5 edition, 2000.

[26] http://www.friedli.com/herbs/phytochem/flavonoids.html.

[27] http://www.charlies-web.com/specialtopics/anthocyanin.html.

[28] Tore Frängsmyr, editor. *Nationalencylopedin, Första bandet.* Bra Böcker, 1989.

[29] http://www.wholehealthmd.com/refshelf/substances_view/1,1525,1026,00.html.

[30] http://school.chem.umu.se/spec_antocyan.html.

[31] http://www.lef.org/magazine/mag2000/mar00-cover1a.html.

[32] http://www-class.unl.edu/biochem/labs/student/exp6.htm.

[33] Casimiro Mantell, Miguel Rodrìguez, and Enrique Martìnez de la Ossa. A Screening Analysis of the High-Pressure Extraction of Anthocyanins from Red Grape Pomace with Carbon Dioxide and Cosolvent. *Engineering in Life Sciences*, 3:38–42, 1900.

[34] http://www.nal.usda.gov/ttic/tektran/data/000007/19/0000071970.html.

[35] http://www.agsci.ubc.ca/courses/fnh/410/colour/3_72.html.

[36] George S. Serris and Costas G. Biliaderis. Degradation kinetics of beetroot pigment encapsulated in polymeric matrices. *Journal of the Science of Food and Agriculture*, 81:691–700, 1900.

[37] Dieter Starck, Thomas Vogt, and Willibald Schliemann. Recent advances in betalain research. *Phytochemistry*, 62:247–269, 2003.

[38] http://home.tnv.mh.se/nils-ekelund/Lab_v_5p.htm.

[39] Yizhong Cai, Mei Sun, Willibald Schliemann, and Harold Corke. Chemical stability and colorant properties of betaxanthin pigments from celosia argentea. *Journal of Agricultural and Food Chemistry*, 49:4429–4435, 2001.

[40] M. A. Pedre no and J. Escribano. Correlation between antiradical activity and stability of betanine from Beta vulgaris L roots under different pH, temperature and light conditions. *Journal of the Science of Food and Agriculture*, 81:627–631, May 2001.

[41] http://www.platinuminfo.net/pgm.html.

[42] http://www.scescape.net/ woods/elements/ruthenium.html.

[43] http://www.bebig.de/downloads/gebr_anw_ru6app_en_02.pdf.

[44] http://pearl1.lanl.gov/periodic/elements/44.html.

[45] Aiga Fumihiko and Tada Tsukasa. Molecular and electronic structures of black dye; an efficient sensitizing dye for nanocrystalline tio$_2$ solar cells. *Journal of Molecular Structure*, 658:25–32, 2003.

[46] http://www.solaronix.com.

[47] Mr Toby Meyer. Solaronix SA, Rue de l'Ouriette 129, CH-1170 Aubonne, Switzerland, 2005.

[48] http://chemed.chem.purdue.edu/genchem/topicreview/bp/ch21/gibbs.html.

[49] Steven S. Zumdahl. *Chemistry.* D. C. Heath and Company, 3 edition, 1993.

[50] http://emsolar.ee.tu-berlin.de/lehre/english/pv1/.

[51] Jörn Rostalski and Dieter Meissner. Monochromatic vs. Solar Efficiencies of Organic Solar Cells. Technical report, Forschungszentrum Jülich, 1998.

[52] John Moore and Nicholas D Spencer, editors. *Encyclopedia of Chemical Physics and Physical Chemistry*, volume 1. Institute of Physics Publishing, 2001. http://ecppc.iop.org/iop.

[53] http://www.britannica.com.

[54] P. W. Atkins. *Physical Chemistry.* Oxford University Press, 6 edition, 1998.

[55] Allen J Bard and Larry R Faulkner. *Electrochemical Methods Fundamentals and Applications.* John Wiley & Sons, 1980.

[56] B. D. Cullity. *Elements of X-ray Diffraction.* Addison-Wesley Publishing Company Inc, 1959.

[57] http://www.pro-lite.uk.com/Light/Labsphere/spectralon.html.

[58] http://www.ne.se/jsp/search/article.jsp?i_art_id=134394&i_word=Bouguer-Lambert-Beers%20lag.

[59] http://de.wikipedia.org/wiki/Ferrocen.

[60] Arne Roos. Use of an integrating sphere in solar energy research. *Solar Energy Materials and Solar Cells*, 30:77–94, 1993.

[61] G. Blom. *Sannolikhetsteori och statistik med tillämpningar.* Studentlitteratur, 1989.